SRESA Journal of

LIFE CYCLE RELIABILITY AND SAFETY ENGINEERING

Vol.1 Issue No.3 July – Sept 2012 ISSN – 2250 0820

Special Issue :

on Paper Presented at "International Symposium on Engineering Under Uncertainty: Safety Assessment and Management – ISEUSAM-2012"

Guest-Editors

Subrata Chakraborty
Sankaran Mahadevan

Chief-Editors

P.V. Varde
A.K. Verma
Michael G. Pecht

SOCIETY FOR RELIABILITY AND SAFETY

Typeset & Printed

EBENEZER PRINTING HOUSE
Unit No. 5 & 11, 2nd Floor, Hind Services Industries,
Veer Savarkar Marg,
Dadar (west), Mumbai -28
Tel.: 2446 2632/ 3872
E-mail: outwork@gmail.com

Life Cycle Reliability and Safety Engineering
Vol.1 Issue 3 (2012) iv-v

Guest Editorial

In engineering applications, it is important to model and treat adequately all the available information during the analysis and design phase. Typically, the information originates from different sources like field measurements, experts' judgments, objective and subjective considerations. Overlaying these features are influences of human errors, imperfections in the construction techniques and production process, and the influences of the boundary and environmental conditions. All these aspects can be brought under one common denominator: that is "*presence of uncertainty*". Uncertainty heavily affects reliability and safety, which are the core issues that need to be addressed during the analysis, design, construction and operation of engineering systems. In this backdrop, the International Symposium on Engineering under Uncertainty: Safety Assessment and Management (ISEUSAM - 2012) was organised at BESU, Shibpur during January 4 to 6, 2012 to facilitate the discussion towards better understanding and management of uncertainty and risk, encompassing various aspects of safety and reliability of engineering systems. Twelve selected papers are compiled in two Special Issues of Society for Reliability and Safety (SRESA) Journal of Life Cycle Reliability and Safety Engineering to provide a snapshot of the various papers discussed in ISEUSAM 2012.

All the six papers included in this July-September issue are revised versions of those presented in the Symposium. The first paper deals with reliability problem of earth slopes under a probabilistic framework. The study is concerned with the determination of the critical probabilistic slip surface and the associated probability of failure. The second paper is focused on robust optimum design of tuned mass damper system in seismic vibration mitigation. The effectiveness of robust design over conventionally adopted interval approach in the absence of complete probabilistic information to describe the system parameters is demonstrated. *The third paper* highlights the role of uncertain hydraulic conductivity parameter of the fill material and its influence on probabilistic assessment of ground water level and sea water interface seems to be useful in quality control purposes in a land reclamation projects. *The fourth paper* focuses on the effect of uncertainty of different parameters of wind field on the performance of container cranes, highly susceptible to damage or even failure during severe windstorms. *The fifth paper* discusses current research and opportunities for uncertainty quantification in performance prediction and risk assessment of engineered systems. This keynote paper draws on illustrative problems in different engineering disciplines to discuss recent research on quantifying various types of errors and uncertainties, framework for integrating information from multiple sources, multiple model development activities and multiple formats; and using uncertainty quantification in risk-informed decision-making throughout the life cycle of engineered systems. *The sixth paper* presents predictive models for time-dependent damages in corrosion-affected RC beams for evaluating time-dependent flexural and shear strengths for corroded beams considering variability in the identified basic variables.

The Guest Editors would like to express their deep gratitude to all authors for their time and effort devoted to the completion of their contributions. We are thankful to Professor Gautam Bhattacharya, one of the organising secretaries of ISEUSAM 2012 for his support and encouragement. We also would like to specially thank Professor Achintya Haldar, Chair, Scientific Committee of ISEUSAM 2012 for his in-depth reviews and recommendations in selecting the papers. In addition, we are most appreciative to the Editors of *SRESA Journal of Life Cycle Reliability and Safety Engineering*, for their kind invitation to edit this Special Issue.

Guest Editors

Subrata Chakraborty Department of Civil Engineering Bengal Engineering and Science University, Shibpur Howrah - 711103 INDIA Ph:03326684561-63(ext 281) Fax:03326682916 Email: schak@civil.becs.ac.in	Sankaran Mahadevan Department of Civil & Environmental Engineering 272 Jacobs Hall Vanderbilt University VU Station B 356077 Nashville, TN 37235-6077 Ph:615-322-3040 Fax:615-322-3365 Email: sankaran.mahadevan@vanderbilt.edu

Dr. Subrata Chakraborty, a fellow of the Indian National Academy Engineering, is currently a Professor at Bengal Engineering and Science University, Shibpur. He did his bachelor of Civil Engineering at Bengal Engineering College, Shibpur, M. Tech. and PhD at IIT Kharagpur. He visited RWTH, Aachen, Germany in 2009, 2010 as a Humboldt Fellow, University of Arizona, Tucson, USA in 2005 as a BOYSCAST Fellow and was a Research Associate at University of Cambridge, UK in 2003. Prof. Chakraborty's research interests include Stochastic Finite Element and Sensitivity Analysis, Dynamic Analysis under Seismic, Wind and Blast load, Seismic Vulnerability Assessment, Reliability under Hybrid Uncertainty, Robust and Reliability Based Optimization, Fibre Reinforced Concrete, Structural Control and Health Monitoring, etc. He has completed a number of research projects funded by DST, UGC, CSIR etc. and international collaborative research in Indo-Italian Cultural Exchange Programme of UGC and CP-STIO programme of DST etc. Prof. Chakraborty has supervised four doctoral and forty master theses. He has authored more than hundred technical articles including international and national journals, conference proceedings, book and book chapters. Prof. Chakraborty has served as a managing editor, associate editor and member of the editorial board of national and international journals. In recognition of his contribution in Engineering Science, Prof Chakraborty has received several awards and laurels as honourable as the Humboldt Fellowship for Experienced Researchers, the INAE Young Engineer Award, the BOYSCAST Fellowship, the Young Faculty Research Award etc.

Dr. Sankaran Mahadevan is John R. Murray Sr. Professor of Engineering at Vanderbilt University, and founder-director of NSF-funded IGERT multidisciplinary doctoral program in Reliability and Risk Engineering and Management at Vanderbilt University. He has twenty five years of research and teaching experience in the areas of reliability and risk analysis, uncertainty quantification, design optimization, materials durability, and structural health monitoring. His research has been funded by many U.S. agencies such as NSF, NASA, FAA, DOD, DOE, DOT, NRC, and private industry such as GM, Chrysler, Union Pacific, and American Association of Railroads. He has directed 34 Ph.D. dissertations and 22 M.S. theses, taught many industry short courses on risk and reliability methods, and authored more than 350 technical publications, including two textbooks and 150 peer-reviewed journal articles.

Professor Mahadevan has served as Technical and General Chair of the AIAA SDM conference and the AIAA Non-Deterministic Approaches Conference. In addition, he has served as Chair of several ASCE committees and is on the Editorial Board of several journals.

Professor Mahadevan obtained his B.Tech from Indian Institute of Technology, Kanpur, M.S. from Rensselaer Polytechnic Institute, Troy, NY, and Ph.D. from Georgia Institute of Technology, Atlanta, GA.

Life Cycle Reliability and Safety Engineering
Vol.1 Issue 3 (2012) 01-07

Slope Reliability Analysis Using the First Order Reliability Method

Subhadeep Metya[1] and Gautam Bhattacharya[2]
[1]*Budge Institute of Technology, Kolkata-700137,*
[2]*Bengal Engineering & Science University, Shibpur, Howrah 711103,*
E-mail:subhadeep.metya@gmail.com

Abstract

The paper pertains to a study on the reliability evaluation of earth slopes under a probabilistic framework. The study is concerned in the first phase with the determination of reliability index and the corresponding probability of failure associated with a given slip surface and then in the second phase the determination of the critical probabilistic slip surface and the associated minimum reliability index and the corresponding probability of failure. The geomechanical parameters of the slope system have been treated as random variables for which different probability distributions have been assumed. The reliability analyses have been carried out using two methods, namely, the approximate yet simple Mean-Value-First-Order Second-Moment method (MVFOSM) and the rigorous First-Order Reliability Method (FORM). Based on a bench mark illustrative example of a simple slope in homogeneous soil with uncertain strength parameters along a slip circle, an effort has been made to numerically demonstrate the nature and level of errors introduced by adopting the MVFOSM method for reliability analysis of earth slopes still widely used in the geotechnical engineering practice, vis-à-vis a more accurate method such as the FORM.

Keywords: *Slope stability; slip surface; uncertainty; random variable; probability distribution; reliability analysis*

1. Introduction

In recent years there has been a growing appreciation amongst the researchers in the field of geotechnical engineering of the fact that geotechnical parameters, especially the strength parameters including pore water pressure, are highly uncertain or random. Conventional deterministic approach is, therefore, being increasingly replaced with probabilistic approach or reliability analysis within a probabilistic framework. Slope stability analysis is one of the important areas where the recent trend is to determine the probability of failure of slopes instead of, or complementary to, the conventional factor of safety.

During the last decade quite a few studies on reliability evaluation of earth slopes have been reported in the literature. Most of these studies used the simple yet approximate reliability analysis method known as the Mean-Value First-Order Second-Moment (MVFOSM) method based on a Taylor series expansion of the factor of safety. However, this method suffers from serious shortcomings such as the following: (i) the method does not use the distribution information about the variables when it is available; (ii) the performance function is linearized at the mean values of the basic variables. When the performance function is nonlinear, significant errors may be introduced by neglecting higher order terms, for the reason that the corresponding ratio of mean of performance function to its standard deviation which is evaluated at the mean values may not be the distance to the nonlinear failure surface from the origin of the reduced variables. (iii) Furthermore, first-order approximations evaluated at the mean values of the basic variates will give rise to the problem of invariance for mechanically equivalent limit states; that is, the result will depend on how a given limit-state event is defined.

The First Order Reliability Method (FORM), on the other hand, does not suffer from the above shortcomings and is, therefore, widely considered to be an accurate method. The method has been finding increasing use especially in structural engineering applications for more than a decade. More recently in the geotechnical engineering field also there have been quite a few attempts at reliability analysis of earth

slopes using the FORM method (Sung Eun Cho,2009, Chowdhury and Rao,2010, Das and Das, 2010)

In this paper, an attempt has been made to develop computational procedures for slope reliability analysis based on the First Order Reliability Method (FORM). Computer programs have been developed to demonstrate the application of FORM in the determination of (i) the reliability index for a given slip surface, and, more importantly, in the determination of (ii) the probabilistic critical slip surface and the associated minimum reliability index. Different probability distributions have been considered for the basic random variables. In determining the probabilistic critical slip surface the basic methodology suggested by Bhattacharya et al. (2003) has been adopted. The above reliability analyses have also been carried out using the approximate MVFOSM method and the results obtained have been compared with those obtained by using the FORM to bring out the difference clearly and demonstrate numerically the shortcomings of the MVFOSM method.

2. Formulation

2.1 Deterministic Analysis

The conventional slope stability analysis follows a deterministic approach wherein out of a number of candidate potential slip surfaces the one with the least value of factor of safety is searched out and is termed the critical slip surface. It has now been widely appreciated that the slope stability analysis is essentially a problem of optimization wherein the co-ordinates defining the shape and location of the slip surface are the design variables and the factor of safety functional expressed as a function of the design variables is the objective function to be minimized subject to the constraints that the obtained critical slip surface should be kinematically admissible and physically acceptable. In practice, analysis is often done based on the assumption that the slip surface is an arc of a circle, as it greatly simplifies the problem. The Ordinary Method of Slices (OMS) (Fellenius, 1936) is the simplest and the earliest method of slices that assumes a circular slip surface geometry.

The factor of safety functional (FS) for the Ordinary Method of Slices (OMS), is given by the following expression [Eq. (1)], where the notations have their usual meaning. Specifically, c' and φ' denote the effective cohesion and effective angle of shearing resistance respectively; W_i and u_i are the weight and the pore water pressure at the base of the i^{th} slice respectively, θ_i is the base inclination of the i^{th} Δl_i slice, and $\hat{L}$ are the base length of the i^{th} slice and the total arc length of the slip circle respectively.

$$FS=\frac{c'\hat{L}+\tan\varphi'\sum_{i=1}^{i=n}(W_i\cos\theta_i - u_i\,\Delta l_i)}{\sum_{i=1}^{i=n}(W_i\sin\theta_i)} \quad (1)$$

Substituting $W_i = \gamma b h_i$, and $u_i = r_u \gamma h_i$, where γ and b are the unit weight of soil and the common width of slice respectively, h_i is the mean height of the ith slice, and r_u is the pore pressure ratio, Eq. (1) reduces to

$$FS=\frac{c'\hat{L}+\tan\varphi'\sum_{i=1}^{i=n}(\gamma b h_i\cos\theta_i - r_u\gamma h_i\Delta l_i)}{\sum_{i=1}^{i=n}(\gamma b h_i\sin\theta_i)} \quad (2)$$

2.2 Reliability Index β based on the MVFOSM method

Taking the performance function as the expression for FS in a limit equilibrium method of slices such as Eq. (1) or (2) for analyzing slope stability, and the corresponding limit state equation as FS - 1 = 0, the reliability index β based on the MVFOSM method is given by

$$\beta = \frac{E[FS]-1}{\sigma[FS]} = \frac{FS(\mu_{x_i})-1}{\sqrt{\sum_{i=1}^{n}\left(\frac{\partial FS}{\partial X_i}\right)^2\sigma^2[X_i] + 2\sum_{i,j=1}^{n}\left(\frac{\partial FS}{\partial X_i}\right)\left(\frac{\partial FS}{\partial X_j}\right)\rho\,\sigma[X_i]\,\sigma[X_j]}} \quad (3)$$

where n = number of soil strength parameters (c', $\tan\varphi'$, r_u, γ etc.) taken as random variables ; E[FS] = expected value of FS; σ[FS]=standard deviation of FS; μ_{xi} = mean value of random variable X_i; σ[X_i] = standard deviationof X_i; and ρ = correlation coefficient between X_i and X_j.

Mechanically Equivalent Limit State

When using MVFOSM method, it is of interest to study how the results of reliability analysis differ when other mechanically equivalent limit states are adopted. A limit state equivalent to FS-1 = 0 mentioned above is given by ln (FS) = 0. For such a limit state, the reliability index is given by

$$\beta = \frac{E[\ln FS]}{\sigma_{\ln FS}} \quad (4a)$$

where,

$$E[\ln FS] = \ln(E[FS]) - \frac{\sigma^2_{\ln FS}}{2} \quad (4b)$$

and

$$\sigma_{\ln FS} = \sqrt{\ln\left(1 + \left(\frac{\sigma_{FS}}{E[FS]}\right)^2\right)} \qquad (4c)$$

2.3 Reliability Index β based on the FORM Method

In this method the reliability index (β) is defined as the minimum distance (D_{min}) from the failure surface [g(**X′**) =0] to the origin of the reduced variates, as originally proposed by Hasofer and Lind (1974). For general nonlinear limit states, the computation of the minimum distance (D_{min}) becomes an optimization problem as stated below:

Minimize $D = \sqrt{x'^t x'}$

Subject to the constraint $g(x') = 0$

where, X′ represents the coordinates of the checking point on the limit state equation in the reduced coordinates system.

Two optimization algorithms are commonly used to solve the above minimization problem to obtain the design point on the failure surface and the corresponding reliability index β (Haldar and Mahadevan, 2000). In the first method (Rackwitz. 1976) referred to as FORM Method I by Haldar and Mahadevan (2000), it is required to solve the limit state equation during the iteration. The second method (Rackwitz and Fiessler, 1978) referred to as FORM Method II by Haldar and Mahadevan (2000) does not require solution of the limit state equation. It uses a Newton-type recursive formula to find the design point. The FORM Method II is particularly useful when the performance function is implicit, that is, when it cannot be written as a closed form expression in terms of the random variables. The FORM method, however, is applicable only for normal random variables. For non-normal variables it is necessary to transform them into equivalent normal variables. This is usually done following the well known Rackwitz–Fiessler method (Haldar and Mahadevan, 2000).

2.4 Probability of Failure:

Once the value of the reliability index β is determined by any of the methods discussed above, the probability of failure, p_F is then obtained as:

$$p_F = \Phi(-\beta) \qquad (5)$$

where, Φ (.) is the standard normal cumulative probability distribution function, values of which are tabulated in standard texts.

2.5 Determination of Probabilistic Critical Slip Surface

Bhattacharya et al. (2003) proposed a procedure for locating the surface of minimum reliability index, β_{min}, for earth slopes. The procedure is based on a formulation similar to that used to search for the surface of minimum factor of safety, $FS_{min,}$ in a conventional slope stability analysis. The advantage of such a formulation lies in enabling a direct search for the critical probabilistic surface by utilizing an existing deterministic slope stability algorithm or software with the addition of a simple module for the calculation of the reliability indexβ. This is definitely an improvement over the indirect search procedure proposed earlier by Hassan and Wolff (1999).

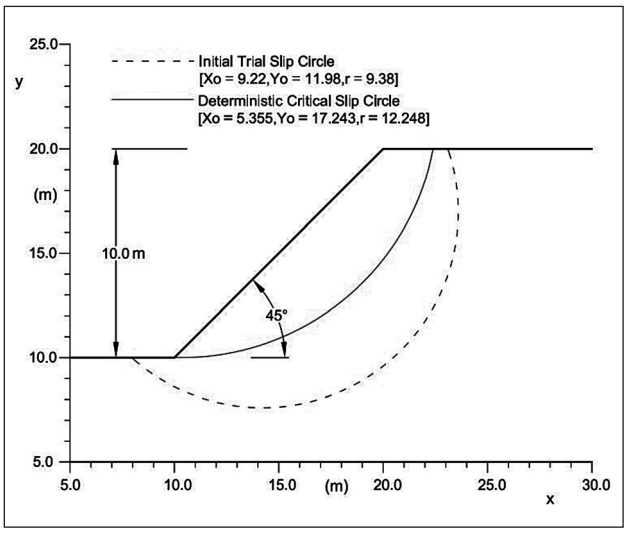

Figure 1: Slope Section and the deterministic critical slip circle in the illustrative example

3. Illustrative Example

Table 1: Statistical properties of soil parameters

Parameter (1)	Mean (2)	Standard deviation (3)	Coefficient of variation (4)
c′	18.0 kN/m²	3.6 kN/m²	0.20
tan φ′	tan 30°	0.0577	0.10
γ	18.0 kN/m³	0.9 kN/m³	0.05
r_u	0.2	0.02	0.10

Figure 1 shows a section of a simple slope of inclination 45° and height 10m in a homogeneous c- φ soil. Previous reliability analyses of this slope under a probabilistic framework include those reported by Li and Lumb (1987), Hassan and Wolff (1999), and

Bhattacharya et al. (2003) using different methods of analysis. Thus this example can well be regarded as a bench mark example problem. In all the previous investigations, all four geotechnical parameters namely, the effective cohesion c', the effective angle of shearing resistance φ', the pore pressure ratio r_u, and the unit weight γ were treated as random variables and their statistical properties (mean, standard deviation and co-efficient of variation) are as in Table 1.

4. Results and Discussion

4.1 Deterministic Analysis

For the purpose of determination of the critical slip circle, a trial slip circle (x_o=9.22m, y_o=11.98m, r =9.38m with reference to the axis system shown in Figure 1) has been arbitrarily selected. Using Eq. (1) or (2) for the Ordinary method of slices, its factor of safety (FS) is obtained as 1.70, when the parameters c′, tan φ′, γ, and r_u are assumed constant at their mean values (Table-1). With this slip circle as the initial slip surface, the developed computer program based on the Sequential Unconstrained Minimization Technique (SUMT) of nonlinear optimization coupled with the Ordinary Method of Slices (OMS) yields a critical slip circle (x_c=5.355m, y_c=17.243m, r_c =12.248m) which passes through the toe, as shown in Figure 2. The associated minimum factor of safety (F_{min}) is obtained as 1.26.

4.2 Reliability Analysis

Reliability analysis of this slope was attempted using two methods, namely, the Mean Value First Order Second Moment (MVFOSM) method and the First Order Reliability Method (FORM), with a view to comparing the two sets of results. All four parameters c′, tan φ′, γ, and r_u are assumed to be normally distributed and uncorrelated. However, reliability analyses were carried out in three phases: In Phase I only two parameters, namely, the cohesion c′ & the effective angle of shearing resistance in the form of tan φ′ were treated as random variables while the other two parameters, γ & r_u were assumed as constants at their mean values. In Phase II, three parameters, namely, the cohesion c′, the effective angle of shearing resistance tan φ′ and r_u were treated as random variables while the parameter γ was assumed as constant at its mean value, while in Phase III all four parameters were assumed as random variables.

4.3 Reliability Analysis for a Given Slip Surface Using MVFOSM

For the two slip surfaces shown in Figure 1, namely, (1) the initial slip circle (x_o=9.22, y_o=11.98, r =9.38) and (2) the deterministic critical slip circle (x_o=5.355, y_o=17.243, r =12.248), the reliability indices were determined by MVFOSM method by taking two mechanically equivalent limit states: FS-1 = 0 and ln(FS) = 0 using Eqs. (3) and (4) respectively, for Phase I, Phase II and Phase III described above. The reliability index values for the different cases are summarized in Table 2.

4.4 Reliability Analysis for a Given Slip Surface Using FORM

Reliability index values have also been determined for the above mentioned slip surfaces using FORM. In particular the algorithm for FORM Method-I (Haldar and Mahadevan, 2000) has been used in this case. All three phases mentioned above have been analyzed. For the sake of comparison as well as numerical demonstration, both the limit states considered in the analyses by MVFOSM have also been used here. The results are summarized in Table 2 again, alongside those obtained by using MVFOSM.

From Table 2, the following observations are made:

(i) For the same slip surface and the same set of random variables (in Phase I, II and III), values of reliability index obtained for different mechanically equivalent limit states are markedly different when MVFOSM is used as the method of reliability analysis, whereas these values are identical when analysed by the FORM method. This observation clearly demonstrates that unlike the FORM method, the MVFOSM method suffers from the 'problem of invariance', i.e., the result depends on how a given limit state event is defined. In this respect another observation from Table 2 is that when the limit state is taken as ln (FS) = 0, the reliability index values are higher in all three phases of analysis.

(ii) It may be noted from Eqs. (1) and (2) that the performance function FS is linear when only c′ and tan φ′ are treated as random variables as in Phase I of reliability analysis. However, when c′, tan φ′ and r_u are treated as random variables as in Phase II, or when c′, tan φ′, r_u and γ are treated as random variables as in Phase III, the performance function FS becomes nonlinear and the degree of nonlinearity increase from Phase II to Phase III. Now, from Table 2 it is seen that for Phase I, the values of reliability index yielded by MVFOSM and FORM are exactly the same, whereas, they are different for Phases II and

III. Further, this difference in case of Phase III is more than in case of Phase II. This observation clearly demonstrates that in those situations where the performance function is linear and all the variables are normally distributed and statistically independent, the values of reliability index by MVFOSM method agrees with those given by the FORM; and the error associated with MVFOSM method increases as the degree of nonlinearity of the performance function (or limit state equation) increases.

(iii) Another important observation from Table 2 is that when the number of random variables increases the value of reliability index (β) decreases and probability of failure increases.

Table-2: Summary of Results of Reliability Analyses for Given Slip Surfaces

Method of Reliability Analysis	Slip Surface	Values of Reliability Index					
		Limit State: FS – 1 = 0			Limit State: ln (FS) = 0		
		Phase I (c′, tan φ′)	Phase II (c′, tan φ′, r_u)	Phase III (c′, tan φ′, r_u,γ)	Phase I (c′, tan φ′)	Phase II (c′, tan φ′, r_u)	Phase III (c′, tan φ′, r_u,γ)
MVFOSM	Initial Slip Circle	3.955 ($3.83X10^{-5}$)	3.812 ($6.89X10^{-5}$)	3.736 ($9.35X10^{-5}$)	5.059 ($2.10X10^{-7}$)	4.874 ($5.46X10^{-7}$)	4.775 ($8.98X10^{-7}$)
	Deterministic Critical Slip Circle	1.671 ($4.73X10^{-2}$)	1.643 ($5.02X10^{-2}$)	1.601 ($5.47X10^{-2}$)	1.815 ($3.47X10^{-2}$)	1.783 ($3.73X10^{-2}$)	1.734 ($4.14X10^{-2}$)
FORM (All random variables are Normally distributed)	Initial Slip Circle	3.955 ($3.83X10^{-5}$)	3.862 ($5.63X10^{-5}$)	3.851 ($5.88X10^{-5}$)	3.955 ($3.83X10^{-5}$)	3.862 ($5.63X10^{-5}$)	3.851 ($5.88X10^{-5}$)
	Deterministic Critical Slip Circle	1.671 ($4.73X10^{-2}$)	1.646 ($4.99X10^{-2}$)	1.625 ($5.21X10^{-2}$)	1.671 ($4.73X10^{-2}$)	1.646 ($4.99X10^{-2}$)	1.625 ($5.21X10^{-2}$)

Note: Figures in the parentheses indicate the values of the Probability of failure for the respective slip surface.

Table-3: Variation of Reliability Index with different probability distributions for the basic variates

Limit State Surface	Probability Distribution		Values of Reliability Index for			
	c′.	tan φ′.	Initial Trial Slip Circle		Deterministic Critical Slip Circle	
			MVFOSM	FORM	MVFOSM	FORM
FS -1= 0	Lognormal	Normal	3.955	4.806	1.671	1.859
	Normal	Lognormal		4.038		1.661
	Lognormal	Lognormal		5.318		1.854
	Normal	Normal		3.955		1.671
ln FS = 0	Lognormal	Normal	5.059	4.806	1.815	1.859
	Normal	Lognormal		4.038		1.661
	Lognormal	Lognormal		5.318		1.854
	Normal	Normal		3.955		1.671

Note: These results correspond to the Phase I analysis, i.e, when only c'.and tanφ'are treated as random variables

4.5 Reliability Analysis for Given Slip Surfaces: Effect of Probability distributions of the basic variates

As already stated, the MVFOSM method does not use the information on probability distribution of the basic random variables. In the FORM method, on the other hand, this information can be incorporated in the analysis. In the present analysis, the effect of variation of probability distributions have been studied using FORM Method-I. Only two distributions have been considered, namely, the normal distribution and the lognormal distribution. Results have been obtained for the Phase I only, i.e., when only two parameters c'.and tanφ'are treated as random variables. Table 3 summarizes the results. It can be observed that there are substantial differences in the values of the reliability index obtained by using

FORM when different combinations of probability distributions for the random variates c'.and tanφ'are considered. It is further observed that the β values from MVFOSM agree with those from FORM only when both the random variables are assumed to be normally distributed. Thus it can be said that the MVFOSM method, though does not make use of any such knowledge regarding distribution of variates, implicitly assumes that all variables are normally distributed.

4.6 Probabilistic Critical Slip Surface and the associated β_{min}

The probabilistic critical slip surface (surface of minimum β) has been determined following the same computational procedure as used for the determination of the deterministic critical slip surface, simply by replacing the objective function FS with β (Bhattacharya et al. 2003). A computer program was developed based on the Sequential Unconstrained Minimization Technique (SUMT) of nonlinear optimization coupled with a method of reliability analysis, MVFOSM or FORM, as the case may be.

For this search, the deterministic critical slip surface shown in Figure 1 has been used as the initial slip surface. Several such probabilistic critical slip surfaces have been determined and the associated minimum reliability index ($\beta_{min)}$ values are summarized in Table 4. For the sake of clarity only two of these critical surfaces are plotted in Figure 2: the probabilistic critical slip surface for Phase III analysis using MVFOSM (x_c=4.907m, y_c=17.311m, r_c =12.311m), and the probabilistic critical slip surface for Phase III analysis using FORM with all four random variables normally distributed (x_c=4.920m, y_c=17.283m, r_c =12.284m). For the sake of comparison, the deterministic critical slip surface (x_c=5.355m, y_c=17.243m, r_c =12.248m) has also been plotted in Figure 2.

investigators. The detailed results presented in Table 4 generally corroborates the observations made earlier from Table 2 with reference to the reliability analyses of the given slip surfaces.

5. Summary and Conclusions

In view of the growing appreciation of the uncertainty associated with the geotechnical parameters, especially, the strength parameters including the pore water pressure, the conventional deterministic approach of analysis is increasingly being replaced by probabilistic approach of analysis or

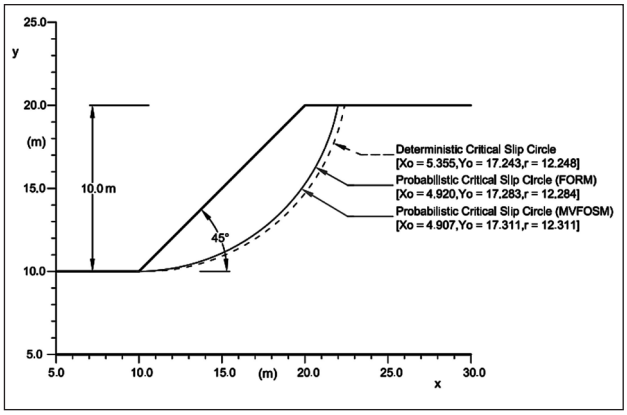

Figures 2: Probabilistic and Deterministic Critical Slip Surfaces

From Figure 2, as well as from the magnitudes of the coordinates of centers and radii, it is seen that the two probabilistic critical slip surfaces are located very close to each other while the deterministic critical slip circle is somewhat apart. The closeness of the deterministic and the probabilistic critical slip surfaces for the case of simple homogeneous slopes are in agreement with those reported by earlier

Table-4: Summary of Results of the Minimum Reliability Analyses Associated with the Probabilistic Critical Slip Surface

Method of Reliability Analysis	Values of Minimum Reliability Index					
	Limit State: FS – 1 = 0			Limit State: ln (FS) = 0		
	Phase I(c′, tan φ′)	Phase II (c′, tan φ′, r_u)	Phase III (c′, tan φ′, r_u,γ)	Phase I (c′, tan φ′)	Phase II (c′, tan φ′, r_u)	Phase III (c′, tan φ′, r_u,γ)
MVFOSM	1.643 (1.671)	1.618 (1.643)	1.576 (1.601)	1.785 (1.815)	1.756 (1.783)	1.707 (1.734)
FORM (All random variables are Normally distributed)	1.643 (1.671)	1.620 (1.646)	1.599 (1.625)	1.643 (1.671)	1.620 (1.646)	1.599 (1.625)

Note: Figures in the parentheses indicate the values of reliability index for the deterministic critical slip surface

reliability analysis under a probabilistic framework. The Mean Value-First Order-Second Moment (MVFOSM) method based on a Taylor series expansion is rather widely used by the practitioners in the geotechnical engineering field mainly due to the simplicity and early origin of the method. However, in other fields of engineering, e.g., in the structural engineering field, it is an established fact for quite some time that the MVFOSM method suffers from serious shortcomings such as the problem of invariance, as mentioned in an earlier section of this paper.

This paper concerns a study on the reliability analysis of earth slopes with uncertain soil strength parameters under a probabilistic framework. Reliability analyses have been carried out using a rigorous method, namely, the First Order Reliability Method (FORM) in conjunction with a simple slope stability model namely, the Ordinary Method of Slices (OMS). For the sake of comparison, results in the form of the reliability index and probability of failure have also been obtained using the MVFOSM method. Computer programs have been developed for the determination of reliability index based on both FORM and MVFOSM method for a given slip surface, and then for the optimization based determination of the probabilistic critical slip surface and the associated minimum reliability index. The developed programs have been applied to a bench mark example problem concerning a simple slope in homogeneous soil in which the geotechnical parameters are treated as random variables with given values of statistical moments. The differences between the two sets of results have been brought out for the cases of an arbitrarily selected given slip surface, the deterministic critical slip surface and, also the probabilistic critical slip surface. The study has been successfully used to demonstrate numerically all the major shortcomings of the approximate MVFOSM method and the error involved vis-à-vis the more accurate FORM method.

References

1. Bhattacharya, G., Jana, D., Ojha, S. and Chakraborty, S (2003) "Direct search for minimum reliability index of earth slopes" Computers and Geotechnics, Volume 30, Issue 6, September 2003, Pages 455-462.
2. Cho SE (2009) "Probabilistic stability analyses of slopes using the ANN-based response surface" Computers and Geotechnics; 36(5):787–97.
3. Chowdhury, Rajib and Rao, B.N (2010) "Probabilistic stability assessment of slopes using high dimensional model representation" , Computers and Geotechnics, Volume 37, Issues 7-8, November 2010,Pages 876-884.
4. Das, Sarat Kumar and Das, Manas Ranjan (2010), Discussion of "Reliability-Based Economic Design Optimization of Spread Foundations- by Y. Wang", J. Geotech. and Geoenvir. Engrg, Volume 136, Issue 11, pp. 1587-1588.
5. Fellenious, W. (1936) "Calculation of Stability of Earth Dams Transaction", Second Congress on Large Dams, Washington, 4; 445.
6. Haldar, A., and S. Mahadevan,(2000). "Probability, Reliability, and Statistical Methods in Engineering Design", John Wiley and Sons, 2000.
7. Hasofer, A. A. and Lind, A. M. (1974) "Exact and Invariant Second Moment Code Format", J. Geotech. Engg. Div., ASCE, 100(1) 111-121.
8. Hassan, A.M. and Wolff, T.F., 1999. Search Algorithm for Minimum Reliability Index of Earth Slopes, J. Geotechnical and Geoenviormental Engrg. 125(4), 301-308.
9. Li, K. S. and Lumb, P. (1987) "Probablistic Design of Slopes", Can. Geotech. J., 24(4), 520-535.
10. Metya, Subhadeep (2011) "First Order Reliability Method in Reliability Analysis of Earth Slopes", M.E. Thesis, Bengal Engineering and Science University, Shibpur, Howrah, India.
11. Rackwitz, R., and Fiessler, B. (1976). "Note on discrete safety checking when using non-normal stochastic models for basic variables." Load Project Working Session, MIT, Cambridge, MA.
12. Rackwitz, R., and Fiessler, B. (1978). "Structural Reliability Under Combined Random Load Sequences." Computers and Struc-tures, Vol. 9, No. 5, pp. 484-494.

Life Cycle Reliability and Safety Engineering
Vol.1 Issue 3 (2012) 08-15

Robust Optimum Design of Tuned Mass Damper in Seismic Vibration Control of Structures Under Uncertain Bounded System Parameters

Bijan Kumar Roy and Subrata Chakraborty
Department of Civil Engineering, Bengal Engineering and Science University, Shibpur
Howrah 711103 India e-mail: bijan.roy@rediffmail.com

Abstract

The optimum design of tuned mass damper (TMD) system considering model parameter uncertainty is usually performed by minimizing the performance measure obtained by the total probability theory concept without any consideration to the variation of the performance of TMD due to uncertainty. However, such a design method does not necessarily correspond to an optimum design in terms of maximum response reduction as well its minimum dispersion. The present study is focused on robust optimum design of TMD system of protection to mitigate the seismic vibration effect of structures considering uncertain but bounded (UBB) type system parameters. The root mean square displacement (rmsd) of the primary structures is considered as the performance index. The robust optimization is obtained by using a two-criterion equivalent deterministic optimization problem where the weighted sum of the nominal value of the performance function and its dispersion is minimized. The conventional interval analysis based bounded optimum solution is also obtained to demonstrate the effectiveness of the robust optimum solution. A numerical study is performed to elucidate the effect of parameter uncertainty on the robust optimum design of TMD parameters by comparing the robust optimization results with the optimization results obtained by solving usually adopted interval optimization procedure.

Keywords: Seismic vibration control, tuned mass damper, uncertain bounded parameters, bounded optimization, robust optimization.

1. Introduction

In the field of passive vibration control, the TMDs are amongst the oldest control devices effectively use to suppress undesirable vibration induced due to wind and earthquake. One of the most important design issues is the parameter optimization. The optimal design of TMD assuming deterministic system parameters are well developed (Warburton and Ayorinde, 1980, Thomson 1980, Rana and Soong 1998). A major limitation of the deterministic approach is that the uncertainties in the performance-related decision variables cannot be included in the optimization process. But, the efficiency of dampers may be drastically reduced if the parameters are off tuned to the vibrating mode it is designed to suppress due to unavoidable presence of uncertainty in the system parameters. Thus, the probabilistic vibration control considering uncertain parameters is gaining more importance in recent past. The reliability based design optimization (RBDO) in passive vibration control applications was originally proposed by Papadimitriou et al. (1997). The control problems for a wide class of mechanical systems with uncertainty were presented in Ferrara and Giacomini (2000). The concept of robust reliability against failure has been introduced by Papadimitriou and Katafygiotis(2001) and it serves as an important metric by which the quality of controlled systems may be judged. Taflanidis et al. (2008) presented theoretical analysis of RBDO for passive or active structural control applications that optimizes a control system explicitly to minimize an upper bound first-passage failure probability.

The studies on optimization of damper parameters allowing model parameter uncertainty as discussed above primarily use the total probability theory concept to obtain the unconditional response or the failure probability of a system which is subsequently used as the performance measure. Such design

approach does not consider the possible dispersion of the performance and the damper parameters so designed may be sensitive to the variations of the input parameter due to uncertainty. However, it is desirable to achieve a balance where an optimum design will also assure less sensitivity with respect to the variations of the parameters due to uncertainty. For this, an additional 'dimension' is required to be introduced in the analysis by using information about the uncertain system parameters. The robustness is generally measured in terms of the dispersion of a performance function from its nominal value which is usually expressed in terms of the variance and percentile difference. In this regard, it is of worth mentioning here that in many real situations, the maximum possible ranges of variations expressed in terms of percentage of the corresponding nominal values of the parameters are only known and can be modelled as UBB type parameters. In such cases, the interval analysis method in the framework of set theoretical description is usually employed (Chen and Zhang 2006, Chen et al. 2007, Chakraborty and Roy 2011). However, the bounded solutions thus obtained are the worst case measures and has little importance for practical design. The robust design optimization (RDO) in which the bounds on the magnitude of uncertain parameters are only required will be a viable alternative in such cases. The concepts of RDO have been developed independently in different scientific disciplines and the developments in the recent past are noteworthy (Zang et al. 2005**,** Park et al. 2006, Beyer and Sendhoff 2007). However, there have been a few applications of RDO with respect to the reduction of vibration levels of structures. Hwang et al. (2001) have minimized the mean and variance of displacement at the first resonance frequency of an automobile mirror system with both stiffness and mass variation. Son and Savage (2007) proposed a probabilistic approach of designing vibration absorber parameters to reduce both the mean and variance of the dynamic performance measure over the excitation frequency range. Marano et al. (2008, 2010) studied the RDO criterion in seismic vibration control of structure considering random system parameters.

The primary objective of the present study is to propose an RDO procedure to obtain the optimum TMD parameters to mitigateseismic vibration effect of structures characterized by *UBB* type uncertain parameters. This involves optimization of TMD parameters that include the frequency and damping properties of TMD considering uncertainty in the properties of the primary structure and ground motion parameters as well. The RDO is obtained by using a two-criterion equivalent deterministic optimization problem, where the weighted sum of the nominal value of the performance function and its dispersion, is optimized. The maximum root mean square displacement (rmsd) of the primary structures is considered as the performance index. The conventional interval analysis based bounded design optimization (BDO) is also performed to demonstrate the effectiveness of the proposed RDO approach. A numerical study elucidates the effect of parameter uncertainty on RDO of TMD system of protection by comparing the present RDO results with those obtained by the usually adopted interval optimization procedure.

2. Stochastic Dynamic Response of TMD - Structure System

The TMD in its' simplest form consists of an additional mass connected to a main system by a spring and a damper.The mechanical model of a TMD structure system is represented in Figure-1which is described by a single mass m_s, linked with the base by a linear spring k_s and a dash pot c_s. It is excited by a base acceleration $\ddot{y}_b(t)$, and it is connected with a secondary mass m_T by a spring k_T and a dash pot c_T. The dynamic equilibrium of the equation of the system can be expressed as:

$$\mathbf{M\ddot{Y}(t) + C\dot{Y}(t) + KY(t) = r}\ddot{y}_b(t) \tag{1}$$

where $\mathbf{Y(t)}$, $\mathbf{\dot{Y}(t)}$and $\mathbf{\ddot{Y}(t)}$, denote the relative displacement, velocity and acceleration vectors, ***r***is the influence coefficient vector; **M C** and **K** are respectively the mass, damping and stiffness matrices of the combined system. The well-known Kanai-Tajimi stochastic process (1960) which is able to characterise input frequency content for a wide range of practical situations is used in the present study and $\ddot{y}_b(t)$ is represented as:

$$\ddot{y}_b(t) = \ddot{x}_f(t) + w(t) = -(2\xi_g\omega_g\dot{x}_f(t) + \omega_g{}^2 x_f(t)) \text{ and}$$
$$\ddot{x}_f(t) + 2\xi_g\omega_g\dot{x}_f(t) + \omega_g{}^2 x_f(t) = -w(t) \tag{2}$$

In the above $x_f(t)$ is the response of the filter representing the ground, ξ_g and ω_g are, respectively, the damping ratio and the frequency of this filter, $w(t)$ being the white noise process, representing the excitation at the bed rock.

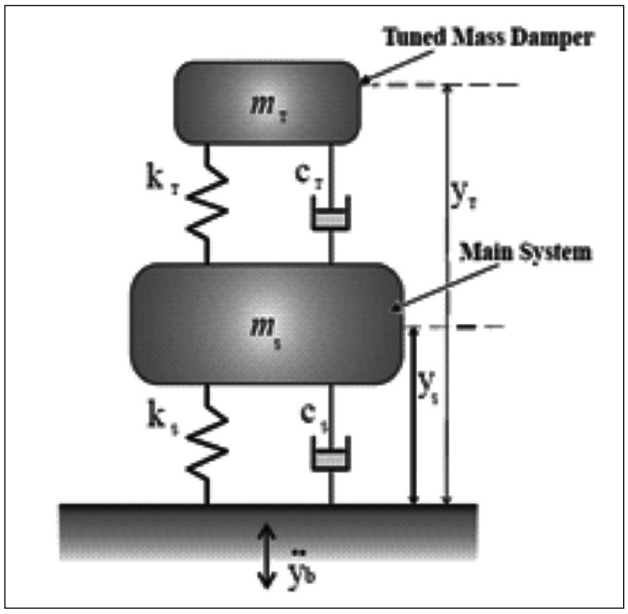

Figure 1. Linear model of TMD system

Introducing the space state vector: $Z = (y_T, y_S, x_f, \dot{y}_T, \dot{y}_S, \dot{x}_f)^T$, the stochastic response of the system can be obtained by using the covariance matrix $\mathbf{R}_{ZZ}$ obtained by solving the following Lyapunov equation:

$$AR_{ZZ} + R_{ZZ}A^T + B = 0 \tag{3}$$

Where the state matrix **A** is:

$$A = \begin{bmatrix} 0 & 0 & 0 & 1 & 0 & 0 \\ 0 & 0 & 0 & 0 & 1 & 0 \\ 0 & 0 & 0 & 0 & 0 & 1 \\ -\omega^2_T & \omega^2_T & \omega^2_f & -2\xi_T\omega_T & 2\xi_T\omega_T & 2\xi_f\omega_f \\ \omega^2_T & -(\mu\omega^2_T + \omega^2_T) & \omega^2_f & \mu 2\xi_T\omega_T & -(\mu 2\xi_T\omega_T + 2\xi_S\omega_S) & 2\xi_f\omega_f \\ 0 & 0 & -\omega^2_f & 0 & 0 & -2\xi_f\omega_f \end{bmatrix} \tag{4}$$

And the matrix **B** has all null elements, except the last on the main diagonal: $[B]_{6,6} = 2\pi S_0$, where S_0 is the intensity of the white noise. System mechanical parameters in matrix are as follows, $\omega_T = \sqrt{k_T / m_T}$, $\omega_S = \sqrt{k_S / m_S}$ $\xi_T = c_T / 2\sqrt{m_T k_T}$, $\xi_S = c_S / 2\sqrt{m_S k_S}$ and, $\mu = m_T / m_S$

where ω is natural frequency and ξ is damping ratio of concerned system.

The space state covariance matrix **R** (of size 6x6) is obtained by solution equation (3). The rmsd of TMD and the primary system can be then obtained as:

$$\sigma_{y_T} = \sqrt{R_{zz}(1,1)}, \sigma_{y_S} = \sqrt{R_{zz}(2,2)} \tag{5}$$

3. Optimization of TMD Parameters

The optimum TMD parameters are generally obtained by minimizing the vibration effect of a structure under dynamic load. The problem of optimization of the TMD system of protection consists of determining optimum frequency (ω_T) and damping ratio (ξ_T) of the damper system. The design vector (DV) can be thus defined as: $\bar{b} = (\omega_T, \xi_T)$. The stochastic structural optimization (SSO) problem under random earthquake load can be formulated as the search of a suitable set of DVs, over a possible admissible domain Ω to minimize a desired objective. For stochastically excited structures, a tractable measure of performance can be given in terms of mean square responses (displacement, acceleration, stress etc.). The failure probability of the structure or the total life-cycle cost of the structure can be also used as the performance index. In the present study, the rmsd of the primary structure is considered as the objective function. The SSO problem so defined leads to a standard nonlinear programming problem (Nigam NC 1972) as following:

$$\text{Find } \bar{b} \in \mathbf{\Omega} \text{ to minimze, } f = \sigma_{y_s} \tag{6}$$

3.1 The Parameter Uncertainty and Optimization of TMD system

The response statistic evaluated under stochastic earthquake load to solve the SSO problem as described by Eqn. (6) intuitively assumes that these parameters characterizing the structure and stochastic earthquake load model are completely known. But, the uncertainty in these parameters may lead to an unexpected excursion of responses affecting the desired safety of the structure. Thus, in the design of optimum TMD system of protection, apart from the stochastic nature of the earthquake load, the uncertainty with regard to these parameters should be taken into account. This will involve sensitivity analysis of stochastic dynamic system. In the present section, the related formulations are briefly discussed for UBB type system parameter. If $\bar{x}_i$ is the nominal value of the i[th] UBB parameter

viewed as the mean value and $\pm \Delta x_i$ represents the maximum deviation from the nominal value, then the UBB parameter value deviates from the nominal value can be expressed as,.

$$x_i^I = [x_i^l, x_i^u] = \bar{x}_i + \Delta x_i[-1,1] = \bar{x}_i + \Delta x_i e_\Delta, \bar{x}_i = \frac{x_i^l + x_i^u}{2},\ e_\Delta = [-1,\ 1]$$

Thus, the i[th] interval variable can be written as:

$$x_i = \bar{x}_i + \delta x_i, \text{ where, } |\delta x_i| \le \Delta x_i, i = 1, 2, .., m.$$

The system matrix **A** , **B** and response covariance matrix **R** can be expanded with respect to 'm' numbers of such UBB parameters in Taylor series about the nominal values in first order terms of δx_i as,

$$\mathbf{A} = \bar{\mathbf{A}} + \sum_{i=1}^{m} \frac{\partial \mathbf{A}}{\partial x_i} \delta x_i + \ldots,\ \mathbf{B} = \bar{\mathbf{B}} + \sum_{i=1}^{m} \frac{\partial \mathbf{B}}{\partial x_i} \delta x_i + \ldots$$
$$\text{and } \mathbf{R} = \bar{\mathbf{R}} + \sum_{i=1}^{m} \frac{\partial \mathbf{R}}{\partial x_i} \delta x_i + \ldots \quad (7)$$

In the above, the over bar represents the matrices correspond to the nominal values of the UBB parameters. The derivatives are evaluated at $x_i = \bar{x}_i$ .Substituting Eqn (7) in Eqn. (3) for i[th] UBB parameters and equating the equal order term after neglecting the higher order term the following equation can be readily obtained:

$$\bar{\mathbf{A}}\bar{\mathbf{R}} + \bar{\mathbf{R}}\bar{\mathbf{A}}^T + \bar{\mathbf{B}} = \mathbf{0} \quad (8)$$

$$\bar{\mathbf{A}} \frac{\partial \mathbf{R}}{\partial x_i} + \frac{\partial \mathbf{R}}{\partial x_i} \bar{\mathbf{A}}^T + \mathbf{B}^I = \mathbf{0} \text{ where, } \mathbf{B}^I = \frac{\partial \mathbf{A}}{\partial x} \bar{\mathbf{R}} + \bar{\mathbf{R}} \frac{\partial \mathbf{A}^T}{\partial x} \quad (9)$$

The mean covariance matrix $\bar{\mathbf{R}}$ is obtained by solving Eqn. (8) considering the mean values of system parameter matrices A i.e. the system matrices correspond to the mean value of the system parameters. The first order sensitivity of the covariance matrix $\partial \mathbf{R} / \partial x_i$ can be obtained by solving Eqn. (8). It may be noted that the equation needs to be solved for each uncertain parameter involved in the problem.

The performance function i.e. the rmsd as defined by Eqn. (5) is also a function of the uncertain parameters and can be expanded in first order Taylor series as the mean and fluctuating part as following:

$$\sigma_x = \bar{\sigma}_x + \sum_{i=1}^{m} \frac{\partial \sigma}{\partial x_i} \delta x_i + \ldots \quad (10)$$

In the above, $\bar{\sigma}_x$ is obtained by using the solution of Eqn. (8) in Eqn. (5). The sensitivity of the rmsd can be obtained by differentiating the appropriate expression of Eqn. (5) with respect to the i[th]UBB parameters as following:

$$\frac{\partial \sigma_x}{\partial x_i} = \frac{1}{2}\left[\frac{\partial \mathbf{R}(2,2)}{\partial x} / \sqrt{\mathbf{R}(2,2)} \right] \quad (11)$$

In which, $\partial \mathbf{R} / \partial x_i$ is obtained by solving Eqn. (9). Now, by making use of interval extension in interval mathematics assuming monotonic responses, the interval extension of the above expression can be obtained. The interval region of the function involving the UBB variables can be then separated out to the upper and lower bound as below:

$$\sigma_x^u = \bar{\sigma}_x + \sum_{i=1}^{m} \frac{\partial \sigma_x}{\partial x_i} \Delta x_i + \ldots \text{ and}$$
$$\sigma_{xl} = \bar{\sigma}_x - \sum_{i=1}^{m} \frac{\partial \sigma_x}{\partial x_i} \Delta x_i + \ldots \quad (12)$$

The optimization now involves two objective function yielding the upper and lower bound solutions.

3.2 Robust Optimization of TMD Parameters

The BDO procedure as presented above does not consider the possible dispersion of the design performance with respect to variation of parameters due to uncertainty. Thus, it may be sensitive due to the variations of the input system parameters. As already mentioned, the RDO solution aims to improve the design by minimizing the variability of the structural response, meeting the requirements of the performance. The robustness of performance function (σ_x) is generally expressed in terms of its dispersion, $\Delta\sigma$ from the nominal value, $\bar{\sigma}_x$ defined as following:

$$\Delta\sigma = \sum_{i=1}^{m} \left| \frac{\partial \sigma}{\partial x_i} \right| \Delta x_i \quad (13)$$

The objective of an ideal design is to achieve the optimal performance as well as less sensitivity of the performance with respect to the variation of system parameters. The two criteria often conflict with each other. The problem is dealt as a multi-objective optimization, where the conventional objective function and its dispersion are two objectives that need to be optimized i.e. find **x**, to minimize $\{\bar{\sigma}_x, \Delta\sigma\}$. The two-criterion optimization problem is transformedto minimization of an equivalent single objective as:

$$\phi = \alpha * \bar{\sigma}_x + (1-\alpha) * \Delta\sigma \quad (14)$$

Where, α is a weighting factor in the bi-objective optimization problem. The maximum robustness will be achieved for α =0.0, and α = 1.0 indicates optimization without any robustness. The optimization can be performed based on the standard unconstrained non-linear optimization routine available with MatLab Optimization Toolbox. Once the optimal design point is obtained by solving Eqn. (14), the dispersion of performance can be estimated at the optimal point using Eqn. (13).

4. Numerical Study

The primary system with an attached TMD as shown in Fig.1 is undertaken to elucidate the proposed RDO of TMD system in seismic vibration control of structure characterized by UBB type system parameters. The uncertainties are considered in $m_S, k_S, m_T, k_T, \xi_g, \omega_g$, S_0 and is represented by the maximum possible dispersion (Δx_i) expressed in terms of the percentage of corresponding nominal value ($\bar{x}_i$). Unless mentioned otherwise, the following nominal values are assumed in the present numerical study: $\xi s = 3\%$, $\mu = 4\%$, $\omega_s = 4.5\pi$, $\omega_f = 7\pi$ rad/sec, $\xi_f = 0.4$, S_{0i}=300 cm^2/sec^3, Δx_i =10%.Based on this, the rmsd of the unprotected system i.e. without TMD is computed to be 3.36 cm. The rmsd of the primary structure is optimized by the proposed RDO procedure. The optimum mean value of the rmsd of the structure versus the mass ratio is plotted in Fig. 2 for different settings of weight factor α .The associated dispersion of the rmsd of the primary structure is shown inFig. 3.The corresponding optimum tuning ratio and damping ratio of the TMD are shown in Figs. 4 and 5, respectively.

The BDO procedure considering the upper and lower bound performance functions as described by Eqn. (12) are also performed.The results are shown in the same plot for ease in comparison with the RDO results. The uncertainty level of 15% and 3% damping ratio is considered to develop these plots. It can be readily observed from the plots that the bounded solutions are too far apart which is obvious as interval method gives a conservative estimate of the upper and lower bound solutions. In such situation, an upper bound solution is usually suggested to be used as the performance function for optimum design is merely a conservative deterministic solution of the problem without any consideration on the possible dispersion of the suggested design. The lower

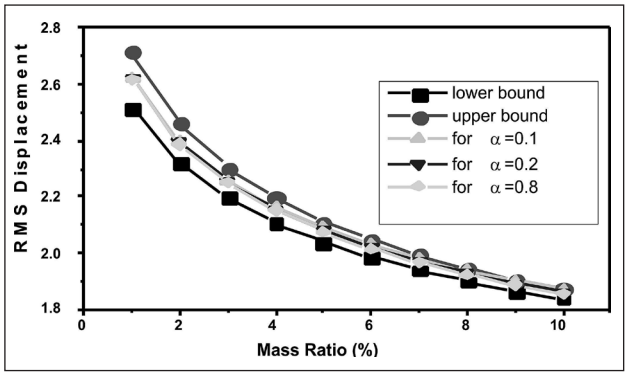

Figures 2: The variation of rmsd of the TMD with varying mass ratio

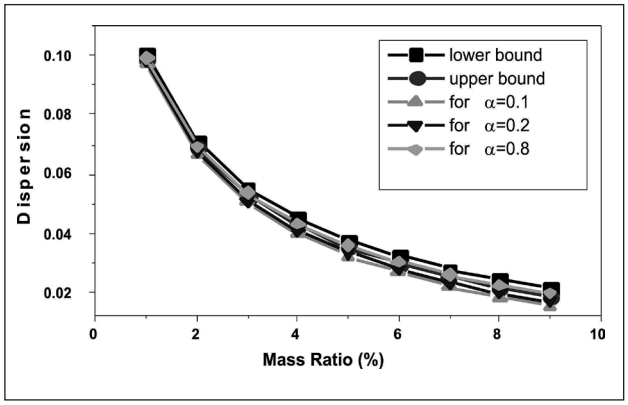

Figures 3:The variation of dispersion of rmsd with varying mass ratio

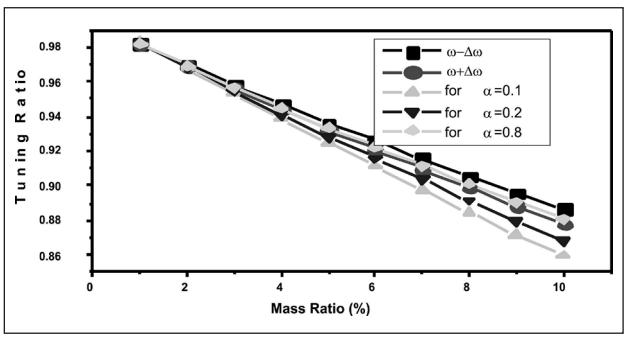

Figures 4: The variation of tuning ratio of the TMD with varying mass ratio

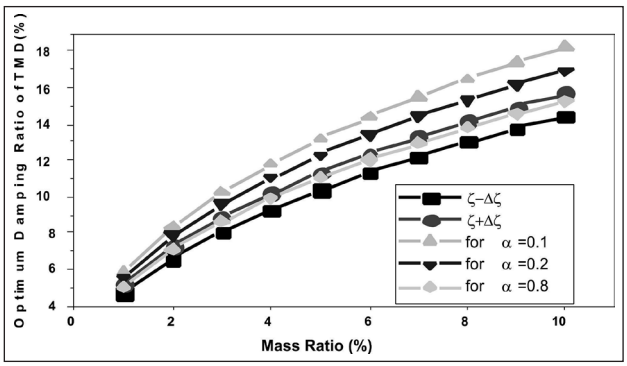

Figures 5: The variation of damping of the TMD with varying mass ratio

bound solution though efficient in terms of response reduction; the associated dispersion of the design is more. The efficiency of the RDO solution is marginally less compare to that of the lower bound solution and lies in between the bounded solutions. However, the dispersion of the design is much lower than the dispersion of the lower bound case solution and the designer has the necessary flexibility to control the design through suitable choice of the weight factor α to achieve the desired level of performance efficiency (i.e. the reduction of vibration level) and its dispersion under parameter uncertainty.

The mean value of the rmsd of the primary structure versus uncertainty range is plotted in

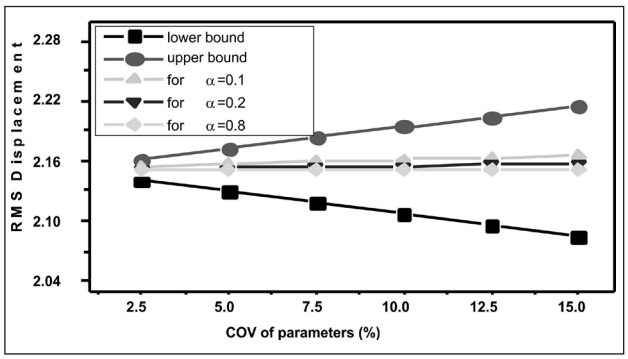

Figure 6:The variation of rmsd with varying level of uncertainty

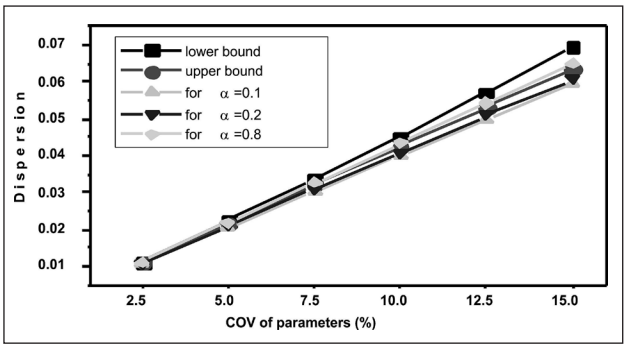

Figure 7: The variation of dispersion of rmsd with varying level uncertainty

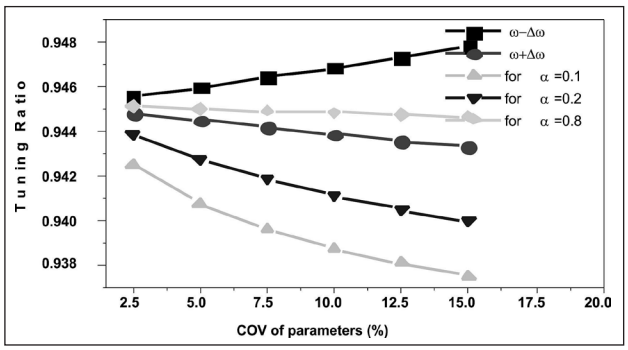

Figure 8:The variation of tuning ration of the TMD with varying uncertainty level

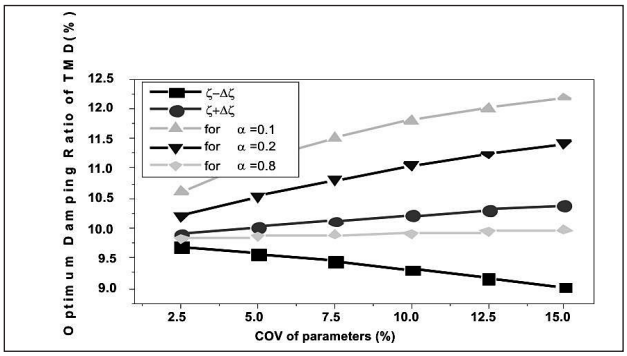

Figure 9: The variation of damping of the TMD with varying uncertainty level.

Fig. 6 for different values of weight factor α . The associated dispersion of the rmsd is shown in Fig. 7. The corresponding optimum tuning ratio and damping ratio are shown in Figs. 8 and 9, respectively. The results of the BDO procedure are also shown in the same plot. The width of the bounded solution increases sharply with increasing level of uncertainty. However the change in the optimum rmsd is nominal by the proposed RDO case. As expected, the dispersion of the rmsd value increases with increasing level of uncertainty for all RDO cases i.e. for all settings of α. However, the dispersion of the design is much smaller than the dispersion of the lower bound case irrespective of uncertainty level. The change in tuning ratio and damping ratio as shown in Fig. 8 and Fig 9 with increasing level of uncertainty is notable. The mass ratio and damping ratio of the primary structure are considered as 4% and 3%, respectively.

It is generally observed that there is a trade-off between the objective values of a design and its robustness. The situation can be studied further in term of Pareto front. The Pareto front is generated by solving the RDO by varying the weight factor α and the results are plotted in Fig. 10 for different mass ratio. The uncertainty ranges for all parameters are taken as 10% and damping is considered to be 3%. It can be observed from the plot that the dispersion of the optimum weight decreases and the rmsd increases as α value decreases. Thus, more robustness is achieved at the cost of sacrificing the performance of TMD. This is one of the important characteristics obtained from multi-objective optimization procedure.

5. Conclusions

The RDO of TMD system of protection in mitigating seismic vibration effect of structures characterized by UBB type system parameters is studied in the present work. The advantage of RDO approach

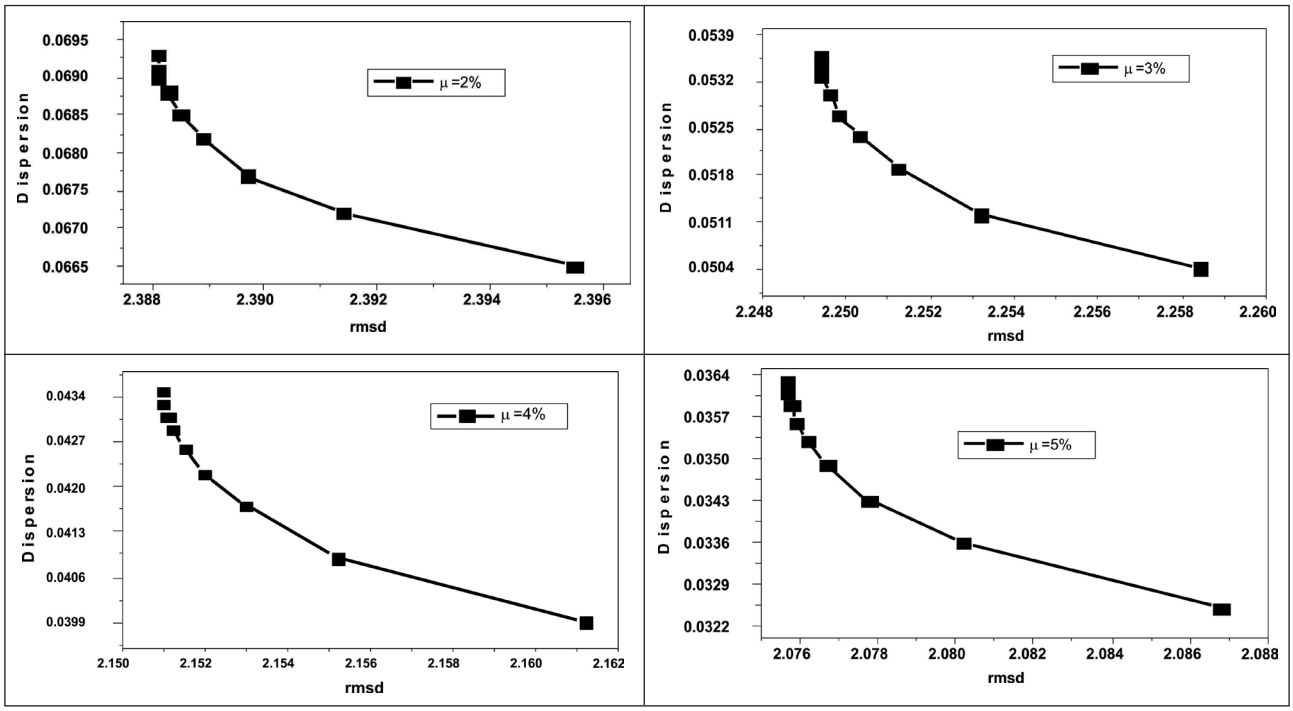

Figure 10: The variation of dispersion with varying rmsd for different mass ratio

in absence of complete probabilistic information to describe the system parameters is demonstrated. The BDO solutions conventionally obtained in such situation are too far apart. The conservative upper bound solution usually suggested in such cases is of little use for practical design application. Moreover, such approach fails to provide information about the possible dispersion of the design performance. But, the RDO approach provides the necessary flexibility to the designer to achieve the desired level of performance efficiency (i.e. the reduction of vibration level) and its dispersion under uncertain environment through suitable choice of parameter α . Thus, one can make more effective use of the resources available in a given structural control situation and provide for more realistic and cost-effective trade-offs between the control performance and its robustness with due importance to the unavoidable presence of system parameter uncertainty. It is generally observed that more robustness is achieved at the cost of sacrificing the optimum weight, an obvious characteristic of results obtained from any multi-objective optimization problem. Though, the efficiency of RDO solution is comparatively less compare to that of the lower bound solution, the dispersion of the design is much lower than the dispersion of the lower bound case solution. The formulation presented here involves linear perturbation based approximation of the responses around the mean values of the UBB parameters. For larger level of uncertainty, alternative approach to linear perturbation analysis is needed which required further study. It may be noted that the approach being generic in nature, can be applied for RDO of TMD for vibration control of MDOF system.

References

1. Beyer H, Sendhoff B. Robust optimization - a comprehensive survey. Computer Methods in Applied Mechanics and Engineering 2007; 196: 3190-3218.
2. Chakraborty S, Roy BK. Reliability based optimum design of tuned mass damper in seismic vibration control of structures with bounded uncertain parameters. Probabilistic Engineering Mechanics 2011; 26(2): 215-221.
3. Chen SH, Zhang XM. Dynamic response of closed-loop system with uncertain parameters using interval finite-element method. ASCE Journal of Engineering Mechanics2006;132(8): 830-840.
4. Chen SH, Song M, Chen YD. Robustness analysis of vibration control structures with uncertain parameters using interval algorithm. Structural Safety 2007; 29: 94-111.
5. Ferrara A., Giacomini L. Control of a Class of Mechanical Systems with Uncertainties via a Constructive adaptive/ second order VSC Approach, J. DynSystMeasContr, Vol. 122, No.1, 2000, p.p. 33-39.
6. Hwang KH, Lee KW, Park GJ. Robust optimization of an automobile rear view mirror for vibration reduction. Structural and Multidisciplinary Optimization2001; 21:300-308.

7. Marano GC, Greco R, Sgobba S. A comparison between different robust optimum design approaches: application to tuned mass dampers. Probabilistic Engineering Mechanics 2010; 25: 108-118.
8. Marano GC, Sgobba S, Greco R, Mezzina M. Robust optimum design of tuned mass dampers devices in random vibrations mitigation. Journal of Sound and Vibration 2008; 313: 472–492.
9. Nigam NC. Structural optimization in random vibration environment. AIAA J 1972;10(4):551_3.
10. Papadimitriou C., Katafygiotis L.S., Updating Robust Reliability using Structural Test Data, Probabilistic Engineering Mechanics, Vol.16, 2001, p.p.103-113
11. Papadimitriou C., Katafygiotis LS., AU SK. Effects of Structural Uncertainties on TMD Design: A Reliability-Based Approach, J. of Structural Control, Vol.4, No.1, 1997, p.p. 65–88
12. Park GJ, Lee TH, Lee K, Hwang KH. Robust design: an overview. AIAA Journal 2006; 44(1): 181-191.
13. Rana R. and Soong TT. Parametric Study and Simplified Design of Tuned Mass Dampers, Engineering Structures, Vol. 20, 1998, p.p. 193-204
14. Son YK, Savage GJ. Optimal probabilistic design of the dynamic performance of a vibration absorber. Journal of Sound and Vibration 2007; 307: 20–37.
15. Taflanidis. A.A., Scruggs J.T., Beck J. L. Reliability-Based Performance Objectives and Probabilistic Robustness in Structural Control Applications, ASCE J. of EngngMech Vol. 134, No. 4, 2008, p.p.291-301.
16. Tajimi H. A statistical method of determining the maximum response of a building during earthquake. In: Proc. of 2nd World Conf. on Earthq. Engng.; 1960.
17. Thomson AG. Optimizing the Tuned Viscous Dynamic Vibration Absorber with Primary System Damping; a Frequency Locus Method, J. of Sound and Vibration, Vol. 73, 1980, p.p. 469-472
18. Warburton GB. andAyorinde EO. Optimum Absorber Parameters for Simple system, Earth Engng and StructDyn, No. 8, 1980, p.p. 197–217
19. Zang C, Friswell MI, Mottershead JE. A review of robust optimal design and its application in dynamics. Computer and Structures 2005; 83: 315–326.

Life Cycle Reliability and Safety Engineering
Vol.1 Issue 3 (2012) 16-22

Geotechnical Uncertainty and Its Influence on Ground Water Level and Sea Water Interface in a Land Reclamation Project

Amit Srivastava
Dept of Civil Engineering, JUET, Guna,
Email: 2002.lala@gmail.com

Abstract

Land reclamation in coastal areas has significant influence on local ground water systems. Steady-state analytical solutions based on Dupuit and Ghyben-Herzberg assumptions are available (Guo and Jiao, 2007) to evaluate the rise in GWT (Ground Water Table) and salt water-fresh water interface. It is established that amount of these changes depends on the extent of reclamation (geometric extent) and the hydraulic conductivity of the fill material. The closed form analytical solutions provide a single value of parameters such as rise in GWT and distance of salt water – fresh water interface. Considering the fact the soil is a natural material which is used as fill material for reclamation purpose, it is difficult to assure a unique value of hydraulic conductivity of the fill material. Uncertainties in the estimation of hydraulic conductivity of the fill material will always lead to the uncertainty in the estimation of output parameters. Conventional approach defines factor of safety to handle uncertainty in geotechnical design and applications which is solely based on past experiences, good engineering judgment and confidence level of the designer. Alternatively, probabilistic approach, which is gaining importance in recent years, can handle uncertainty in a mathematical framework. In the present study, the role of uncertain parameter, i.e., "hydraulic conductivity of the fill material" and its influence on probabilistic assessment of Ground water level and sea water interface in a coastal land reclamation projects is highlighted. Two situations are considered, both with ground water flow resulting from precipitation recharge: (i) the coastal aquifer of an extensive landmass and (ii) an island.

Keywords: coastal land reclamation, probabilistic, hydraulic conductivity, ground water, uncertainty

1. Introduction

Most large urban centers lie in coastal regions, which are home to about 25% of the world's population. Rapid industrial and commercial expansion in recent years has created the need for more land. It is estimated that the current coastal urban population of 200 million is projected to almost double in the next 20 to 30 years. To meet the growing demand for more housing and other land uses, land has been reclaimed from the sea in coastal areas in many countries, including China, Britain, Korea, Japan, Malaysia, Saudi Arabia, Italy, the Netherlands, and the United States. As well known to everyone, one of the most famous case histories is Palm Jumeirah (Nakheel 2007) in Dubai, which is artificial archipelago created using coastal land reclamation.

The direct impact of land reclamation on coastal engineering, environment and marine ecology is well recognized and widely studied (Seasholes, 2003; Lumb, 1976; Suzuki, 2003; Stuyfzand, 1995). It is also recognized that reclamation change the regional groundwater regime, including groundwater table (GWT) as well as interface between seawater and fresh groundwater. Extensive studies on impact of coastal land reclamation on ground water level and the sea water interface have been carried out in the recent past (Bear and Dagan, 1964; Strack 1976; Jiao, 2000; Jiao et al., 2001). Guo and Jiao (2007) provided analytical solutions for the alternation of the salt water interface in response to land reclamation with the assumption that flow satisfies the Ghyben-Herzberg relationship and the Dupuit assumption. The study is useful in assessing long term impact of the land reclamation on both the GWT and the salt water interface in a coastal landmass and an island with unconfined ground water condition. The following section provides a brief review of work carried out by Guo and Jiao (2007).

1.1 Impact of Reclamation in an Extensive Landmass

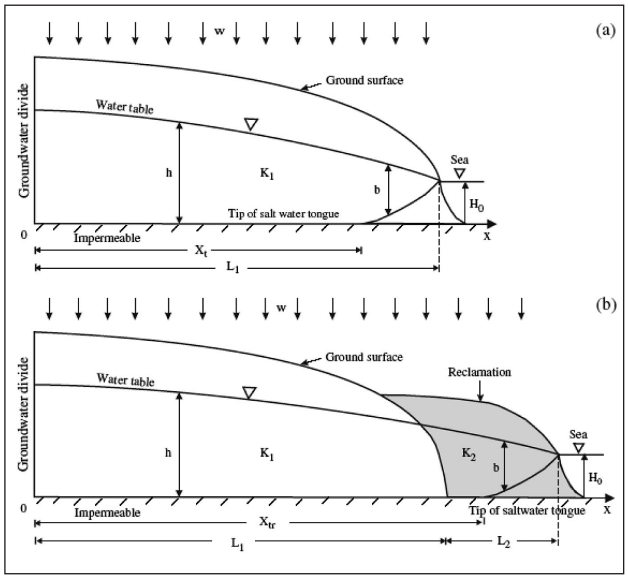

Figure 1: Sketch of an unconfined aquifer system and the salt water interface in a coastal extensive landmass (a) before reclamation and (b) after reclamation (Guo and Jiao, 2007)

Figure 1(a) shows a coastal unconfined ground water system receiving uniform vertical recharge *w*. The hydraulic conductivity of the aquifer is K_1. The distances from the water divide to the coastline and the tip of the salt water tongue are denoted as L_1 and X_t, respectively. The head in the fresh water, h, is measured in relation to the horizontal impermeable bottom of the aquifer, which is H_o below sea level. Figure 1(b) shows the influence of reclamation when steady state condition is reached. It is indicated that coastline moves seaward by a distance L_2 and the hydraulic conductivity of the fill material is K_2 (the boundary between K_1 and K_2 is approximated as vertical). The distance of tip of saltwater water tongue from the water divide after reclamation is assumed to be X_{tr}. The following closed form analytical solutions were derived to obtain the depth of GWT (h) and distance X_{tr} for the reclaimed land.

$$h = \sqrt{w\left[\frac{1}{K_1}\left(L_1^2 - X^2\right) + \frac{1}{K_2}(2L_1 + L_2)L_2\right] + \frac{\rho_s}{\rho_f}H_o^2}, \quad 0 \le X \le L_1 \qquad (1)$$

$$h = \sqrt{\frac{w}{K_2}\left[(L_1 + L_2)^2 - X^2\right] + \frac{\rho_s}{\rho_f}H_o^2}, \quad L_1 \le X \le X_{tr} \qquad (2)$$

$$h = \sqrt{\frac{w(\rho_s - \rho_f)}{K_2\rho_s}\left[(L_1 + L_2)^2 - X^2\right]} + H_o, \quad X_{tr} \le X \le L_1 + L_2 \qquad (3)$$

The location of the tip of the salt water tongue (X_{tr}) can be obtained from the following expression:

$$X_{tr} = \sqrt{(L_1 + L_2)^2 - \frac{K_2\left(\rho_s^2 - \rho_s\rho_f\right)}{w\rho_f^2}H_o^2} \qquad (4)$$

For more detailed study on the topic, it is suggested that this paper should be read in the light of Guo and Jiao (2007). The proposed analytical solutions can be used in estimating the increase in GWT (Δh) as well as location of the tip of the salt water tongue (X_{tr}) for the reclaimed land.

1.2 Impact of Reclamation in an Island

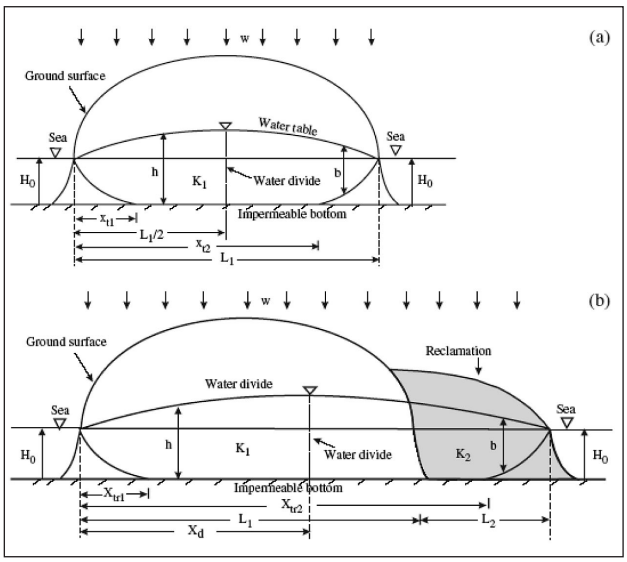

Figure 2: A schematic sketch of the ground water flow system in an oceanic island receiving uniform vertical recharge (a) before reclamation (b) after reclamation (Guo and Jiao, 2007)

Jiao (2000) indicated that in an island, the water divide will be moved when reclamation is significant compared to the size of the original ground water catchments. The reclamation on one side changes the ground water flow in the whole island, including the water level and position of the salt water interface on the other side. The analytical solutions derived for h (with reference to Figure 2) is as follows:

$$h = \sqrt{\frac{w(\rho_s - \rho_f)}{K_1\rho_s}\left(L_1X - X^2\right)} + H_o, \; 0 \le X \le X_{t1} \text{ or } X_{t2} \le X \le L_1 \qquad (5)$$

$$h = \sqrt{\frac{w}{K_1}\left(L_1X - X^2\right) + \frac{\rho_s}{\rho_f}H_o^2}, \; X_{t1} \le X \le X_{t2} \qquad (6)$$

The locations of the tips of the salt water tongues can be readily obtained by setting h equal to $\rho_s H_o/\rho_f$ in either Eq. (5) or Eq. (6) and then solving for X_{t1} and X_{t2}.The reclamation length and hydraulic conductivity of the reclamation material are taken as L_2 and K_2, respectively. The current distances from the coastline on the un-reclaimed side to the tips of salt water tongues are X_{tr1} and X_{tr2}, and the ground water divide after reclamation is assumed to be at $X = X_d$.

The solution for X_d is obtained as below:

$$X_d = \frac{K_1 L^2 + (K_2 - K_1) L_1^2}{2(L_1 K_2 + L_2 K_1)} \quad (7)$$

The final solutions of the head distributions (h) are as follows:

$$h = \sqrt{\frac{w(\rho_s - \rho_f)}{K_1 \rho_s}(\beta X - X^2)} + H_o, \quad 0 \le X \le X_{tr1} \quad (8)$$

$$h = \sqrt{\frac{w}{K_1}(\beta X - X^2) + \frac{\rho_s}{\rho_f} H_o^2}, \quad X_{t1} \le X \le L_1 \quad (9)$$

$$h = \sqrt{\frac{w}{K_2}(\beta X - X^2 + 2\gamma/w) + \frac{\rho_s}{\rho_f} H_o^2}, \quad L_1 \le X \le X_{tr2} \quad (10)$$

$$h = \sqrt{\frac{w(\rho_s - \rho_f)}{K_2 \rho_s}(\beta X^2 - X^2 + 2\gamma/w)} + H_o, \quad X_{t2} \le X \le L \quad (11)$$

Where $\beta = \left|K_1 L^2 + (K_2 - K_1) L_1^2\right| / (L_1 K_2 + L_2 K_1)$ and $\gamma = w L_1 L_2 L (K_2 - K_1) / 2(L_1 K_2 + L_2 K_1)$ Afterreclamation, the locations of the tips of the salt water tongues can be obtained by setting h equal to $\rho_s H_o/\rho_f$ in either Eq. (9) or Eq. (10) and then solving for X_{tr1} and X_{tr2}. The displacement of the water divide, Δd, can be calculated as:

$$\Delta d = X_d - \frac{L_1}{2} = \frac{K_1 L_2 (L_1 + L_2)}{2(L_1 K_2 + L_2 K_1)} \quad (12)$$

Eq. (12) shows that the water divide will move toward the new coastline after reclamation, indicating that ground water discharge to the sea on the non-reclamation side will be increased by an amount of $w\Delta d$ per unit width of flow.

In the development of analytical solutions, it is assumed that the Dupuit assumptions and the Ghyben-Herzberg relationships are valid. Guo and Jiao (2007) indicated that although the results obtained using these expressions are accurate in many cases, one of the major shortcomings of the Ghyben-Herzberg relationships is that there is no seepage face at the coastline. Further, the model does not include the more complicated cases like (*i*) heterogeneity of the aquifer system, (*ii*) complicated topography at the coast, and (*iii*) the transient process immediately after the reclamation.

It can be noted that in the proposed analytical solutions, the permeability of the *in situ* soil (K_1) and also reclamation material (K_2) are the governing parameters in deciding the water heads of GWT and location of the tip of the salt water tongue (X_{tr}). Being soil a natural material and heterogeneous in nature, deterministic estimate of K_1 and K_2 (i.e., single value) is virtually impossible. The uncertainty in estimation on these parameters brings uncertainty in determination of water heads of GWT and location of the tip of the salt water tongue. Hence, probabilistic assessment of these parameters becomes imperative in which the input parameters are treated as random variables and the influence of these input variables on the output responses, i.e., water heads of GWT and location of the tip of the salt water tongue are studied.

2. Objectives of the Present Study

In the present study, the work proposed by Guo and Jiao (2007) is studied in the light of probabilistic analysis. The heterogeneity of the aquifer system is taken into consideration to study the impact of coastal land reclamation on GWT (h) and sea water interface (X_{tr}). Monte Carlo simulations are done to obtain the statistical information on mean and variance of output parameters h and X_{tr}. Using FORM, the reliability of getting a particular value of h and X_{tr} are evaluated.

3. Geotechnical Uncertainties and Its Quantification

Quantitative assessment of soil uncertainty modeling requires use of statistics, as well as probabilistic modeling to process data from laboratory or *in situ* measurements. In the probabilistic analysis, the input parameters are modeled as either discrete or continuous random variables defined by their probability density functions (*pdf*) or the parameters of distributions (Baecher and Christian, 2003).

Normally, in geotechnical practice, the soil parameters are either modeled as normally distributed or log-normally distributed continuous random variables. The parameters of the normal and log-normal probability distribution function (*pdf*) are directly related to the unbiased estimates of statistical moments, i.e., sample mean (μ) and variance (σ^2) of

the measured data set. The coefficient of variation (*CoV%*), which is obtained by dividing the sample standard deviation (σ) by the sample mean (μ), is commonly used in quantifying the geotechnical uncertainty analysis because of the advantages of being dimensionless as well as providing a meaningful measure of relative dispersion of data around the sample mean.

Where site-specific data are not available to estimate parameters of random variables, uncertainty can be characterized by assuming that the coefficient of variation (CoV%) of a parameter is similar in magnitude to that observed at other sites. Typical values of coefficients of variation for soil properties have been compiled and reported by Uzielli *et al.*, (2007). Typical values of range of coefficient of variation (*CoV%*) for selected geotechnical parameters are provided in Table 1.

Consideration of these uncertainties in the input soil parameters and its impact on the performance of a geotechnical system are studied using the reliability-based design procedures. Reliability analysis focuses on the most important aspect of performance, i.e., probability of failure (p_f).

Table 1:*CoV*% for the selected geotechnical parameters

Property	*CoV*% range
Dry unit weight (γ_d)	2 – 13
Undrained shear strength (c_u)	6 – 80
Effective Friction angle (φ')	7 – 20
Elastic Modulus (E_s)	15 – 70
Coefficient of permeability (k)	68 - 90

4. Methods of Reliability Analysis

In FORM, if the demand is defined as *D* and capacity is defined as *C*; the margin of safety or the performance function *G(x)* or *M* is defined as below:

$$G(x) = M = C - D \tag{13}$$

If both *C* and *D* are uncorrelated continuous random variables defined by their probability distribution and parameters of distribution means (μ_C, μ_D) and standard deviations (σ_C, σ_D), In the case of log-inormally distributed *C* and *D*, the expression of β is as below (Baecher and Christian, 2003):

$$\beta = \frac{\ln\left[\left(\frac{\mu_C}{\mu_D}\right)\sqrt{(1+\delta_C^2)(1+\delta_D^2)}\right]}{\sqrt{\ln\left[\frac{(1+\delta_C^2)}{(1+\delta_D^2)}\right]}} \tag{14}$$

where, δ_C,δ_D is coefficient of variation in *C*, and *D*, respectively.

USACE (1997) made specific recommendation on target probability of failure (p_f) and reliability indices (β) in geotechnical and infrastructure projects. The suggested guidelines say that a reliability index (β) value of at least 5.0 is considered to indicate high performance of the system and 3.0 for the above average performance.

5. Results of Analysis and Discussion

5.1 Deterministic Solutions

A typical case of reclamation site of an extensive landmass in Hong Kong (Jiao et al., 2001) with the numerical values of the following parameters: K_1 = 0.1 m/day, L_1 = 1000 m, ρ_s = 1.025 g/cm^3, ρ_f = 1.000 g/cm^3, w = 0.0005 m/day and H_o = 20m, is considered. The land reclamation will increase the GWT and change the fresh water and sea water interface. From the available analytical solutions, it can be seen that the highest GWT increase is at the original coastline. For L_2 = 500m and K_2 = 0.5 m/day, the increase is 20.74 m.

Figure 3 shows the displacement of the tip of the salt water tongue with hydraulic conductivity of the reclamation material and for different reclamation length (given values of K_1 = 0.1 m/day, L_1 = 1000 m, ρ_s = 1.025 g/cm^3, ρ_f = 1.000 g/cm^3, w = 0.0005 m/day and H_o = 20m). It can be noted that permeability of reclamation material has high impact on displacement of the tip of the salt water tongue. As the permeability value reduces the tip of the sea water tongue moves sea side. Hence, it is always beneficial to keep the permeability of the reclamation material as low as possible.

Considering the case of an island, assuming L_1 = 2000 m and other parameters same as K_1 = 0.1 m/day, L_1 = 1000 m, ρ_s = 1.025 g/cm^3, ρ_f = 1.000 g/cm^3, w = 0.0005 m/day and H_o = 20m, the calculations show that the displacement of the tip of the salt water tongue near the coastline on the reclamation side is similar to the results obtained in Figure 3.

It is observed that after reclamation, the salt water interface on the reclamation side is pushed toward the post-reclamation coastline. The salt water

interface on the un-reclaimed side will similarly be pushed seaward. This is because the water-divide moves toward the reclaimed side, increasing the recharge to the aquifer and the ground water discharge to the sea on both sides of the island. The water table increases throughout the island as a result of the reclamation. The results are similar to those obtained for reclamation of extensive landmass.

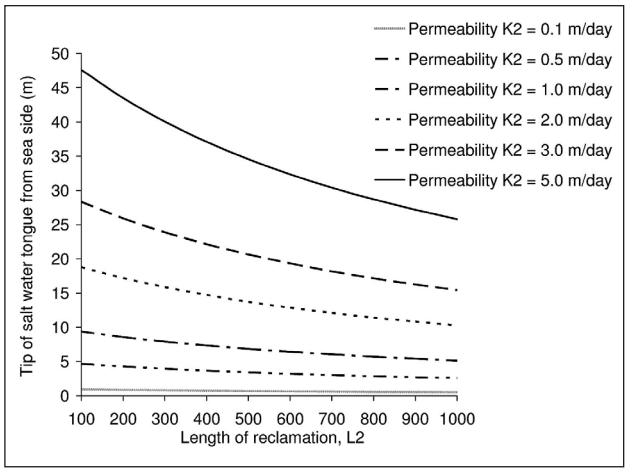

Figure 3: Displacement of the tip of the salt water tongue with hydraulic conductivity of the reclamation material and for different reclamation length

5.2 Probabilistic Solutions

It can be noted that the deterministic values obtained for increase in GWT (Δh) and distance of sea water – fresh water interface (X_{tr}) are reliable to the extent the accuracy with which the permeability parameters of the soil are obtained from field or laboratory test results. As indicated earlier it is almost impossible to attain a single (deterministic) value of K_1 and K_2 parameters for the *in situ* soil and reclamation material, respectively.

From Table 1, it is evident that the coefficient of variation (*CoV*%) in the permeability parameter can be expected in the range of 68% to 90%. Hence, assessment of ground water level and sea water interface in a reclamation project is extremely difficult in an uncertain environment. Through reliability analysis, the uncertainty in permeability parameters can be handled in a mathematical framework and the best way to answer to the following questions is probabilistically:

1. What is the reliability of getting tip of the salt water tongue at a particular distance (X_{tr})?
2. What is the reliability of getting increased value of GWT (Δh) of some numerical value?

For the reliability index calculations, the mean capacity (μ_C) is taken as the calculated value of Δh or X_{tr} and the demand (μ_D) is taken as deterministic (predefined numerical) values of Δh and X_{tr}. The results of the reliability analysis of reclamation of extensive landmass are presented. Similar calculations can be performed for the reclamation of an island.

For the reliability analysis of the given problem in hand, the permeability parameter (K_2) is considered as log-normally distributed continuous random variable. The coefficient of variation in demand is taken as zero, i.e., δ_D=0. The information on mean (μ_C) and coefficient of variation (δ_C) in capacity are obtained through Monte Carlo simulation results. For the parametric study, different values of mean (K_2 parameter = 0.1m/day, 0.5 m/day and 1.0 m/day) and the coefficients of variation (as 60%, 70%, 80%, and 90%) of permeability parameter (K_2) are assumed that constitutes the following cases:

CASE – A: Mean K_2 = 0.1 m/day and CoV = 60%, 70%, 80%, and 90%

CASE – B: Mean K_2 = 0.5 m/day and CoV = 60%, 70%, 80%, and 90%

CASE – C: Mean K_2 = 1.0 m/day and CoV = 60%, 70%, 80%, and 90%

For each case; 30000 random numbers for K_2parameter are generated to perform Monte Carlo simulations and to estimate the statistical information on mean and variance of Δh and X_{tr}. For that purpose corresponding to each value of K_2, proposed analytical solutions (Guo and Jiao, 2007) are utilized to obtain the corresponding values Δh and X_{tr}. The simulation provides 30000 numerical values of Δh and X_{tr}, which can be utilized in calculating mean (μ_C) and coefficient of variation (δ_C) in the capacity, as the case may be. It is further assumed that output values are random variables following lognormal distribution so that Eq. (14) can be utilized to calculate reliability index (β).

Table 2(a) shows typical results of the reliability analysis obtained for X_{tr} for CASE – A. It can be noted that the deterministic value of X_{tr} from analytical solution is 1499.317m. From the results of the reliability analysis, it can be noted that as X_{tr} is increased from 1495 m to 1498 m the reliability index value decreases for the range of CoV% values assumed for K_2. For 60% CoV in K_2 parameter, an acceptable value of β≥ 5.0 is achieved when the value of $X_{tr} \leq$ 1496.71 m. If the CoV in K_2 parameter is 90%, β ≥ 5.0 is achieved when $X_{tr} \leq$ 1495.0 m. Since the permeability of the reclamation material is very low (0.1 m/day in Case A), a very

low value of coefficient of variation is obtained in X_{tr} through Monte Carlo simulations. Hence, not much variation in X_{tr} in observed for which reliability index (β) $\geq$ 5.0.

Table 2a: Results of the reliability analysis of X_{tr} for CASE – A

Mean X_{tr} (μ_C)	1499.203	1499.168	1499.123	1499.086
CoV% in X_{tr} (δ_C)	0.033	0.039	0.049	0.055
	Reliability Index (β) values ← (CoV% in K_2 parameter) →			
X_{tr}(m)	**60%**	**70%**	**80%**	**90%**
1495	8.46	7.11	5.58	4.94
1496	6.44	5.40	4.22	3.73
1497	4.43	3.70	2.87	2.52
1498	2.42	1.99	1.52	1.31

Table 2b: Results of the reliability analysis of X_{tr} for CASE – B

Mean X_{tr} (μ_C)	1496.187	1496.078	1495.948	1495.826
CoV% in X_{tr} (δ_C)	0.152	0.185	0.215	0.272
	Reliability Index (β) values ← (CoV% in K_2 parameter) →			
X_{tr}(m)	**60%**	**70%**	**80%**	**90%**
1480	7.14	5.84	4.99	3.91
1485	4.92	4.02	3.42	2.67
1490	2.72	2.20	1.85	1.44
1495	0.52	0.39	0.30	0.20

Table 2c: Results of the reliability analysis of X_{tr} for CASE – C

Mean X_{tr} (μ_C)	1493.291	1493.479	1493.579	1493.855
CoV% in X_{tr} (δ_C)	0.270	0.299	0.360	0.382
	Reliability Index (β) values ← (CoV% in K_2 parameter) →			
X_{tr}(m)	**60%**	**70%**	**80%**	**90%**
1470	5.82	5.29	4.42	4.22
1475	4.56	4.16	3.48	3.33
1480	3.31	3.03	2.54	2.44
1485	2.06	1.90	1.60	1.56

Table 3a: Results of the reliability analysis of Δh for CASE – A

Mean Δh (μ_C)	64.971	65.893	66.765	68.494
CoV% in Δh (δ_C)	34.91	41.95	44.27	55.26
	Reliability Index (β) values ← (CoV% in K_2 parameter) →			
Δh (m)	**60%**	**70%**	**80%**	**90%**
10	5.69	4.88	4.70	3.99
12	5.15	4.43	4.27	3.63
14	4.70	4.05	3.90	3.33
16	4.30	3.72	3.59	3.07
18	3.95	3.42	3.31	2.85
20	3.64	3.16	3.06	2.64

Table 3b: Results of the reliability analysis of Δh for CASE – B

Mean Δh (μ_C)	22.994	23.831	24.499	25.367
CoV% in Δh (δ_C)	42.65	54.99	57.00	64.87
	Reliability Index (β) values ← (CoV% in K_2 parameter) →			
Δh (m)	**60%**	**70%**	**80%**	**90%**
1	7.87	6.43	6.30	5.75
2	6.18	5.08	4.99	4.58
3	5.19	4.29	4.22	3.90
4	4.48	3.73	3.68	3.41
5	3.94	3.30	3.26	3.04
6	3.49	2.94	2.92	2.73

Table 3c: Results of the reliability analysis of Δh for CASE – C

Mean Δh (μ_C)	15.135	16.296	17.574	19.334
CoV% in Δh (δ_C)	45.56	52.67	60.56	69.234
	Reliability Index (β) values ← (CoV% in K_2 parameter) →			
Δh (m)	**60%**	**70%**	**80%**	**90%**
1	6.47	5.89	5.41	5.05
2	4.88	4.49	4.17	3.94
3	3.94	3.67	3.44	3.29
4	3.28	3.09	2.93	2.83
5	2.77	2.64	2.53	2.47
6	2.35	2.27	2.20	2.18

In other two cases B & C, in which mean value of K_2 parameter is relatively high, the influence of

variation in K_2 parameter is remarkably observed. The results of the reliability analysis for Case B & C are presented in Table 2(b) and Table 2(c), respectively. For CASE – B; it can be noted that the deterministic value of X_{tr} from analytical solution in 1496.579 m. The results of the reliability analysis indicate that a reliability index (β) ≥ 5.0 is achieved when X_{tr} is assumed at 1484.8 m and 1475.6 m for 60% and 90% CoV in K_2 parameter, respectively. Similarly for CASE – C; it can be noted that the deterministic value of X_{tr} from analytical solution in 1493.152 m. The results of the reliability analysis indicate that a reliability index (β) ≥ 5.0 is achieved when X_{tr} is assumed at 1473.2 m and 1465.6 m for 60% and 90% CoV in K_2 parameter, respectively. Similar calculations were performed for the reliability index (β) evaluation of Δh value and results are presented in Table 3 for all the three cases. It can be noted that as CoV% in K_2 parameter increases the reliability index (β) values decreases for the given value of Δh. The β value also decreases with increase in Δh values.

The results of the reliability analysis can be interpreted as follows: If the mean and CoV% in K_2 parameter are 0.1 m/day and 60%, respectively, the reliability of getting $\Delta h \leq 12.6$ m is very high($\beta \geq 5.0$). The reliability decreases as Δh increases. It can be noted that for the same case analytical solution provides a deterministic value of $\Delta h = 61.61$m. With due consideration of variability in estimating K_2 parameters, the reliability of getting $\Delta h = 61.61$ m is extremely low. From these observations it can be stated that probabilistic assessment of Ground water level and sea water interface in coastal land reclamation projects is essential in view of heterogeneity of the material and uncertainties associated with the estimation of permeability properties governing the flow characteristics of reclaimed site.

6. Conclusions

The study highlights the influence of extent of variation in the permeability parameter in the increase in Ground water level and sea water interface in coastal land reclamation projects. The probabilistic analysis approach gives an opportunity to handle variability in a mathematical framework and it is a useful tool in decision making process. The results of the reliability analysis provide more rational information on selection of appropriate value of X_{tr} and Δh that can be based upon the extent of variation in input K_2 parameter and desired value of reliability index (β) acceptable to decision makers. It is noted that low mean value and low coefficient of variation in permeability of reclamation material is always beneficial and insures higher chances of getting increased X_{tr} and Δh values. These observations are essentially useful in quality control purposes in a land reclamation projects.

References

1. Baecher, G.B. and Christian, J.T. (2003).Reliability and statistics in geotechnical engineering, Chichester, NJ: John Wiley Publications, NY.
2. Bear, J. and Dagan,G. (1964). "Some exact solutions of interface problems by means of the holograph method,"Journal of Geophysical Research, 69(8), 1563-1572.
3. Guo, H. and Jiao,J. (2007). "Impact of coastal land reclamation on ground water level and the sea water interface,"Ground water, 45(3), 362 – 367.
4. Jiao, J.J. (2000). "Modification of regional groundwater regimes by land reclamation,"Hong Kong Geologist, 6, 29-36.
5. Jiao, J.J., Nandy,S. and Li, H. (2001). "Analytical studies on the impact of reclamation on groundwater flow,"Ground Water, 39(6), 912–920.
6. Lumb, P. (1976). Land reclamation in Hong Kong. In Proceedings of Residential Workshop on Materials and Methods for Low Coast Road, Rail and Reclamation Works, Leura, Australia, 299-314.
7. Nakheel (2007). The Palm Jumeirah (http://www.nakheel.com/Developments/The_Palm/The_Palm_Jumeirah:Retrieved 2007-06-19)
8. Seasholes, N.S. (2003). Gaining ground: a history of landmaking in Boston. Cambridge, Mass.: MIT Press.
9. Strack, O.D.L. (1976). "A single-potential solution for regional interface problems in coastal aquifers,"Water Resources Research, 12(6), 1165–1174.
10. Stuyfzand, P.J. (1995). "The impact of land reclamation on groundwater quality and future drinking water supply in the Netherlands," Wat. Sci. Tech., 31(8), 47-57.
11. Suzuki, T. (2003). "Economic and geographic backgrounds of land reclamation in Japanese ports,"Marine Pollution Bulletin, 47, 226-229.
12. USACE (1997). Risk-based analysis in Geotechnical Engineering for Support of Planning Studies, Engineering and Design. US Army Corps of Engineers, Department of Army, Washington, DC, 1997. 20314-100.
13. Uzielli, M., LacasseS., Nadim F. and Phoon K.K. (2007). Soil variability analysis for geotechnical practice. Characterization and engineering properties of natural soils – In Tan, Phoon, Hight& Leroueil (eds), Taylor & Francis group, London, ISBN 978-0-415-42691-6.

Life Cycle Reliability and Safety Engineering
Vol.1 Issue 3 (2012) 23-30

Probabilistic Assessment of Container Crane Under Wind Loading

Sourav Gur and Samit Ray Chaudhuri
Indian Institute of Technology Kanpur,
sourav.gur.1987@gmail.com

Abstract

Container cranes are highly susceptible to damage or even failure during severe windstorms. Damage of container crane causes significant amount of economic loss both in terms of repair/ replacement and downtime. This paper focuses on the effect of uncertainty of different parameters of wind field on the performance of container cranes. A representative crane of tower height 72.60 m and total boom length of 131.00 m is chosen and modeled in a commercial software considering both material and geometric nonlinearities. Stochastic fluctuating wind fields have been simulated by means of spectral representation method using the Kaimal and Simiu power spectra in conjunction with along and across wind coherence functions. Nonlinear time history analyses are carried out using simulated wind fields and the performance of the crane is assessed in terms of fragility curves. Further, a sensitivity analysis is conducted by means of a tornado diagram and first-order second-moment analysis to rank different uncertain parameters of wind field. Based on these results, a few considerations for design have been provided.

Keywords: Container crane; parametric uncertainty; stochastic wind field; nonlinear dynamic analysis; Fragility curve; Sensitivity analysis.

1. Introduction

Seaports are essential nodes of national and international transport system of a country. It is thus essential to minimize the damage of ports under natural disasters such as earthquakes and severe windstorms. In a port facility, container cranes are one of the most important types of structures that facilitate the movement of cargos between a ship and storage yards. Thus, damage or collapse incidents of cranes can hinder smooth port operation, causing significant amount of economic loss in terms of repair or replacement, downtime, and enduring loss of business due to permanent traffic rerouting. Although significant advancements have been achieved in terms of design and construction of modern-day huge cranes, recent failure incidents such as (a) in 2003, at Pusan port of S. Korea and (b) in 1996, the Zhanjiang port of Guangdong indicate that these cranes are highly vulnerable to windstorm induced loadings. Several researchers such as McCarthy and Vazifdar (2004), McCarthy *et al.* (2007), and McCarthy *et al.* (2009) carried out a few studies to identify different components of container cranes that are highly susceptible to failure during severe windstorm (tie-down wharf bracket and stowage-pin system, link plates, and turnbuckles) and different retrofitting schemes. In addition, several numerical and experimental studies are conducted [viz., Eden *et al.* (1980); Huang *et al.* (2006); Lee *et al.* (2007); and Lee and Kang (2007)] to determine values of different governing parameters for design of container crane due to wind load. Important conclusions of all those studies are: *(a)* effect of Reynolds number (R_e) and Strouhal number (S) on different aerodynamic coefficients is negligible and *(b)* maximum value of uplifting force at any support occurs either for yaw angles between 20^0 and 40^0 or between 130^0 and 150^0 and minimum value occurs at the yaw angle 90^0.

It can be observed from previous research that no systematic studies have been carried out to investigate the effect of different parameters on failure of container crane as well as all those previous studies did not explicitly consider the influence of spatial variation of wind field on failure vulnerability of container crane. The primary purpose of this study is twofold: *(a)* identification of different parameters that have significant influence on failure vulnerability of container cranes, and *(b)* estimate the influence of these parameters on failure of container cranes.

2. Stochastic Wind Field Simulation

Wind speed at any point and any instant of time [$V(x,y,z;t)$] consist of two parts: *(a)* mean wind speed [$\bar{\boldsymbol{V}}(z)$], which is independent of space and time but only varies along the height and *(b)* fluctuating wind speed [$v(x, y, z; t)$], which varies both in space and time (Paola, 1998), as given by:

$$\boldsymbol{V}(\boldsymbol{x},\boldsymbol{y},\boldsymbol{z};\boldsymbol{t}) = \bar{\boldsymbol{V}}(\boldsymbol{z}) + \boldsymbol{v}(\boldsymbol{x},\boldsymbol{y},\boldsymbol{z};\boldsymbol{t}) \quad (1)$$

In this study, wind fields are simulated by means of spectral representation method [viz., Shinozuka and Deodatis (1991); Shinozuka and Deodatis (1988) and Shinozuka and Jan (1972)].

2.1 Mean Wind Field Simulation

For the simulation of mean wind speed, at first, the original coordinate system (x, y, y) is transformed to the coordinate system of the wind flow direction (x_1, y_1, z_1) considering wind flow as horizontal, and varying the yaw angle (θ, in degree). It is considered that the value of mean wind speed is zero at ground level and varying only with height according to the well-known power law, which is given as:

$$\bar{V}(Z) = V_g \left(\frac{Z}{Z_g}\right)^{\alpha} \quad (2)$$

where $\bar{V}(Z)$ is the mean wind speed at height Z, V_g, is the gradient wind velocity at gradient height Z_g (the height at which wind velocity become constant) and α is a power law exponent that depends on terrain conditions.

2.2 Fluctuating Wind Field Simulation

Fluctuating part of wind speed is simulated as a zero mean, one-dimensional, multivariate (1D-mV) stationary Gaussian stochastic wind field and can be rewritten as:

$$v_j^{(i)}(p\Delta t) = Re\left\{\sum_{q=1}^{j}\sum_{l=0}^{M-1} B_{jql}\exp\left[i\,l\,p\,\frac{2\pi}{M}\right]\right\} \quad (3)$$

$j = 1, 2, \ldots\ldots, m;\ \ p = 0, 1, \ldots\ldots, M\text{-}1;$
$l = 0, 1, \ldots\ldots, N\text{-}1$

where

$$B_{jql} = 2\left|H_{jk}(l\Delta\omega)\right|\sqrt{\Delta\omega}\exp\left[-i\theta_{jq}(l\Delta\omega)\right]\exp\left[i\Phi_{ql}\right] \quad (3a)$$

$$\Delta\omega = \frac{\omega_u}{N};\ \Delta t = \frac{2\pi}{M\Delta\omega};\ \text{and } M = 2N \quad (3b)$$

$$S^0(\omega) = H(\omega)H^{*T}(\omega) \quad (3c)$$

$$\theta_{jq}(l\Delta\omega) = \tan^{-1}\left(\frac{Im[H_{jq}(l\Delta\omega)]}{Re[H_{jq}(l\Delta\omega)]}\right) \quad (3d)$$

$H_{jk}(l\Delta\omega)$ is the lower triangular matrix obtained from decomposing the spectral density matrix $[S^0(\omega)]$ using Cholesky's method. Elements of the spectral density matrix $[S^0(\omega)]$ can be expressed as:

$$S_{jj}^0(\omega) = S_j(\omega) \quad j = 1, 2, \ldots, m \quad (4.a)$$

$$S_{jk}^0(\omega) = \sqrt{S_j(\omega)\,S_k(\omega)}\ *\eta_{jk}*\gamma_{jk}$$

$$j, k = 1, 2, \ldots, m, j \neq k \quad (4.b)$$

where

$$S_j(\omega) = \frac{1}{2}\frac{1}{2\pi}\,200\,u_*^2\,\frac{Z}{V(Z)}\,\frac{1}{\left[1+50\,\frac{|\omega|Z}{2\pi V(Z)}\right]^{5/3}}$$

(Kaimal and Simiu power spectra) (4.c)

$$\eta_{jk}(\omega, dX) = exp\left[-\frac{|\omega|\,C_X\,dX}{2\pi\,V_{m_{jk}}(Z)}\right]$$

(Along wind coherence function) (4.d)

$$\gamma_{jk}(\omega, dY, dZ) = exp\left[-\frac{|\omega|\sqrt{(C_Y\,dY)^2 + (C_Z\,dZ)^2}}{2\pi\,V_{m_{jk}}(Z)}\right]$$

(Across wind coherence function) (4.e)

Therefore, the Total wind speed at any point of the structure and at any instant of time is given by:

$$V(x,y,z;t) = V_g\left(\frac{Z}{Z_g}\right)^{\alpha} + Re\left\{\sum_{q=1}^{j}\sum_{l=0}^{M-1} B_{jql}\,exp\left[i\,l\,p\,\frac{2\pi}{M}\right]\right\} \quad (5)$$

For simulation, the values of different parameters are assumed as $N = 2048$, M = 4096, and $\omega_u = 4\pi$. Realizations of the wind speed time histories are simulated for 1023.75 sec with an interval of 0.25 sec. Figure 1(a) shows a realization of simulated wind speed data for Z_g of 30.0 m and V_g of 60.0 m/sec at different nodes for a time window of 400 sec to 500 sec. To check the accuracy of simulated wind speed, Cross Power Spectral Density Function (CPSDF) between these two nodes (node 55 and 40) are calculated from the simulated wind field data and then considering 20 samples, the average is calculated. Figure 1(b) shows the comparison of generated CPSDFs (a sample, the average CPSDF computed from 20 realizations obtained using a moving average method with a window size of 16 and the assumed-one) for a frequency range of 0.1 Hz to 1.0 Hz. It shows that in mean sense, the CPSDFs generated from the wind speed data are in very good agreement with the assumed CPSDF.

2.3 Wind Force Computation

Only the drag and lift forces at each node are considered in the direction of wind and perpendicular to the plane of wind flow *i.e.*, in the vertical direction. The drag force F_D and lift force F_L at any point can be expressed as (Simiu and Scanlan, 1986):

$$F_D(x,y,z;\ t) = \frac{1}{2}\ \rho\ [V(x,y,z;t)]^2\ C_D\ A\ \ and$$

$$F_L(x,y,z;\ t) = \frac{1}{2}\ \rho\ [V(x,y,z;t)]^2\ C_L\ A \qquad (6)$$

where F_D and F_L are the drag and lift forces, respectively; ρ is the density of air (1.225 Kg/m^3), C_D and C_L are the drag and lift coefficients, respectively;

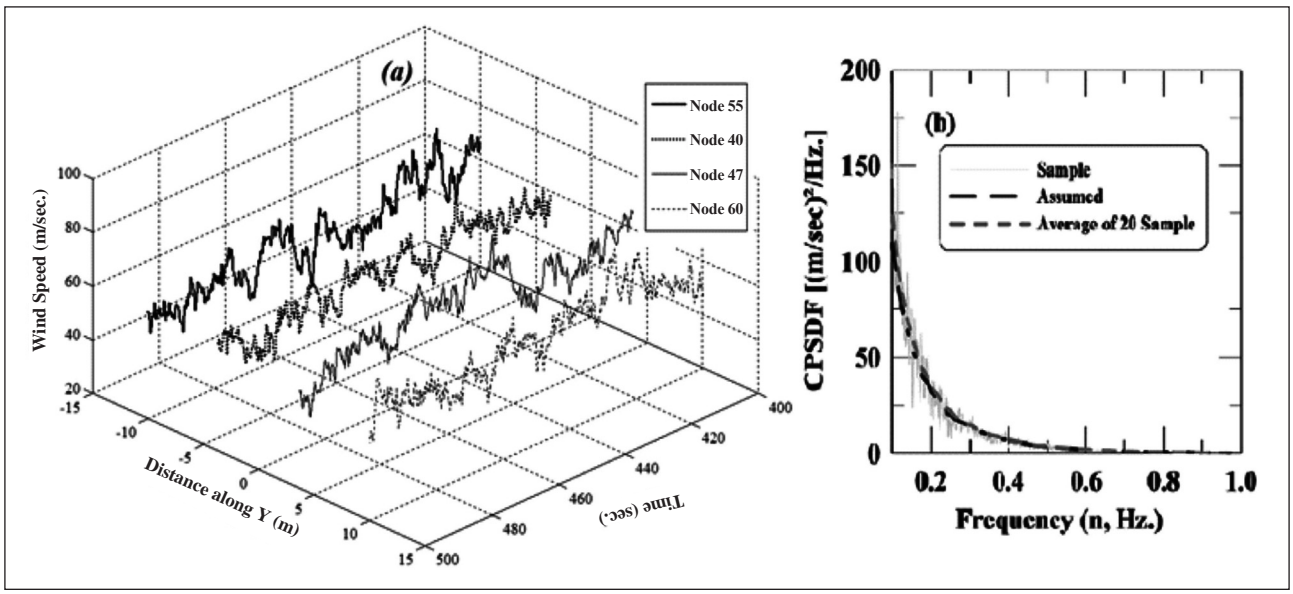

Figure 1: (a) Total wind speed along 'X' at different points plotted with respect to time and distance and (b) Comparison of CPSDFs of wind speed between nodes 40 and 55

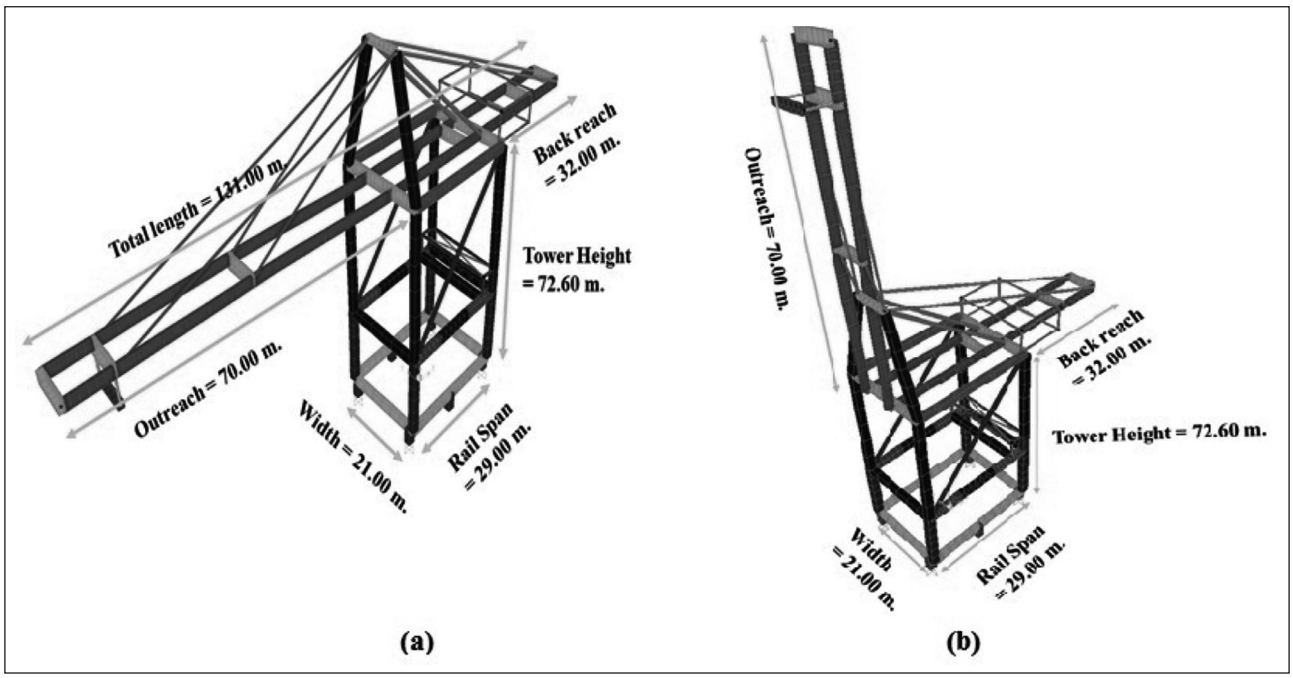

Figure 2: Representative container crane model at two different boom positions: (a) Boom-down and (b) Boom-up

and A is the effective area of any node in the direction of wind flow. Drag (C_D) and lift (C_L) coefficient values are taken from Lee and Kang (2007).

3. Numerical Modeling and Analysis

For this study, a container crane of tower height 72.60 m, total boom length of 131.0 m (back reach

length 32.0 m, rail span 29.0 m and outreach length 70.0 m) has been considered (Figure 2). The lifting capacity of the container crane model is 65.0 tones. The proposed container crane at different boom positions is modeled in SAP 2000 V14 (Computers and Structures, 2009) using frame element (67 nodes, connected by 109 elements). For modeling, isotropic tendon-type steel [Unit weight (γ): 76972.86 N/m^3, Modulus of elasticity (E): 1.999 x 10^{11} N/m^2, Poisson's ratio (ν): 0.30, Shear Modulus (G): 7.690 x 10^{10} N/m^2, Minimum yield stress (F_y): 1.493 x 10^9 N/m^2] with 3 % kinematic hardening is considered.

3.1 Modal Properties

Analysis is performed to estimate natural frequencies and mode shapes of the models. Ritz vector method is employed to extract only the first six modes of the model. Table 1 provides the natural periods of the first six modes of container crane models. It can be observed from these results that the periods in all modes of boom-up model is higher than the corresponding boom-down position, thereby implying that the boom-up position is more flexible, as one can expect.

Table 1: Natural periods and mode shape of the first six modes

Mode Number	Time Periods (in sec.)		Mode Shape Type	
	Boom Down	Boom Up	Boom Down	Boom Up
1st	3.14162	3.66817	LOB	LOB
2nd	2.38287	2.58208	LBB	TOB1
3rd	1.30613	2.11273	LTV	L
4th	1.06751	1.50134	T	LT
5th	0.80840	0.99998	VB	T
6th	0.71979	0.73545	LT	TOB2

Note: LOB: Lateral motion of outreach of boom girder; LBB: Lateral motions of back reach of boom girder; LTV: Lateral torsion with vertical motion; T: Transverse motion; VB: Vertical motion of boom girder; LT: Lateral torsion motion; TOB1: Transverse motion of outreach of boom girder; L: Lateral motion; TOB2: Torsional motion of outreach of boom girder.

3.2 Static and Wind Load Analysis

For a container crane, static load comes from different sources. These loads are applied at each nodes of the crane model and analysis is performed to obtain the state of stress and deformation of the model. For static analysis, geometric nonlinearity (P-Δ effect and large deformation) is considered. At first, the static load analysis is performed. Then holding the states of deformation and stress due to the applied static loads, the wind load analysis is performed. The wind load time history is applied at each node in both the directions (horizontal and vertical). Nonlinear time history analysis is carried out using Newmark's direct integration technique.

4. Covergence Test and Sensitivity Analysis

Since wind fields are stochastic in nature, a convergence test of response parameters (normalized base moment) has been performed for Z_g of 30.0 m and V_g of 60.0 m/sec to determine the approximate sample size of random wind field required for simulation convergence. Sensitivity analysis is then carried out to identify parameters that may have significant influence on failure of container cranes. Tornado diagram method and FOSM analysis is used for the purpose of sensitivity study. In tornado diagram method, all the uncertain parameters are considered as random variables and their two extreme values are chosen as mean - standard deviation and mean + standard deviation. The mean values and coefficients of variation of different uncertain parameters considered for the sensitivity analysis are given in Table 2.

Table 2: Input parameter uncertainties

Parameter	Unit	Mean	COV (in %)
Yaw angle [θ]	In degree	90.0	33.33
Gradient Height [Z_g]	In m	25.0	10.0
Gradient Wind Speed [V_g]	In m/s	50.0	10.0
Power Law Exponent [α]	-	1/7	20.0
Roughness Height [z_0]	In m	0.01	20.0
Coherence Function Constant [C_X, C_Y, C_Z]	-	6.0, 10.0, 16.0	15.0
Boom Position	-	Boom Down	Boom Articulated and Boom Up
Yield Strength [F_y]	In N/m^2	1.493 x 10^9	20.0
Elastic Modulus [E]	In N/m^2	200 x 10^9	20.0
Kinematic Hardening Ratio [n]	In %	3.00	15.0
Damping Ratio [ξ]	In %	2.00	15.0

Swings have been plotted for all random variables from top to bottom in a decreasing size. These swings demonstrate relative contribution of each variable on the desired response parameter. Here larger swing implies higher influence of a random variable on the response parameter than the shorter one. FOSM analysis is performed to determine relative variance contribution by neglecting correlation terms.

5. Vulnerability Assessment

Windstorm can sustain for a long duration, which can cause high magnitude of stress concentration along with frequent stress reversals. This may lead to low-cycle fatigue failure of the members connected to the supports. Now, the ratio R of the absolute value of the developed moment (M) in a member connected to any support to the plastic moment capacity (M_p) of the section can be used to determine the failure probability of the member. In mathematical form, this can be expressed as:

$$M_P = F_y Z_P \quad \text{and} \quad R = \frac{|M|}{M_P} \tag{7}$$

where Z_p is the plastic section modulus and F_Y is the yield stress. For any loading case, if the value of this ratio (R) becomes more than or equal to unity, the section, and thus the structure, can be considered to have been failed. After defining the damage state, fragility analysis is performed to determine failure probability of the container crane. In this method of fragility analysis, the median and log-standard deviation of fragility curve for different damage states are estimated simultaneously with the aid of maximum likelihood method [viz., Shinozuka *et al.* (2000); Shinozuka *et al.* (2001)]. Due to use of a single log-standard deviation for different damage states, fragility curves for different damage states do not cross each other in this method. If failure of the structure is assessed with respect to the parameter a, then the failure probability of the structure at a particular damage state of E_k is expressed as:

$$P_{ik} = P(a_i; E_k) \tag{8a}$$

$$F_k(a_i; c_k, \zeta) = \Phi\left[\frac{ln\left(\frac{a_i}{c_k}\right)}{\zeta}\right] \tag{8b}$$

where

$$P_{i1} = P(a_i; E_1) = 1 - F_1(a_i; c_1, \zeta)\ ;\ P_{ik} = P(a_i; E_k) = F_{k-1}(a_i; c_{k-1}, \zeta) - F_k(a_i; c_k, \zeta)$$

and $P_{in} = P(a_i; E_n) = F_{n-1}(a_i; c_{n-1}, \zeta)$.

To calculate different medians for different damage states ($c_1, c_2, \ldots c_n$) and a common log-standard deviation (ζ) for all the damage states, the method of maximum likelihood method is used here.

6. Results and Discussions

Important results of this study are listed as follows:

- Figure 3 shows that the normalize base moment value converges for a sample size of approximately 60.
- Figure 4 and 5 show the sensitivity analysis results. From both of the figures, it can be observed that the gradient wind speed, boom position, yaw angle, and gradient height are the most important wind field parameters (in decreasing sequence of importance) to control the failure vulnerability of the container crane.
- From Figure 6 it can be observed that considerable amount of variation in the failure probability occurs due to a change in boom position. Since the boom-up position is more flexible than the boom-down position, the failure probability at boom-up position is much more that of the boom-down position.
- Figure 7 depicts that the failure probability of container crane also changes significantly with the change in yaw angle. At boom-down position, the failure probability decreases with the yaw angle

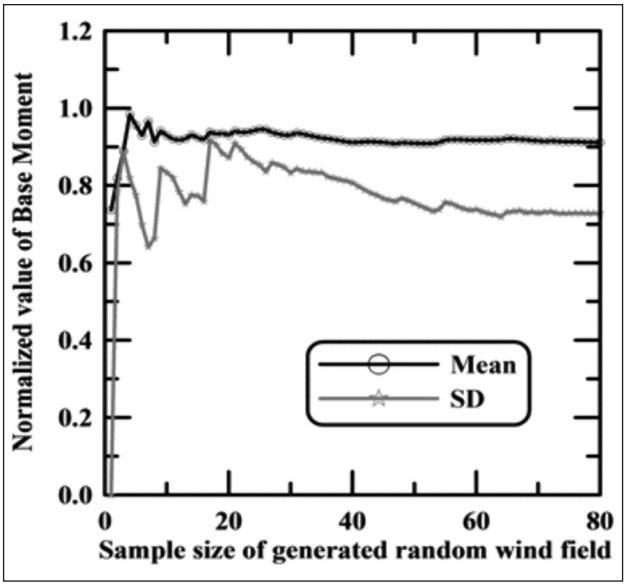

Figure 3: Median and standard deviation (SD) of the normalized base moment for different sample sizes of generated random wind field

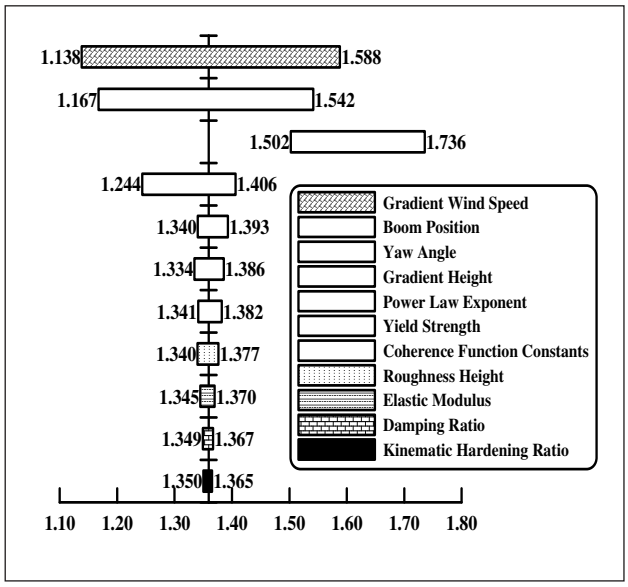

Figure 4: Tornado diagram considering uncertainty in different parameters

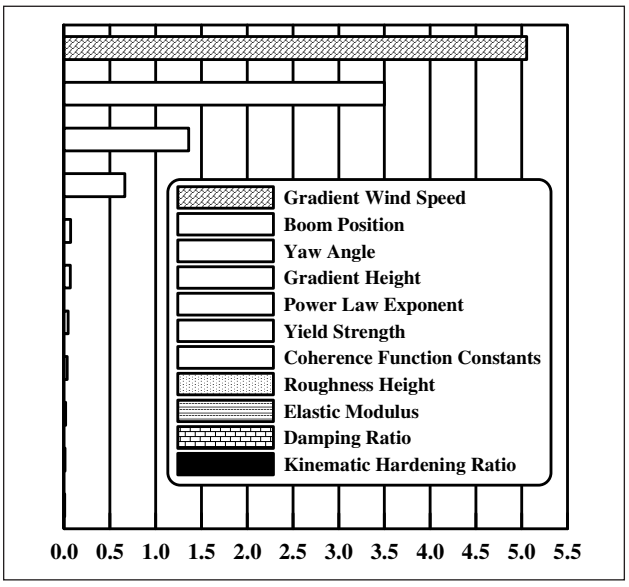

Figure 5: Relative variance contribution (neglecting correlation terms) from FOSM analysis

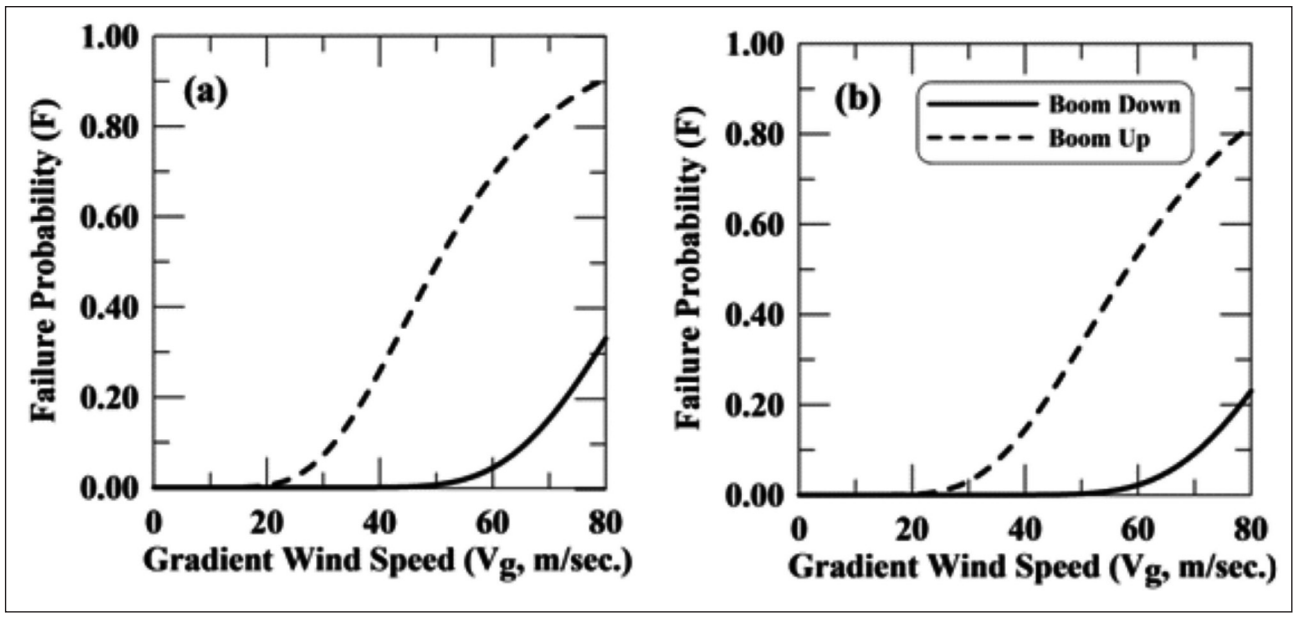

Figure 6: Fragility curve at boom-down and boom-up condition for a particular yaw angle and gradient Height

in the sequence of 60^0, 120^0, 90^0, 30^0, 150^0, 180^0, and 0^0. However, at boom-up condition, this sequence of the yaw angle becomes 60^0, 120^0, 0^0, 180^0, 90^0, 30^0, and 150^0.

- From Figure 8 it can be observed that at a particular yaw angle and boom position, failure probability reduces with an increase in gradient height. A probable reason behind this is at lower value of gradient height, the mean wind field becomes very stiff, which causes higher application of wind load on the structure and thus, increases the failure probability.

7. Conclusions

A parametric study is conducted to identify different wind field parameters that significantly influence the failure of container crane. Influence of these significant parameters on failure vulnerability of the container crane is then assessed in terms of fragility curves. It is observed from the results that the gradient wind speed, boom position, yaw angle, and gradient height are the most important parameters that significantly influence the failure of container crane. It is also observed that the boom-up position is much more vulnerable than the boom-down

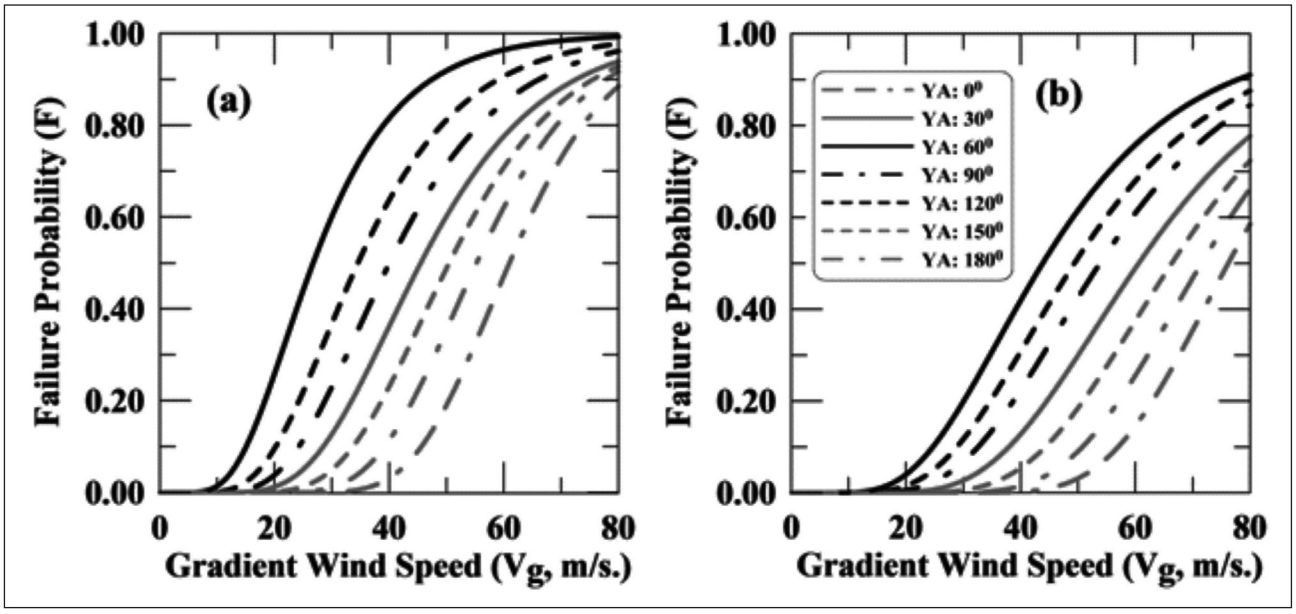

Figure 7: Fragility curve at boom-down condition for a particular gradient height and different yaw angle

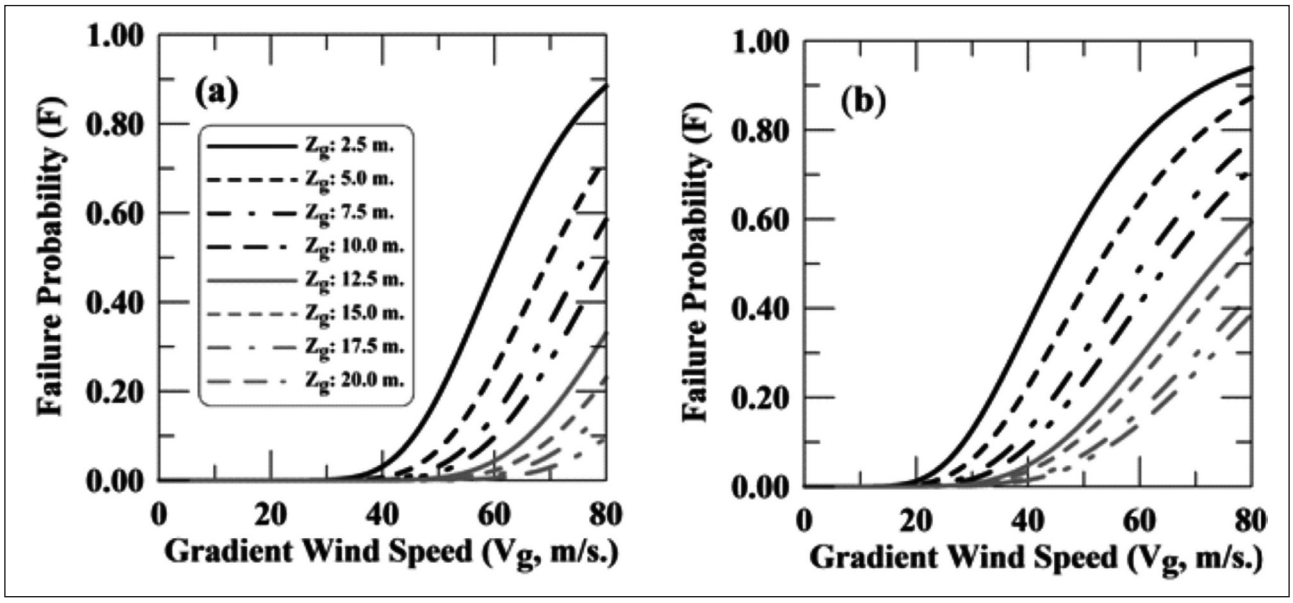

Figure 8: Fragility curve at boom-down condition for a particular yaw angle and different gradient height

position. Considerable amount of variation in the failure probability can occur with the change in yaw angle. It is also found that the failure probability of container crane increases with an increase in gradient wind speed and decreases with an increase in gradient height.

References

1. Eden, J.F, Iny, A. and Butler A.J. (1980). "Cranes in storm winds." engineering structure, 1981, Vol.3.engineering and science, EPMESC X, Aug. 21-23, 2006, Sanya, Hainan, China.
2. Huang, P., Wang J.Y. and Gu, M. (2006). "Wind tunnel test and numerical simulation of mean wind loads on a container crane." The fourth international symposium on Computational Wind Engineering (CWE2006), Yokohama, 2006.
3. Lee, J.S. and Kang H.J. (2007). "Wind load on a container crane located in atmospheric boundary layers." Journal of Wind engineering and Industrial Aerodynamics, 96, 193-208.
4. Lee, S.W., Kim, Y., Han D.S. and Han G.J. (2007). "Wind tunnel study on the structural stability of a container crane according to the boom shape." Proceedings of the 4th WSEAS International Conference on Fluid Mechanics, Gold Coast, Queensland, Australia.
5. McCarthy, P. and Vazifdar, F. (2004). "Securing cranes for storm wind: Uncertainties and Recommendations." ASCE Ports 2004 Conference, Houston, Teaxas.

6. McCarthy, P., Jordan, M., Lee, K., and Werner, S. (2007). "Increasing hurricane winds dockside crane retrofit recommendations." ASCE Ports 2007 Conference, San Diego, CA.
7. McCarthy, P., Soderberg, E. and Dix, A. (2009). "Wind damage to dockside cranes: Recent failures and recommendations." TCLEE 2009 Conference Oakland, CA.
8. Paola, M.D. (1998). "Digital simulation of wind field velocity." Journal of Wind engineering and Industrial Aerodynamics, 74-76 (1998), 91-109.
9. Shinozuka, M. and Deodatis, G. (1991). "Simulation of stochastic processes by spectral representation." Applied Mechanics Reviews vol. 44, no 4, April 1991, ASME Book No AMR094.
10. Shinozuka, M. and Deodatis, G. (1996). "Simulation of multi-dimensional Gaussian stochastic field by spectral representation." Applied Mechanics Reviews vol. 49, no 1, January 1996, ASME Book No AMR183.
11. Shinozuka, M., Feng, M.Q., Kim, H.K., and Kim, S.H. (2000). "Statistical analysis of fragility curves." Journal of Engineering mechanics, 2000, Vol. 126, No. 12.
12. Shinozuka, M., Feng, M.Q., Lee, J., and Naganuma, T. (2000). "Statistical analysis of fragility curves." Journal of engineering mechanics, 2000, Vol. 126, No. 12.
13. Simiu, E., and Scanlan, H.R. (1986). "Wind effects on structure" John Wiley & Sons, Inc., Second Edition.

Life Cycle Reliability and Safety Engineering
Vol.1 Issue 3 (2012) 31-44

Uncertainty Quantification for Decision-Making in Engineered Systems

Sankaran Mahadevan
John R. Murray Sr. Professor of Civil & Environmental Engineering
Vanderbilt University, Nashville, TN, USA
sankaran.mahadevan@vanderbilt.edu

Abstract

This paper discusses current research and opportunities for uncertainty quantification in performance prediction and risk assessment of engineered systems. Model-based simulation becomes attractive for systems that are too large and complex for full-scale testing. However, model-based simulation involves many approximations and assumptions, and thus confidence in the simulation result is an important consideration in risk-informed decision-making. Sources of uncertainty are both aleatory and epistemic, stemming from natural variability, information uncertainty, and modeling approximations. The paper draws on illustrative problems in aerospace, mechanical, civil, and environmental engineering disciplines to discuss (1) recent research on quantifying various types of errors and uncertainties, particularly focusing on data uncertainty and model uncertainty (both due to model form assumptions and solution approximations), (2) framework for integrating information from multiple sources (models, tests, experts), multiple model development activities (calibration, verification, validation), and multiple formats; and (3) using uncertainty quantification in risk-informed decision-making throughout the life cycle of engineered systems, such as design, operations, health and risk assessment, and risk management.

Keywords: uncertainty quantification, model based simulation, surrogate models

1. Introduction

Uncertainty quantification is important in the assessing and predicting performance of complex engineering systems, especially given limited experimental or real-world data. Simulation of complex physical systems involves multiple levels of modeling, ranging from the material to component to subsystem to system. Interacting models and simulation codes from multiple disciplines (multiple physics) may be required, with iterative analyses between some of the codes. As the models are integrated across multiple disciplines and levels, the problem becomes more complex and assessing the predictive capability of the overall system model becomes more difficult. Many factors contribute to the uncertainty in the prediction of the system model including: inherent variability in model input parameters, sparse data, measurement errors, and modeling errors, assumptions and approximations.

The various sources of uncertainty in performance prediction can be grouped into three categories:

- Physical variability,
- Data uncertainty, and,
- Model error.

Physical variability: This type of uncertainty also referred to as aleatory or irreducible uncertainty, arises from natural or inherent random variability of physical processes and variables, due to many factors such as environmental and operational variations, construction processes, and quality control. This type of uncertainty is present both in system properties (e.g., material strength, porosity, diffusivity, geometry variations, chemical reaction rates) and external influences and demands on the system (e.g., concentration of chemicals, temperature, humidity, mechanical loads). As a result, in model-based prediction of system behavior, there is uncertainty regarding the precise values for model parameters and model inputs, leading to uncertainty about the precise values of the model output. Such quantities are represented in engineering analysis as random variables, with statistical parameters such as

mean values, standard deviations, distribution types, etc., estimated from observed data or in some cases assumed. Variations over space or time are modeled as random processes.

Data uncertainty: This type of uncertainty falls under the category of epistemic uncertainty (i.e., knowledge or information uncertainty) or reducible uncertainty (i.e., the uncertainty is reduced as more information is obtained). Data uncertainty occurs in different forms. In the case of a quantity treated as a random variable, the accuracy of the statistical distribution parameters depends on the amount of data available. If the data is sparse, the distribution parameters themselves are uncertain and may need to be treated as random variables. Alternatively, information may be imprecise or qualitative, or as a range of values, based on expert opinion. Both probabilistic and non-probabilistic methods have been explored to represent epistemic uncertainty. Measurement error (either in the laboratory or in the field) is another important source of data uncertainty.

Model error: This results from approximate mathematical models of the system behavior and from numerical approximations during the computational process, resulting in two types of error in general – solution approximation error, and model form error. The performance assessment of a complex system involves the use of several analysis models, each with its own assumptions and approximations. The errors from the various analysis components combine in a complicated manner to produce the overall model error (described by both bias and uncertainty).

The roles of several types of uncertainty in the use of model-based simulation for performance assessment can be easily seen in the case of reliability analysis. Consider the probability of an undesirable event denoted by $g(\mathbf{X}) < k$, which can be computed from Equation 1:

$$P(g(\mathbf{X}) < k) = \int_{g(\mathbf{X})<k} f_{\mathbf{X}}(\mathbf{x})\ d\mathbf{x} \qquad (1)$$

where $\mathbf{X}$ is the vector of input random variables, $f_{\mathbf{X}}(\mathbf{x})$ is the joint probability density function of $\mathbf{X}$, $g(\mathbf{X})$ is the model output, and k is the regulatory requirement in performance assessment. Every term on the right hand side of Equation 1 has uncertainty. There is inherent variability represented by the vector of random variables $\mathbf{X}$; data uncertainty (due to inadequate data) regarding the distribution type and distribution parameters of $f_{\mathbf{X}}(\mathbf{x})$; and model errors in the computation of $g(\mathbf{X})$. Thus it is necessary to systematically identify the various sources of uncertainty and develop the framework for including them in the overall uncertainty quantification in the performance assessment of engineering systems.

The uncertainty analysis methods covered in this paper are grouped by sections along the four major groups of analysis activities that are needed for performance assessment under uncertainty:

1. Input uncertainty quantification;
2. Uncertainty propagation analysis (includes model error quantification);
3. Model calibration, verification, validation, and extrapolation; and,
4. Probabilistic performance assessment.

A brief summary of the analysis methods covered in the four groups is as follows:

Input uncertainty quantification: Physical variability of parameters can be quantified through random variables by statistical analysis. Parameters that vary in time or space are modeled as random processes or random fields with appropriate correlation structure. Data uncertainty that leads to uncertainty in the distribution parameters and distribution types can be addressed using confidence intervals and Bayesian statistics. Recent methods to include several sources of data uncertainty, namely, sparse data, interval data and measurement error, are discussed in this paper.

Uncertainty propagation analysis: Both classical and Bayesian probabilistic approaches can be investigated to propagate inherent variability and data uncertainty through individual sub-models and the overall system model. To reduce the computational expense, surrogate models can be constructed using several different techniques. Methods for sensitivity analyses in the presence of uncertainty are discussed. The uncertainty in the overall model output also includes model errors and approximations in each step of the analysis; therefore approaches to quantify model error are included in the discussion.

Model calibration, verification, validation and extrapolation: Model calibration is the process of adjusting model parameters to obtain good agreement between model predictions and experimental observations. Both classical and Bayesian statistical methods are discussed for model calibration with available data. One particular concern is how to properly integrate different types of data, available at different levels of the model hierarchy. Assessment

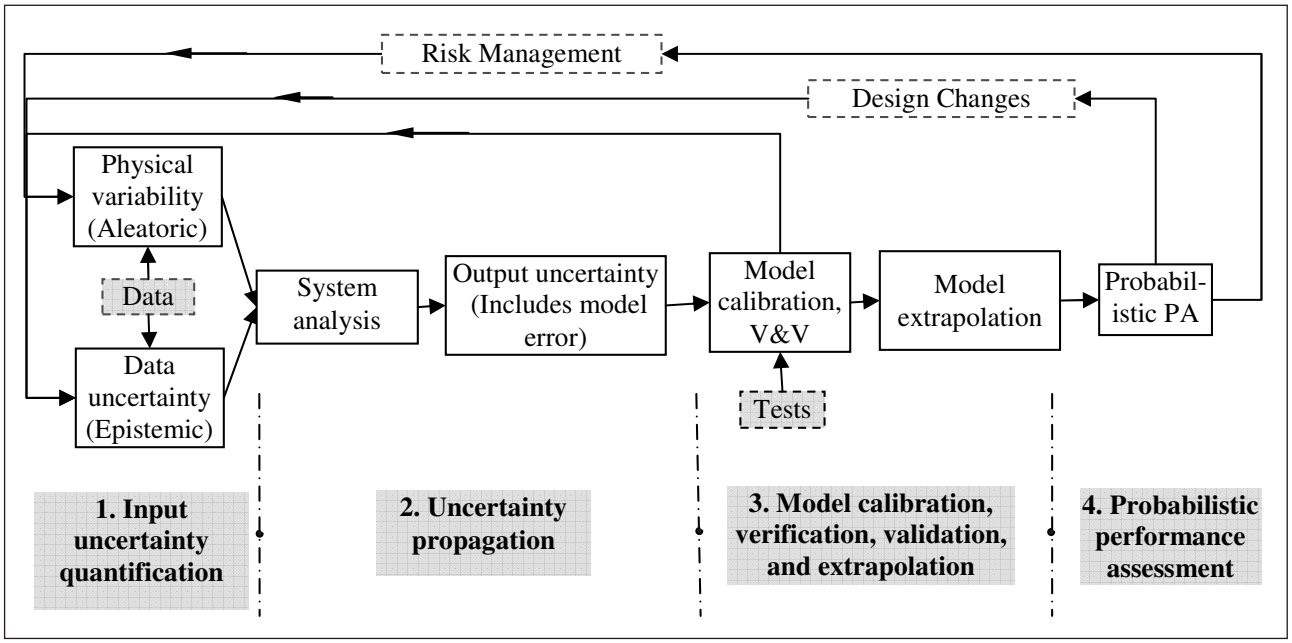

Figure 1. Uncertainty quantification, propagation and management

of the "correct" implementation of the model is called verification and assessment of the degree of agreement of the model response with the available physical observation is called validation. Model verification and validation activities help to quantify model error (both model form error and solution approximation error). A Bayesian network framework is discussed for quantifying the confidence in model prediction based on data, models, and activities at various levels of the system hierarchy. Such information is available in heterogeneous formats from multiple sources, and a consistent framework to integrate such disparate information is important.

Performance assessment: Limit state-based reliability analysis methods are available to help quantify the assessment results in a probabilistic manner. Monte Carlo simulation with high-fidelity analyses modules is computationally expensive; hence surrogate (or abstracted) models are frequently used with Monte Carlo simulation. In that case, the uncertainty or error introduced by the surrogate model also needs to be quantified.

Figure 1 shows the four groups of activities, within a conceptual framework for systematic quantification, propagation and management of various types of uncertainty. The methods discussed in this paper address all the four steps shown in Figure 1. The different steps of analysis in Figure 1 are not strictly sequential. While uncertainty has been dealt with using probabilistic as well as non-probabilistic (e.g., fuzzy sets, possibility theory, evidence theory etc.) formats in the literature, this paper will only focus on probabilistic analysis.

In Figure 1, the box "Data" in the input uncertainty quantification step includes laboratory data, historical field data, literature sources, and expert opinion. The box "Design Changes" may refer to conceptual, preliminary, or detailed design, depending on the development stage. The boxes "Design Changes" and "Risk Management" are outside the scope of this paper, although they are part of the overall uncertainty management framework.

2. Input Uncertainty Quantification

2.1 Physical Variability

Examples of model input variables with physical variability (i.e., inherent, natural variability) include:

a. Material properties (e.g., mechanical and thermal properties, soil properties, chemical properties)
b. Geometrical properties (e.g., Structural dimensions, concrete cover depth)
c. External conditions (e.g., mechanical loading, boundary conditions, physical processes such as freeze-thaw, chemical processes such as carbonation, chloride or sulfate attack)

Many uncertainty quantification studies have only focused on quantifying and propagating the inherent variability in the input parameters. Well-established statistical (both classical and Bayesian) methods are available for this purpose.

In probabilistic analysis, the sample to sample variations (random variables) in the parameters are addressed by defining them as random variables with probability density functions (PDFs). Some parameters may vary not only from sample to sample (as is the case for random variables), but also in spatial or time domain. Parameter variation over time and space can be modeled as *random processes or random fields*.

Some well-known methods for simulating random processes are spectral representation (SR) (Gurley, 1997), Karhunen-Loeve expansion (KLE) (Ghanem and Spanos, 2003, Huang *et al*., 2007; Mathelin *et al*., 2005), and polynomial chaos expansion (PCE) (Huang *et al*., 2007; Mathelin *et al*., 2005; Red-Horse and Benjamin, 2004). The PCE method has been used to represent the stochastic model output as a function of stochastic inputs.

Consider an example of representing a random process using KLE, expressed as

$$\varpi(x,\chi) = \varpi(x) + \sum_{i=1}^{\infty} \sqrt{\lambda_i}\,\xi_i(\chi) f_i(x) \qquad (2)$$

where $\varpi(x)$ is the mean of the random process $\varpi(x,\chi)$, λ_i and $f_i(x)$ are eigen values and eigen functions of $C(x_1,x_2)$, and $\xi_i(\chi)$ is a set of uncorrelated standard normal random variables (x is a space or time coordinate, and χ is an index representing different realizations of the random process). Using Equation 2, realizations of the random process $\varpi(x,\chi)$ can be easily simulated by generating samples of the random variables $\xi_i(\chi)$, and these realizations of $\varpi(x,\chi)$ can be used in the reliability analysis.

Some boundary conditions (e.g. temperature and moisture content) might exhibit a recurring pattern over shorter periods and also a trend over longer periods. Both can be numerically represented by a seasonal model using an autoregressive integrated moving average (ARIMA) method generally used for linear[1] non stationary processes[2] (Box *et al*., 1994). This method can be used to predict the temperature or the rainfall magnitudes in the future so that it can be used in the durability analysis of the structures under future environmental conditions.

It may also be important to quantify the statistical correlations between some of the input random variables. Many previous studies on uncertainty quantification simply assume either zero or full correlation, in the absence of adequate data. A Bayesian approach may be pursued for this purpose, as described in subsection 2.2.

2.2 Data Uncertainty

This section discusses methods to quantify uncertainty due to limited statistical data and measurement errors (ε_{exp}). Data may also be available in interval format (e.g., expert opinion). A Bayesian approach, consistent with the framework proposed in Figure 1, can be used in the presence of data uncertainty. The prior distributions of different physical variables and their distribution parameters can be based on available data and expert judgment, and these are updated as more data becomes available through experiments, analysis, or real-world experience.

Data qualification is an important step in the consideration of data uncertainty. All data points may not have equal weight; a careful investigation of data quality will help to assign appropriate weights to different data sets.

Sparse statistical data

For any random variable that is quantitatively described by a probability density function, there is always uncertainty in the corresponding distribution parameters due to small sample size. As testing and data collection activities are performed, the state of knowledge regarding the uncertainty changes, and a Bayesian updating approach can be implemented. The Bayesian approach also applies to joint distributions of multiple random variables, which also helps to include the uncertainty in correlations between the variables. A prior joint distribution is assumed (or individual distributions and correlations are assumed), and then updated as data becomes available.

Instead of assuming a well-known prior distribution form (e.g., uniform, normal) for sparse data sets, either empirical distribution functions, or flexible families of distributions based on the data can be constructed. A bootstrapping[3]

[1]*The current observation can be expressed as a linear function of past observations.*

[2]*A process is said to be non-stationary if its probability structure varies with the time or space coordinate.*

[3]*Bootstrapping is a data-based simulation method for statistical inference by re-sampling from an existing data set (Efron et al., 1994).*

technique can then be used to quantify the uncertainty in the distribution parameters. The *empirical distribution function* is constructed by ranking the observations from lowest to highest value, and assigning a probability value to each observation. Examples of flexible distribution families include the: Johnson family, Pearson family, gamma distribution, and stretched exponential distribution (e.g., McDonald *et al.*, 2008). Recently, Sankararaman and Mahadevan (2010) developed a likelihood-based approach to construct non-parametric probability distributions in the presence of both sparse and interval data.

Transformations have been proposed from a non-probabilistic to probabilistic format, through the maximum likelihood approach (Langley, 2000; Ross *et al.*, 2002). Such transformations have attracted the criticism that information is either added or lost in the process. Two ways to address the criticism are to: (1) construct empirical distribution functions based on interval data collected from multiple experts or experiments (Ferson *et al.*, 2007); or (2) construct flexible families of distributions with bounds on distribution parameters based on the interval data, without forcing a distribution assumption (McDonald *et al.*, 2008). These can then be treated as random variables with probability distribution functions and combined with other random variables in a Bayesian framework to quantify the overall system model uncertainty. The use of families of distributions will result in multiple probability distributions for the output, representing the contributions of both physical variability and data uncertainty. The non-parametric approach of Sankararaman and Mahadevan (2010) also has the ability to quantify the contributions of aleatory and epistemic uncertainty to the probabilistic representation of an uncertain variable.

Measurement error

The measurement error in each input variable in many studies (e.g., Barford, 1985) is assumed to be independent and identically distributed (IID) normal with zero mean and an assumed variance, i.e., $\varepsilon_{exp} \sim N(0,\sigma_{exp}^2)$. Due to the measurement uncertainty, the distribution parameter σ_{exp} cannot be obtained as a deterministic value. Instead, it is a random variable with a prior density $\tau(\sigma_{exp})$. Thus, when new data is available after testing, the distribution of σ_{exp} can be easily updated using the Bayes theorem. Another way to represent measurement error ε_{exp} is through an interval only, and not as a random variable.

3. Uncertainty Propagation Analysis

In this section, methods to quantify the contributions of different sources of uncertainty and error as they propagate through the system analysis model, including the contribution of model error, are discussed, in order to quantify the overall uncertainty in the system model output.

This section covers two issues: (1) quantification of model output uncertainty, given input uncertainty (both physical variability and data uncertainty), and (2) quantification of model error (due to both model form selection and solution approximations).

Several uncertainty analysis studies, including a study with respect to the proposed Yucca Mountain high-level waste repository, have recognized the distinction between physical variability and data uncertainty (Helton and Sallaberry, 2009a & 2009b). As a result, these methods evaluate the variability in an inner loop calculation and data uncertainty in an outer loop calculation.

3.1 Propagation of Physical Variability

Various probabilistic methods (e.g., Monte Carlo simulation and first-order or second-order analytical approximations) have been studied for the propagation of physical variability in model inputs and model parameters (Haldar and Mahadevan, 2000a, expressed through random variables and random process or fields. Stochastic finite element methods (e.g., Ghanem and Spanos, 2003; Haldar and Mahadevan, 2000b) have been developed for single discipline problems, in structural, thermal and fluid mechanics. An example of such propagation is shown in Figure 2. Several types of combinations of system analysis model and statistical analysis techniques are available:

- Monte Carlo simulation with the deterministic system analysis as a black-box (e.g., Robert and Cesalla, 2004) to estimate model output statistics or probability of regulatory compliance;
- Monte Carlo simulation with a surrogate model to replace the deterministic system analysis model (e.g., Ghanem and Spanos, 2003; Isukapalli *et al.*, 1998; Xiu and Karniadakis, 2003; Huang *et al.*, 2007), to estimate model output statistics or probability of regulatory compliance;
- Local sensitivity analysis using finite difference, perturbation or adjoint analyses, leading to estimates of the first-order or second-order moments of the output (e.g., Blischke and Murthy, 2000); and,

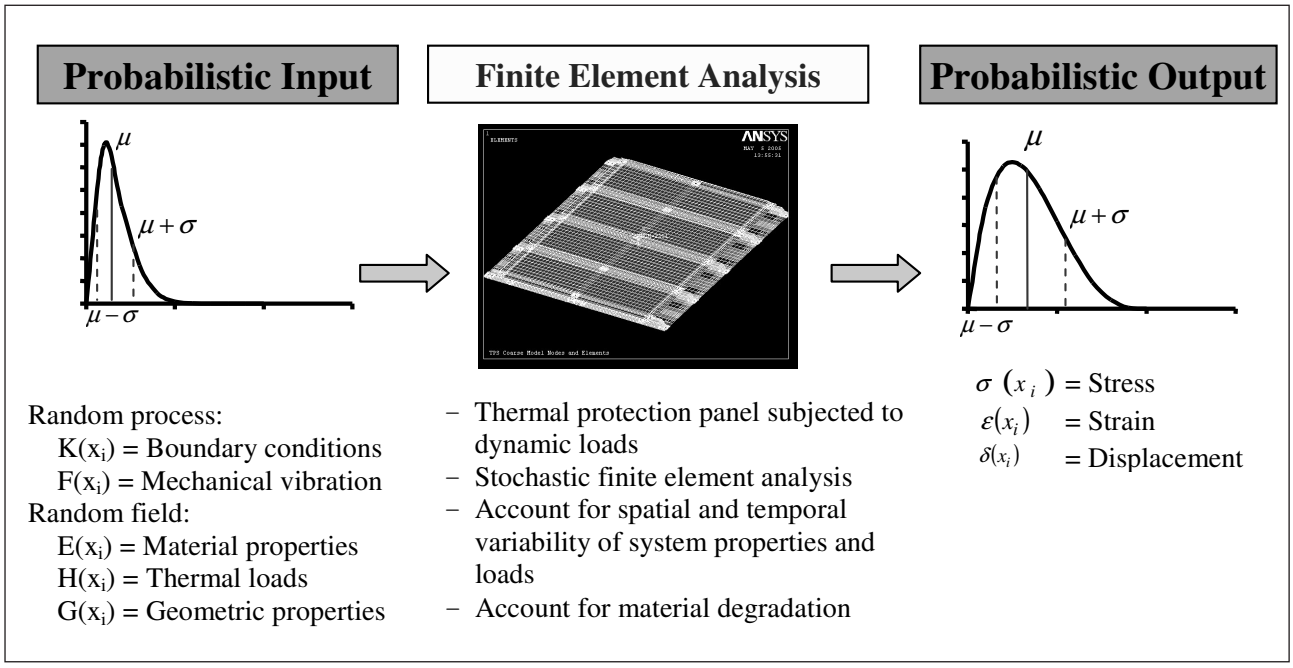

Figure 2. Example of physical variability propagation.

- Global sensitivity and effects analysis, and analysis of variance in the output (e.g., Box *et al.*, 1978).

These techniques are generic, and can be applied to engineering systems with multiple component modules and multiple physics. However, most applications of these techniques have only considered physical variability. The techniques need to include the contribution of data uncertainty and model error to the overall model prediction uncertainty. Computational effort is a significant issue in practical applications, since these techniques involve a number of repeated runs of the system analysis model. The system analysis may be replaced with an inexpensive surrogate model in order to achieve computational efficiency; this is discussed in Section 3.3 of this report. Efficient Monte Carlo techniques have also been pursued to reduce the number of system model runs, include *Latin hypercube sampling* (LHS) (Mckay *et al*., 1979; Farrar *et al*., 2003) and *importance sampling* (Mahadevan and Raghothamachar, 2000; Zou *et al*. 2003).

When multiple requirements are defined, computation of the overall probability of satisfying multiple performance criteria requires integration over a multidimensional space defined by unions and intersections of individual events (of satisfaction or violation of individual criteria).

3.2 Propagation of Data Uncertainty

Three types of data uncertainty were discussed in Section 2. Sparse point data results in uncertainty about the parameters of the probability distributions describing quantities with physical variability. In that case, uncertainty propagation analysis takes a nested implementation. In the outer loop, samples of the distribution parameters are randomly generated, and for each set of sampled distribution parameter values, probabilistic propagation analysis is carried out as in Section 3.1. This results in the computation of multiple probability distributions of the output, or confidence intervals for the estimates of probability of failure.

In the case of measurement error, choice of the uncertainty propagation technique depends on how the measurement error is represented. If the measurement error is represented as a random variable, it is simply added to the measured quantity, which is also a random variable due to physical variability. Thus a sum of two random variables may be used to include both physical variability and measurement error in a quantity of interest. If the measurement error is represented as an interval, one way to implement probabilistic analysis is to represent the interval through families of distributions or upper and lower bounds on probability distributions, as discussed in Section 2.2.3. In that case, multiple probabilistic analyses, using the same nested approach as in the case of sparse data, can be employed to generate

multiple output distributions or confidence intervals for the model output. The same approach is possible for interval variables that are only available as a range of values, as in the case of expert opinion.

Propagation of uncertainty is conceptually very simple, but computationally quite expensive to implement, especially when both physical variability and data uncertainty are to be considered. The presence of both types of uncertainty requires a nested implementation of uncertainty propagation analysis (simulation of data uncertainty in the outer loop and simulation of physical variability in the inner loop). If the system model runs are time-consuming, then uncertainty propagation analysis could be prohibitively expensive. One way to overcome the computational hurdle is to use an inexpensive surrogate model to replace the detailed system model, as discussed next.

3.3 Surrogate Models

Surrogate models (also known as response surface models) are frequently used to replace the expensive system model, and used for multiple simulations to quantify the uncertainty in the output. Many types of surrogate modeling methods are available, such as linear and nonlinear regression, polynomial chaos expansion, Gaussian process modeling (e.g., Kriging model), splines, moving least squares, support vector regression, relevance vector regression, neural nets, or even simple look-up tables. For example, Goktepe *et al.*, 2006 used neural network and polynomial regression models to simulate expansion of concrete specimens under sulfate attack. All surrogate models require training or fitting data, collected by running the full-scale system model repeatedly for different sets of input variable values. Selecting the sets of input values is referred to as statistical design of experiments, and there is extensive literature on this subject. Two types of surrogate modeling methods are discussed below, that might achieve computational efficiency while maintaining high accuracy in output uncertainty quantification. The first method expresses the model output in terms of a series expansion of special polynomials such as Hermite polynomials, and is referred to as a stochastic response surface method (SRSM). The second method expresses the model output through a Gaussian process, and is referred to as Gaussian process modeling.

Stochastic response surface method (SRSM)

The common approach for building a surrogate or response surface model is to use least squares fitting based on polynomials or other mathematical forms based on physical considerations. In SRSM, the response surface is constructed by approximating both the input and output random variables and fields through series expansions of standard random variables (e.g. Isukapalli *et al.*, 1998; Xiu and Karniadakis, 2003; Huang *et al.*, 2007). This approach has been shown to be efficient, stable and convergent in several structural, thermal and fluid flow problems. A general procedure for SRSM is as follows:

a. Representation of random inputs (either random variables or random processes) in terms of Standard Random Variables (SRVs) by K-L expansion, as in Equation 2.
b. Expression of model outputs in chaos series expansion. Once the inputs are expressed as functions of the selected SRVs, the output quantities can also be represented as functions of the same set of SRVs. If the SRVs are Gaussian, the output can be expressed a Hermite polynomial chaos series expansion in terms of Gaussian variables. If the SRVs are non-Gaussian, the output can be expressed by a general Askey chaos expansion in terms of non-Gaussian variables (Ghanem and Spanos, 2003).
c. Estimation of the unknown coefficients in the series expansion. The improved probabilistic collocation method (Isukapalli *et al.*, 1998) is used to minimize the residual in the random dimension by requiring the residual at the collocation points equal to zero. The model outputs are computed at a set of collocation points and used to estimate the coefficients. These collocation points are the roots of the Hermite polynomial of a higher order. This way of selecting collocation points would capture points from regions of high probability (Tatang *et al.*, 1997).
d. Calculation of the statistics of the output that has been cast as a response surface in terms of a chaos expansion. The statistics of the response can be estimated with the response surface using either Monte Carlo simulation or analytical approximation.

Kriging or Gaussian process models

Gaussian process (GP) models have several features that make them attractive for use as surrogate models. The primary feature of interest is the ability of the model to "account for its own uncertainty". That is, each prediction obtained from a Gaussian process model also has an associated variance, or uncertainty. This prediction variance primarily depends on the

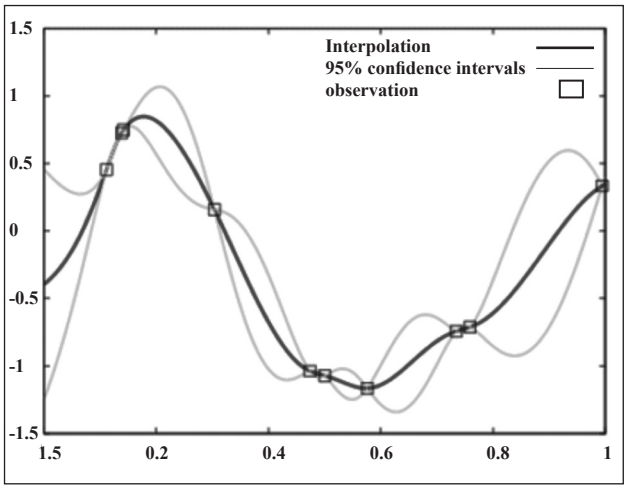

Figure 3. Gaussian process model with uncertainty bounds.

closeness of the prediction location to the training data, but it is also related to the functional form of the response. For example, see Figure 4, which depicts a one-dimensional Gaussian process model. Note how the uncertainty bounds are related to both the closeness to the training points, as well as the shape of the curve.

The basic idea of the GP model is that the output quantities are modeled as a group of multivariate normal random variables. A parametric covariance function is then constructed as a function of the inputs. The covariance function is based on the idea that when the inputs are close together, the correlation between the outputs will be high. As a result, the uncertainty associated with the model prediction is small for input values that are close to the training points, and large for input values that are not close to the training points. In addition, the GP model may incorporate a systematic trend function, such as a linear or quadratic regression of the inputs (in the notation of Gaussian process models, this is called the mean function, while in Kriging it is often called a trend function). The effect of the mean function on predictions which interpolate the training data is small, but when the model is used for extrapolation, the predictions will follow the mean function very closely.

Within the GP modeling technique, it is also possible to adaptively select the design of experiments to achieve very high accuracy. The method begins with an initial GP model built from a very small number of samples, and then one intelligently chooses where to generate subsequent samples to ensure the model is accurate in the vicinity of the region of interest. Since the GP model provides the expected value and variance of the output quantity, the next sample may be chosen in the region of highest variance, if the objective is to minimize the prediction variance. The method has been shown to be both accurate and computationally efficient for arbitrarily shaped functions (Bichon *et al*., 2007).

3.4 Sensitivity Analysis

Sensitivity analysis serves several important functions: (1) identification of dominant variables or sub-models, thus helping to focus data collection resources efficiently; (2) identification of insignificant variables or sub-models of limited significance, helping to reduce the size of the problem and computational effort; and (3) quantification of the contribution of solution approximation error. Both local and global sensitivity analysis techniques are available to investigate the quantitative effect of different sources of variation (physical parameters, models, and measured data) on the variation of the model output. The primary benefit of sensitivity analysis to uncertainty analysis is to enable the identification of which physical parameters have the greatest influence on the output (Campolongo *et al*., 2000; Saltelli *et al*., 2000).

Sensitivity analysis can be local or global. Local sensitivity analysis utilizes first-order derivatives of system output quantities with respect to the parameters. It is usually performed for a nominal set of parameter values. Global sensitivity analysis typically uses statistical sampling methods, such as Latin Hypercube Sampling, to determine the total uncertainty in the system output over the entire range of the input uncertainty and to apportion that uncertainty among the various parameters.

3.5 Model Error Quantification

Model errors may relate to governing equations, boundary and initial condition assumptions, loading description, and approximations or errors in solution algorithms (e.g., truncation of higher order terms, finite element discretization, curve-fitting models for material damage such as S-N curve). Overall model error may be quantified by comparing model prediction and experimental observation, properly accounting for uncertainties in both. This overall error measure combines both model form and solution approximation errors, and so it needs to be considered in two parts. Numerical errors in the model prediction can be quantified first, using sensitivity analysis,

uncertainty propagation analysis, discretization error quantification, and truncation (residual) error quantification. The measurement error in the input variables can be propagated to the prediction of the output. The error in the prediction of the output due to the measurement error in the input variables is approximated by using a first-order sensitivity analysis (Rebba *et al*., 2006). Then the model form error can be quantified based on all the above errors, following the approach illustrated for a heat transfer problem by Rebba *et al*., 2006.

Solution approximation error

Several components of prediction error, such as discretization error (denoted by ε_d) and uncertainty propagation analysis error (ε_s) can be considered. Several methods to quantify the discretization error in finite element analysis are available in the literature. However, most of these methods do not quantify the actual error; instead, they only quantify some indicator measures to facilitate adaptive mesh refinement. The Richardson extrapolation (RE) method comes closest to quantifying the actual discretization error (Richards, 1997). (In some applications, the model is run with different levels of resolution, until an acceptable level of accuracy is achieved; formal error quantification may not be required).

Errors in uncertainty propagation analysis (ε_s) are method-dependent, i.e. sampling error occurs in Monte Carlo methods and truncation error occurs in response surface methods (either conventional or polynomial chaos-based). For example, sampling error could be assumed to be a Gaussian random variable with zero mean and variance given by σ^2/N where N is the number of Monte Carlo runs and σ^2 is the original variance of the model output (Rubinstein, 1981) The truncation error is simply the residual error in the response surface.

Rebba *et al.* (2006), and Liang and Mahadevan (2011) used the above concept to construct a surrogate model for finite element discretization error in structural analysis, using the stochastic response surface method (SRSM). Gaussian process models may also be employed for this purpose. Both options are helpful in quantifying the solution approximation error.

Model form error

The overall prediction error is a combination of errors resulting from numerical solution approximations and model form selection. A simple way is to express the total observed error (difference between prediction and observation) as the sum of the following error sources:

$$\varepsilon_{obs} = \varepsilon_{num} + \varepsilon_{model} - \varepsilon_{exp} \quad (3)$$

where ε_{num}, ε_{model}, and ε_{exp} represent numerical solution error, model form error, and output measurement error, respectively. However solution approximation error results from multiple sources and is probably a nonlinear combination of various errors such as discretization error, round-off and truncation errors, stochastic analysis errors etc. One option is to construct a regression model consisting of the individual error components (Rebba *et al*., 2006). The residual of such a regression analysis will include the model form error (after subtracting the experimental error effects). By denoting ε_{obs} as the difference between the data and prediction, i.e., $\varepsilon_{obs} = y_{exp} - y_{pred}$, we can construct the following relation by considering a few sources of numerical solution error (Rebba *et al*., 2006):

$$\varepsilon_{obs} = f(\varepsilon_h, \varepsilon_d, \varepsilon_s) + \varepsilon_{model} - \varepsilon_{exp} \quad (4)$$

where ε_h, ε_d, and ε_s represent output error due to input parameter measurement error, finite element discretization error, and uncertainty propagation analysis error, respectively, all of which contribute to numerical solution error. Rebba *et al*., 2006 illustrated the estimation of model form error using the above concept for a one-dimensional heat conduction problem, using a polynomial chaos expansions for the input-output model as well as numerical solution error. Kennedy and O'Hagan (2001) calibrated Gaussian process surrogate models for both the input-output model and the model form error (which is also referred to as model discrepancy or model inadequacy term). Both approaches incorporate the dependence of model error on input values.

4. Model Calibration, Validation And Extrapolation

After quantifying and propagating the physical variability, data uncertainty and model error for individual components of the overall system model, the probability of meeting performance requirements (and our confidence in the model prediction) needs to be assessed based on extrapolating the model to field conditions (which are uncertain as well), where sometimes very limited or no experimental data is available. Rigorous verification, validation and calibration methods are needed to establish credibility in the modeling and simulation. Both classical and Bayesian statistical methodologies have been

investigated during recent years. The methods have the capability to consider multiple output quantities or a single model output at different spatial and temporal points.

This section discusses methods for (1) calibration of model parameters, based on observation data; (2) validation assessment of the model, based on observation data; and (3) estimation of confidence in the extrapolation of model prediction from laboratory conditions to field conditions.

4.1 Model Calibration

Two types of statistical techniques may be pursued for model calibration uncertainty, the least squares approach and the Bayesian approach. The least squares approach estimates the values of the calibration parameters that minimize the discrepancy between model prediction and experimental observation. This approach can also be used to calibrate surrogate models or low-fidelity models, based on high-fidelity runs, by treating the high-fidelity results similar to experimental data.

The second approach is Bayesian calibration (Kennedy and O'Hagan, 2001) using Gaussian process surrogate models. This approach is flexible and allows different forms for including the model errors during calibration of model parameters (McFarland and Mahadevan, 2007). Recently, Sankararaman and Mahadevan (2010) extended least squares, likelihood and Bayesian calibration approaches to include imprecise and unpaired input-output data sets, a commonly occurring situation when using historical data or data from the literature, where all the inputs to the model may not be reported.

Markov Chain Monte Carlo (MCMC) simulation is used for numerical implementation of the Bayesian updating analysis. Several efficient sampling techniques are available for MCMC, such as Gibbs sampling, the Metropolis algorithm, and the Metropolis-Hastings algorithm (Gilks *et al*., 1996).

4.2 Model Validation

Model validation involves comparing prediction with observation data (either historical or experimental) when both have uncertainty. Since there is uncertainty in both model prediction and experimental observation, it is necessary to pursue rigorous statistical techniques to perform model validation assessment rather than simple graphical comparisons, provided data is even available for such comparisons. Statistical hypothesis testing is one approach to quantitative model validation under uncertainty, and both classic and Bayesian statistics have been explored. Classical hypothesis testing is a well-developed statistical method for accepting or rejecting a model based on an error statistic (see e.g., Trucano *et al*., 2001). Validation metrics have been investigated in recent years based on Bayesian hypothesis testing (Zhang and Mahadevan, 2003; Mahadevan and Rebba, 2005; Rebba and Mahadevan, 2006), reliability-based methods (Rebba and Mahadevan, 2008), and risk-based decision analysis (Jiang and Mahadevan, 2007a & 2007b). Ling and Mahadevan (2012) provide detailed discussion of the interpretations of various metrics, their mathematical relationships, and implementation issues, with the example of a MEMS device reliability prediction problem and validation data.

In Bayesian hypothesis testing, we assign prior probabilities for the null and alternative hypotheses; let these be denoted as $P(H_0)$ and $P(H_a)$ such that $P(H_0) + P(H_a) = 1$. Here H_0: model error < allowable limit, and H_a: model error > allowable limit When data D is obtained, the probabilities are updated as $P(H_0 \mid D)$ and $P(H_a \mid D)$ using the Bayes theorem. Then a Bayes factor (Jeffreys, 1961) B is defined as the ratio of likelihoods of observing D under H_0 and H_a; i.e., the first term in the square brackets on the right hand side of Eq. (12).

$$\frac{P(H_0 \mid D)}{P(H_a \mid D)} = \left[\frac{P(D \mid H_0)}{P(D \mid H_a)}\right]\frac{P(H_0)}{P(H_a)} \tag{4}$$

If $B > 1$, the data gives more support to H_0 than H_a. Also the confidence in H_0, based on the data, comes from the posterior null probability $P(H_0 \mid D)$, which can be rearranged from above Eq. as .

$$\frac{P(H_0)B}{P(H_0)B + 1 - P(H_0)}$$

Typically, in the absence of prior knowledge, we may assign equal probabilities to each hypothesis and thus $P(H_0) = P(H_a) = 0.5$. In that case, the posterior null probability can be further simplified to $B/(B+1)$. Thus a B value of 1.0 represents 50% confidence in the null hypothesis being true.

The Bayesian hypothesis testing is also able to account for uncertainty in the distribution parameters (mentioned in Section 2). For such problems, the validation metric (Bayes factor) itself becomes a random variable. In that case, the probability of

the Bayes factor exceeding a specified value can be used as the decision criterion for model acceptance/ rejection.

Notice that model validation only refers to the situation when controlled, target experiments are performed to evaluate model prediction, and both the model runs and experiments are done under the same set of input and boundary conditions. The validation is done only by comparing the outputs of the model and the experiment. Once the model is calibrated, verified and validated, it may be investigated for confidence in extrapolating to field conditions different from laboratory conditions. This is discussed in the next section.

4.3 Overall Uncertainty Quantification

While individual methods for calibration, verification, and validation have been developed as mentioned above, it is necessary to integrate the results from these activities for the purpose of overall uncertainty quantification in the model prediction. This is not trivial because of several reasons. First, the solution approximation errors calculated as a result of the verification process need to be accounted for during calibration, validation, and prediction. Second, the result of validation may lead to a binary result, i.e. the model is accepted or rejected; however, even when the model is accepted, it is not completely correct. Hence, it is necessary to account for the degree of correctness of the model in the prediction. Third, calibration and validation are performed using independent data sets and it is not straightforward to compute their combined effect on the overall uncertainty in the response.

The issue gets further complicated when system-level behavior is predicted based on a hierarchy of models. As the complexity of the system under study increases, there may be several components and subsystems at multiple levels of hierarchy, which integrate to form the overall multi-level system. Each of these components and subsystems are represented using component-level and subsystem-level models which are mathematically connected to represent the overall system model which is used to study the underlying system. In each level, there is a computational model with inputs, parameters, and outputs, experimental data (hopefully available for calibration and validation separately), and several sources of uncertainty – physical variability, data uncertainty (sparse or imprecise data, measurement errors, expert opinion), and model uncertainty (parameter uncertainty, solution approximation errors and model form error).

Recent studies by the author and coworkers have demonstrated that the Bayes network methodology provides an efficient and powerful tool to integrate multiple levels of models, associated sources of uncertainty and error, and available data at multiple levels and in multiple formats. While the Bayesian approach can be used to perform calibration and validation individually for each model in the multi-level system, it is not straightforward to integrate the information from these activities in order to compute the overall uncertainty in the system-level prediction. Sankararaman and Mahadevan (2012) extend the Bayesian approach to integrate and propagate information from verification, calibration, and validation activities in order to quantify the margins and uncertainties in the overall system level prediction.

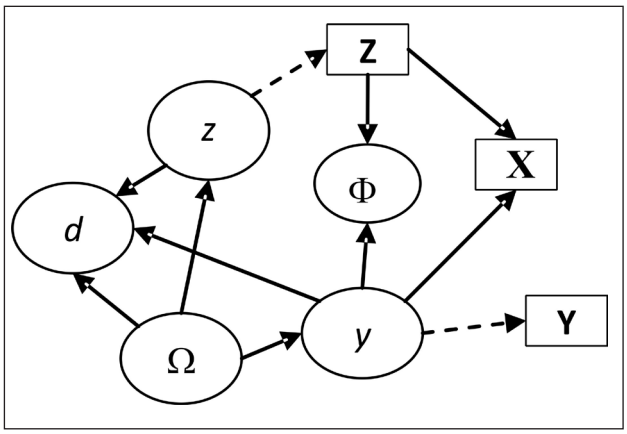

Figure 4. Bayes network.

Bayes networks (Jensen and Jensen, 2001) are directed acyclic graphical representations with nodes to represent the random variables and arcs to show the conditional dependencies among the nodes. Data in any one node can be used to update the statistics of all other nodes. This property makes the Bayes network a powerful tool to integrate information generated from multiple activities and to quantify the uncertainty in prediction under actual usage conditions (Mahadevan and Rebba, 2005).

Figure 4 shows an illustrative Bayes network for confidence extrapolation. An ellipse represents a random variable and a rectangle represents observed data. A solid line arrow represents a conditional probability link, and a dashed line arrow represents the link of a variable to its observed data if available.

The probability densities of the variables **Ω,** z, and *y* are updated using the validated data **Y**. The updated statistics of **Ω**, *z*, and *y* are then used to estimate the updated statistics of the decision variable *d* (i.e., assessment metric). In addition, both model prediction and predictive experiments are related to input variables **X** via physical parameters **Φ**. Note that there is no observed data available for d; yet we are able to calculate the confidence in the prediction of *d*, by making use of observed data in several other nodes and propagation of posterior statistics through the Bayes network.

The Bayes network thus links the various simulation codes and corresponding experimental observations to facilitate two objectives: (1) uncertainty quantification and propagation, and (2) confidence assessment in system behavior prediction in the application domain, based on data from the laboratory domain, expert opinion, and various computational models at different levels of the system hierarchy.

5. Conclusion

Uncertainty quantification in performance assessment involves consideration of three sources of uncertainty – inherent variability, information uncertainty, and model errors. This paper surveyed probabilistic methods to quantify the uncertainty in model-based prediction due to each of these sources, and addressed them in four stages – input characterization based on data; propagation of uncertainties and errors through the system model; model calibration, validation and extrapolation; and performance assessment. Flexible distribution families as well as a non-parametric Bayesian approach were discussed to handle sparse data and interval data. Methods to quantify model errors resulting from both model form selection and solution approximation were discussed. Bayesian methods were discussed for model calibration, validation and extrapolation. An important issue is computational expense, when iterative analysis between multiple codes is necessary. Uncertainty quantification multiplies the computational effort of deterministic analysis by an order of magnitude. Therefore the use of surrogate models, sensitivity and screening analyses, and first-order approximations of overall output uncertainty, are available to reduce the computational expense.

Many of the methods described in the paper have been applied to mechanical systems that are small in size, or time-independent, and the uncertainties considered were not very large. None of these simplifications are available in the case of long-term performance assessment of civil infrastructure systems, and real-world data to validate long-term model predictions are not available. Thus the extrapolations are based on laboratory data or limited term observations, and come with large uncertainty. The application of the methods described in this paper to such complex systems needs to be investigated. However, it should be recognized that the benefit of uncertainty quantification is not so much in predicting the actual failure probability or similar measures, but in facilitating engineering decision making, such as comparing different design and analysis options, performing sensitivity analyses, and allocating resources for uncertainty reduction through further data collection and/or model refinement.

Acknowledgement

The research described in this paper by the author and his students/colleagues has been funded by many sources during the past decade. A partial listing the recent sources includes: (1) National Science Foundation (IGERT project on Reliability and Risk Assessment and Management at Vanderbilt University); (2) Sandia National Laboratories (Bayesian framework for model validation, calibration and error estimation); (3) U. S. Department of Energy (uncertainty quantification in micro-electro-mechanical systems (MEMS) reliability prediction; long-term durability of cementitious barriers); (4) National Aeronautics and Space Administration (space vehicle performance uncertainty quantification; uncertainty quantification in diagnosis and prognosis; Bayes network development for testing resource allocation); (5) U. S. Air Force Office of Scientific Research (multi-disciplinary uncertainty analysis of aircraft components); and (6) Federal Aviation Administration (uncertainty quantification in fracture mechanics simulation of rotorcraft components). The support is gratefully acknowledged.

References

1. ANSYS Inc. 2000, 'Ansys user's manual', Technical Report, Ansys Inc.
2. Bichon, BJ, Eldred, MS, Swiler, LP, Mahadevan, S & McFarland, JM 2007, 'Multimodal reliability assessment for complex engineering applications using efficient global optimization,' Proceedings of 9th AIAA Non-Deterministic Approaches Conference, Waikiki, HI.
3. Barford, NC 1985, Experimental measurements: precision, error, and truth, Wiley, NewYork.
4. Blischke, WR & Murthy, DNP 2000, Reliability: modeling, prediction, and optimization, Wiley, New York.

5. Box, GEP, Hunter, WG & Hunter JS 1978, Statistics for experimenters, an introduction to design, data analysis, and model building, Wiley Interscience.
6. Box, GEP, Jenkins, GM & Reinsel GC 1994, Time series analysis forecasting and control, 3rd edition, Prentice Hall, Englewood Cliffs, New Jersey.
7. Chen, D 2006, Computational framework for durability assessment of reinforced concrete structures under coupled deterioration processes, Ph.D. Dissertation, Department of Civil and Environmental Engineering, Vanderbilt University.
8. Ferson, S, Kreinovich, V, Hajagos, J, Oberkampf W & Ginzburg, L 2007, 'Experimental Uncertainty Estimation and Statistics for Data Having Interval Uncertainty,' Sandia National Laboratories Technical Report, SAND2003-0939, Albuquerque, New Mexico.
9. Ghanem, R & Spanos, P 2003, Stochastic Finite Elements: A Spectral Approach, Springer-Verlag, New York.
10. Gilks, WR, Richardson, S & Spiegelhalter, DJ 1996, Markov Chain Monte Carlo in Practice, Interdisciplinary Statistics Series, Chapman and Hall, Boca Raton, Florida.
11. Glimm, J & Sharp, DH 1999, 'Prediction and the quantification of uncertainty,' Physica D, 133(1-4), 152–170.
12. Gulikers, J 2006, 'Considerations on the reliability of service life predictions using probabilistic approach,' Journal de Physique IV, 136, 233-241, 2006.
13. Gurley, KR 1997, Modeling and simulation of non-Gaussian processes, PhD thesis, University of Notre Dame, April 1997.
14. Haldar, A & Mahadevan, S 2000a, Probability, Reliability and Statistical Methods in Engineering Design, J. Wiley & Sons, New York.
15. Haldar, A & Mahadevan, S 2000b, Reliability Analysis using the Stochastic Finite Element Method, J. Wiley & Sons, New York.
16. Hanson, KM 1999, 'A framework for assessing uncertainties in simulation predictions,' Physica D, 133(1-4), 179–188.
17. Helton, JC & Sallabery, CJ 2009a, 'Conceptual basis for the definition and calculation of expected dose in performance assessments for the proposed high-level radioactive waste repository at Yucca Mountain, Nevada,' Reliability Engineering and System Safety 94, 677- 698.
18. Helton, JC & Sallabery, CJ 2009b, 'Computational implementation of sampling-based approaches to the calculation of expected dose in performance assessments for the proposed high-level radioactive waste repository at Yucca Mountain, Nevada,' Reliability Engineering and System Safety 94, 699-721.
19. Hills, RG & Leslie, I 2003, 'Statistical validation of engineering and scientific models: Validation experiments to application,' Sandia National Laboratories Technical Report, SAND2003-0706, Albuquerque, New Mexico.
20. Hills, RG & Trucano, TG 2002, 'Statistical validation of engineering and scientific models: A maximum likelihood based metric,' Sandia National Laboratories Technical Report, SAND2001-1783, Albuquerque, New Mexico.
21. Huang, S, Mahadevan, S & Rebba, R 2007, 'Collocation-based stochastic finite element analysis for random field problems,' Probabilistic Engineering Mechanics, 22, 194–205, 2007.
22. Isukapalli, SS, Roy, A & Georgopoulos, PG 1998, 'Stochastic response surface methods (SRSMs) for uncertainty propagation: Application to environmental and biological systems,' Risk analysis, 18(3), 351–363.
23. Jeffreys, H 1961, Theory of Probability, 3rd edition, Oxford University Press, London.
24. Jensen, FV & Jensen, FB 2001, Bayesian Networks and Decision Graphs, Springer-Verlag, New York.
25. Jiang, X & Mahadevan, S 2007a, 'Bayesian risk-based decision method for model validation under uncertainty,' Reliability Engineering and System Safety, 92(6), 707–718.
26. Kennedy, MC & O'Hagan, A 2001, 'Bayesian calibration of computer models (with discussion),' Journal of the Royal Statistical Society, Series B, 63(3), 425–464.
27. Langley, RS 2000, 'A unified approach to the probabilistic and possibilistic analysis of uncertain systems,' ASCE Journal of Engineering Mechanics, 126, 1163-1172.
28. Liang, B. & Mahadevan, S 2011 , "Error and Uncertainty Quantification and Sensitivity Analysis of Mechanics Computational Models," *International Journal for Uncertainty Quantification*, accepted, in press.
29. Ling, Y. & Mahadevan, S 2011, 'Quantitative Model Validation Metrics: New Insights,' *Reliability Engineering & System Safety*, under review.
30. Mahadevan, S & Rebba, R 2005, 'Validation of reliability computational models using Bayes networks,' Reliability Engineering and System Safety, 87(2), 223–232.
31. Mahadevan, S & Raghothamachar, P 2000, 'Adaptive simulation for system reliability analysis of large structures,' Computers and Structures, 77(6), 725–734.
32. McDonald, M, Zaman, K and Mahadevan, S 2011, "Representation and First-Order Approximations for Propagation of Aleatory and Distribution Parameter Uncertainty," *AIAA Journal*.
33. McFarland, JM 2008, Uncertainty analysis for computer simulations through validation and calibration, PhD dissertation, Vanderbilt University, Nashville, TN.
34. Pandey, MD 1998, 'An effective approximation to evaluate multinormal integrals,' Structural Safety, 20(1), 51–67.
35. Rackwitz, R & Fiessler B 1978, 'Structural reliability under combined load sequences,' Computers and Structures, 9(5), 489–494.
36. Rebba, R 2005, Model Validation and Design under Uncertainty. PhD dissertation, Vanderbilt University, Nashville, TN, USA.
37. Rebba, R & Mahadevan, S 2006, 'Model predictive capability assessment under uncertainty,' AIAA Journal, 44(10), 2376–2384.
38. Rebba, R & Mahadevan, S 2008, 'Computational methods for model reliability assessment,' Reliability Engineering and System Safety, 93, 1197–1207.
39. Rebba, R, Mahadevan, S & Huang, S 2006, 'Validation and error estimation of computational models,' Reliability Engineering and Safety System, 91(10-11), 1390–1397.
40. Red-Horse, JR & Benjamin, AS 2004, 'A probabilistic approach to uncertainty quantification with limited information,' Reliability Engineering and System Safety, 85, 183–190, 2004.
41. Robert, CP & Casella, G 2004, Monte Carlo Statistical Methods. 2nd ed. Springer-Verlag, New York.
42. Ross, TJ, Booker, JM & Parkinson, WJ 2002, Fuzzy Logic and Probability Applications: Bridging the Gap, Society for Industrial and Applied Mathematics, Philadelphia, PA.
43. Richards, SA 1997, 'Completed Richardson extrapolation in space and time,' Communications in Numerical Methods in Engineering, 13(7), 558–573.

44. Rubinstein, RY 1981, Simulation and the Monte Carlo method. New York, Wiley.
45. Saltelli, A, Chan, K & Scott, EM 2000, Sensitivity Analysis, John Wiley & Sons.
46. Sankararaman, S & Mahadevan, S 2011, "Likelihood-Based Representation of Epistemic Uncertainty due to Sparse Point Data and Interval Data," *Reliability Engineering and System Safety*.
47 Sankararaman, S., Y. Ling, & Mahadevan, S 2011, "Model Validation and Uncertainty Quantification of Fatigue Crack Growth Analysis," *Engineering Fracture Mechanics*, accepted, in press.
48. Sankararaman, S. and Mahadevan, S 2012, "Roll-up of Calibration and Validation Results towards System-Level QMU," Proceedings of 15th AIAA Non-Deterministic Approaches Conference, Honolulu, Hawaii.
49. Urbina, A & Mahadevan, S 2009, 'Uncertainty quantification in hierarchical computational model development,' Proceedings of 12th AIAA Non-Deterministic Approaches Conference, Palm Springs, California.
50. Xiu, D & Karniadakis, GE 2003, 'Modeling uncertainty in flow simulations via generalized polynomial chaos,' Journal of Computational Physics, 187(1), 137-167.
51. Zaman, K., McDonald, M. & Mahadevan, S 2011, "A Probabilistic Approach for Representation of Interval Uncertainty," *Reliability Engineering and System Safety,* Vol. 96, No. 1, pp. 117-130, 2011.
52. Zaman, K., McDonald, M. & Mahadevan, S 2011 "Probabilistic Framework for Propagation of Aleatory and Epistemic Uncertainty," *ASME Journal of Mechanical Design*, accepted, in press.
53. Zhang, R & Mahadevan, S 2003, 'Bayesian methodology for reliability model acceptance,' Reliability Engineering and System Safety, 80(1), 95–103.
54. Zou, T, Mahadevan, S & Mourelatos, Z 2003, 'Reliability-based evaluation of automotive wind noise quality,' Reliability Engineering and System Safety, 82(2), 217–224.

Life Cycle Reliability and Safety Engineering
Vol.1 Issue 3 (2012) 45-60

Probabilistic Assessment of Strengths of Corrosion Affected RC Beams

Kapilesh Bhargava[1], Yasuhiro Mori[2] and A. K. Ghosh[3]
[1] *Nuclear Recycle Board, Bhabha Atomic Research Center, Mumbai, India,*
[2] *Graduate School of Environmental Studies, Nagoya University, Nagoya, Japan*
[3] *Health Safety and Environment Group, Bhabha Atomic Research Center, Mumbai, India*
kapilesh_66@yahoo.co.uk

Abstract

Corrosion of reinforcement causes premature deterioration in reinforced concrete (RC) structures and reduces their intended residual service life. Damages to RC structures due to reinforcement corrosion generally manifest in the form of expansion, cracking and eventual spalling of the cover concrete, loss of steel cross-sectional area, and loss of bond between corroded reinforcement and surrounding cracked concrete. These damages may sometime result in structural failure. This paper initially presents predictive models for time-dependent damages in corrosion-affected RC beams, recognized as loss of mass and cross-sectional area of reinforcing bar, and loss of concrete section owing to the peeling of cover concrete. Then these models have been used to present analytical formulations for evaluating time-dependent flexural and shear strengths for corroded RC beams based on the standard composite mechanics expressions for RC sections. Further by considering variability in the identified basic variables that could affect the time-dependent strengths of corrosion-affected RC beams, an attempt is made in this paper to present simple estimations for the time-dependent mean strengths and time-dependent coefficient of variation (c.o.v.) associated with the strengths for a typical simply supported RC beam. Comparison of presented simple estimations of mean strengths and c.o.v. associated with strengths has been made with those obtained using Monte Carlo Simulation.

Keywords: reinforcement corrosion; annual mean corrosion rate; time-dependent flexural strength; time-dependent shear strength; time-dependent c.o.v.; Latin Hypercube Sampling

1. Introduction

The basic safety requirements of a nuclear power plant (NPP) include the safe shutdown of the reactor, to remove decay heat and to limit the release of radioactivity to the environment. Safety evaluation of the structures is an important issue for any NPP, which has to be carried out to take care of number of factors including the ageing effects, if any. As NPP structures age, a number of degradation mechanisms start affecting the load carrying capacity and serviceability of these structures. Some of the degradation mechanisms for RC structures include corrosion of steel reinforcement, alkali-silica reaction, freeze-thaw damage, sulphate attack, etc. Out of these mechanisms, corrosion of steel has been identified as being the most widespread and predominant mechanism responsible for the deterioration of RC structures. Corrosion causes the reduction of reinforcement cross-sectional area which in extreme forms, can be significant enough to reduce the strength of structural members below the minimum requirements. It also results in cracking and spalling of cover concrete due to formation of expansive of corrosion products, and reduction of bond between the corroded reinforcement and concrete, thereby resulting in further structural damage. By proper control and monitoring of the reinforcement corrosion, premature failure of RC structures can be prevented. Also the assessment of performance of corrosion damaged RC structures to withstand extreme events during their anticipated service life would help in arriving decisions pertaining to the inspection, repair, strengthening, replacement and demolition of such structures.

In this paper initially, predictive models are presented for the quantitative assessment of time-dependent damages in RC beams, recognized as loss of concrete section owing to the peeling of cover concrete and loss of mass and cross-sectional area of reinforcing bar. Then these models have been used

to present analytical formulations for evaluating time-dependent flexural and shear strengths of corroded RC beams based on the standard composite mechanics expressions for RC sections. For the corroded RC beams, loss of flexural and shear strengths would be mainly due to loss of cross-section for concrete and reinforcing steel. The scope of flexural strength estimation has been limited to either by the yielding of tensile reinforcement or by the crushing of concrete in compression zone. Although the continued rebar corrosion would also affect the composite action of concrete and reinforcing steel due to bond deterioration between them, the evaluation of time-dependent flexural strength due to loss of bond has not been considered in the present study. The performance of the presented formulations has been evaluated through their ability to reproduce the available experimental trends. The paper further presents probabilistic assessment of time-dependent strengths for a typical simply supported corroded RC beam. The basic variables that can affect time-dependent strengths for a corroded RC beam are identified as material strengths of concrete and reinforcement, modulus of elasticity of reinforcing steel plus expansive corrosion products combine, creep-coefficient for concrete, dimensions of the beams and annual mean corrosion rate. By considering variability in these variables, simple estimations of following are presented: (i) time-dependent mean strength and c.o.v. associated with the strength, and (ii) time-dependent mean degradation function and c.o.v. associated with the degradation function, wherein, the degradation function is defined as the ratio of strength at time, *t*, to the initial strength for an un-corroded RC beam. The estimation of time-dependent strengths and degradation functions are carried out for two limit states: (a) flexural failure, and (b) shear failure. An attempt has also been made to present analytical models for estimating time-dependent c.ov. associated with the degradation functions. The performance of simple estimations of mean strengths and c.o.v. associated with strengths and degradation functions has been evaluated by comparing their results with those obtained using Monte Carlo Simulation.

2. Corrosion Propagation in RC Beams

A quantitative description of corrosion propagation is generally given in terms of the loss of metal per unit surface area per unit time and this can be obtained by measuring the mass differences in the reinforcing steel with reference to its surface area exposed to corrosion. Most of the non-destructive techniques used for the corrosion monitoring are based on the electrochemical measurements, in which the annual mean corrosion rate is estimated in terms of the corrosion current density, i_{COR} (Val et al. 1998). This i_{COR} can be transformed into the loss of metal by using the diffusion law related to the growth of expansive corrosion products (Liu and Weyers 1998; Bhargava et al. 2003; Bhargava et al. 2005; Bhargava et al. 2006). Reduction in cross-sectional area of reinforcing bars shall result in the reduced flexural and shear strengths of the corrosion-damaged RC beams (Bhargava 2008). Corrosion of reinforcement causes cracking, and eventually spalling and/or peeling of the cover concrete. Reduction in concrete section owing to the peeling of cover concrete shall also result in the reduced flexural and shear strengths of the corrosion-damaged RC beams (Rodriguez et al. 1997). Following sub-sections present estimation of time-dependent loss of concrete and steel sections for the purpose of corrosion propagation in RC beams.

2.1 Loss of Concrete Section

Reduction in concrete section occurs due to peeling of bottom, top and side covers to the reinforcements. Methodology for estimating the time required for peeling of cover concrete is adopted from Bhargava (2008). Figure 1 shows the crack propagating condition for the concrete block with two reinforcing bars of initial diameter D_i. The bars have clear cover, *C*, and the centre line spacing, S_b. Due to the formation of corrosion products; the propagation of radial splitting cracks shall take place in all the directions to the same distance R_c, i.e., the radius of crack front. With $R_i = (D_i / 2)$ and $R_o = (R_i + C)$, the cover concrete is assumed to be fully cracked when R_c becomes equal to R_o (Bhargava et al. 2006). Bazant (1979) reported that failure may occur in two different modes in case of R_c becoming equal to R_o: (i) when $C > (S_b - D_i)/2$, then the failure shall consist of peeling of cover concrete, and (ii) when the spacing of bars, S_b, is large (say $S_b > 6 \cdot D_i$), the failure shall consist of inclined cracking. Based on the suggested failure philosophy of Bazant (1979), the cover peeling time for top, bottom, and side covers are evaluated using corrosion cracking model of Bhargava et al. (2006).

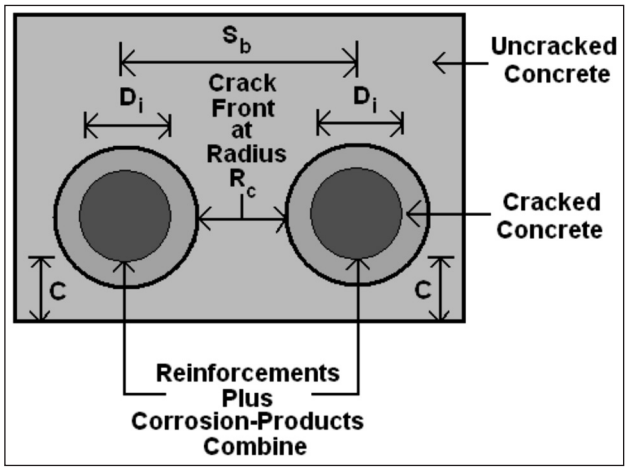

Figure 1: Crack propagating condition for concrete block with two reinforcing bars due to reinforcement corrosion (Bhargava 2008)

2.2 Loss of Reinforcing Steel

Corrosion process is a dynamic process; growth of expansive corrosion products is given by Eq. 1 (Liu and Weyers 1998; Bhargava et al. 2003; Bhargava et al. 2005; Bhargava et al. 2006).

$$\frac{dW_r}{dt} = \frac{k_p}{W_r} \tag{1}$$

where W_r = mass of expansive corrosion products (mg/mm); t = corrosion time (years); k_p = function of rate of metal loss. k_p is expressed by Eq. (2) (Bhargava et al. 2006).

$$k_p = 2.48614 \cdot \pi \cdot D_i \cdot i_{COR} \tag{2}$$

where D_i = initial diameter of reinforcement (mm); i_{COR} = annual mean corrosion rate (μA/cm^2). Various parameters associated with the loss of reinforcing steel at time, t, since initiation of corrosion are evaluated by Eqs. (3 – 6) (Bhargava 2008).

$$W_s(t) = 2.42362 \cdot \sqrt{D_i \cdot i_{COR} \cdot t} \tag{3}$$

$$D_r(t) = \sqrt{D_i^2 - 0.39245 \cdot \sqrt{D_i \cdot i_{COR} \cdot t}} \tag{4}$$

$$A_{cor}(t) = 0.30835 \cdot \sqrt{D_i \cdot i_{COR} \cdot t} \tag{5}$$

$$X(t) = \frac{1}{2} \cdot \left[D_i - D_r(t)\right] \tag{6}$$

where, $W_s(t)$ = mass of steel per unit length of the reinforcement (mg/mm) getting consumed by corrosion process; $D_r(t)$ = reduced bar diameter (mm); $A_{cor}(t)$ = loss of cross-sectional area of steel (mm^2); $X(t)$ = corrosion penetration depth (mm).

2.3 Predictions for Loss of Reinforcing Steel – Comparison with Experimental Results

Analytical predictions for W_s and X are made for the available experimental data by using Eqs. (3 and 6) (Rasheeduzzafar et al. 1992; Andrade et al. 1993; Liu 1996; Rodriguez et al. 1997; Mangat and Elgarf 1999; Torres-Acosta 1999). Figure 2 presents the comparison between W_s^P and W_s^E for the available experimental data. Similarly, Figure 3 presents the comparison between X^P and X^E for the same experimental data. The superscripts P and E correspond to the analytically predicted and the experimental observed values, respectively. The data in both the figures are presented by different symbols to represent the analytical predictions made for different experimental data. It is clear from the same figures that the deviation between the analytically predicted and the experimentally observed values is generally less than by a factor of two and this is a considerably good agreement in view of the large variability associated with the corrosion phenomena.

To test the goodness of Eqs. (3 and 6), the correlation between the predicted and experimental values is estimated. Assuming that $x = W_s^P$ (the independent variable) and $y = W_s^E$ (the dependent variable), the values of both r^2_{xy} and s^2_{yx} are estimated as 0.895 and 0.126 gm^2/cm, respectively for Eq. (3); wherein, r, is the coefficient of correlation between x and y, and, s, is the root mean square error of estimate of y on x. Similarly, by assuming $x = X^P$

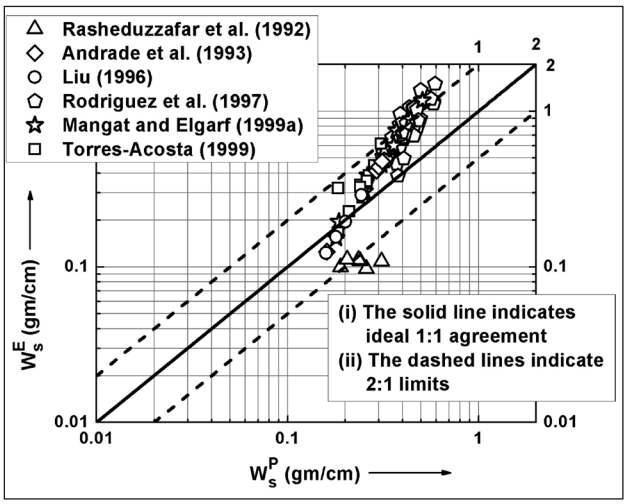

Figure 2: Comparison between experimental W_s^E and predicted W_s^P using Eq. (3)

and $y = X^E$, the values of both r^2_{xy} and s^2_{yx} are estimated as 0.851 and 0.028 mm^2, respectively for Eq. (6). The quite high values associated with r^2_{xy} in both the predictions suggest that Eqs. (3 and 6) can be effectively used for estimating the values of W_s and X for the reinforced concrete members exposed to the corrosive environment.

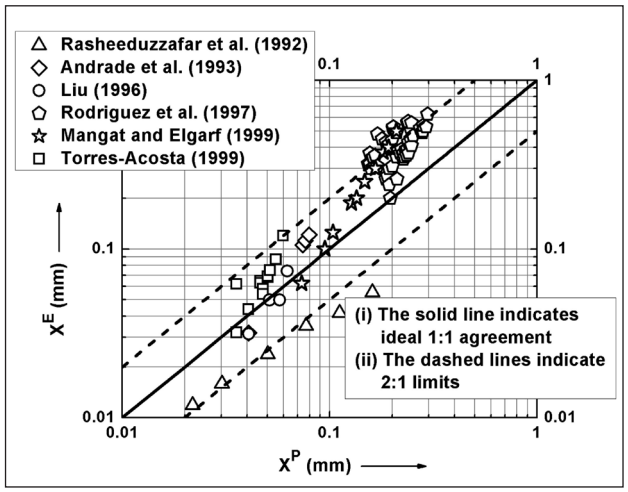

Figure 3: Comparison between experimental X^E and predicted X^P using Eq. (6)

3. Time Dependent Strengths of Corroded RC Beams

Figure 4 shows typical cross-section of a simply supported un-corroded RC beam, which is subjected to flexure and shear under loads. This doubly reinforced beam has *b* and *D* as its width and depth, respectively. The beam is reinforced with bottom tensile reinforcing steel bars having initial area, A_{sti} and top compressive reinforcing steel bars having initial area, A_{sci}. The distance between the centroid of tensile steel and the edge of the compression zone is *d* (also known as effective depth). The shear stirrups are having an initial area, A_{svi} and are provided at spacing, S_v.

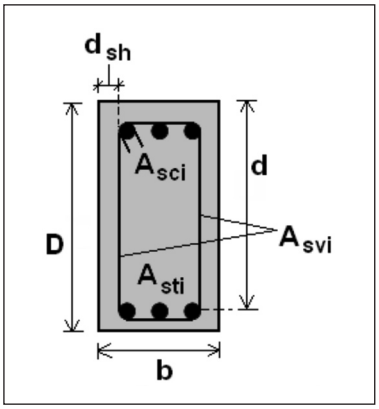

Figure 4: Typical cross-section of an un-corroded RC beam

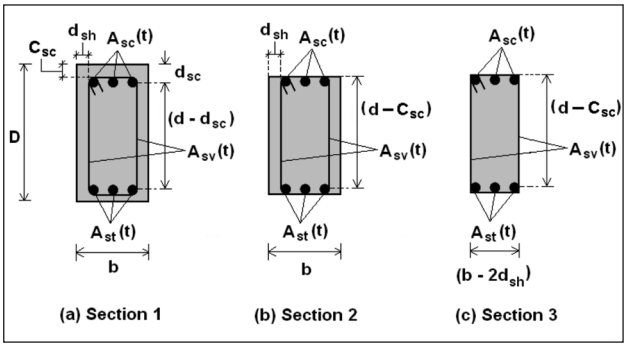

Figure 5: Different schemes of deteriorated reinforced concrete sections for corroded RC beams (Rodriguez et al. 1997)

Figure 5 shows three representative schemes of deteriorated reinforced concrete sections for a corrosion affected RC beam (Rodriguez et al. 1997). The Section 1 indicates the intact concrete section, wherein the peeling of covers is yet to occur. The section 2 indicates the reduced concrete section due to the peeling of top and bottom covers. In section 2, effective depth to tensile reinforcement of the beam is reduced to $(d - C_{sc})$, wherein C_{sc} is clear cover to the compression steel. The section 3 indicates the reduced concrete section due to the peeling of all the top, bottom and side covers. In section 3, effective depth to tensile reinforcement and effective width of the beam are reduced to $(d - C_{sc})$ and $(b - 2 \cdot d_{sh})$ respectively; wherein d_{sh} is the clear cover to the shear stirrups. All the three sections also indicate the reduced sections of main bars and shear stirrups at time, *t*. It is very important to point out that, the reduced concrete section for a deteriorated corroded beam at time, *t*, is governed by the individual cover peeling time for top, bottom and side covers and in some cases it may be different than those shown in Figure 5. Formulations for time-dependent flexural and shear strengths of corroded RC beams are proposed with the considerations that the loss of strengths is mainly due to reduction in cross-sectional areas of reinforcing steel and concrete.

3.1 Time Dependent Flexural Strength

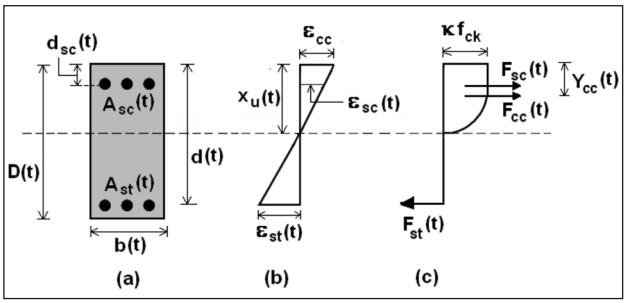

Figure 6: Formulation of time-dependent flexural strength of corroded RC beams: (a) beam section; (b) strain distribution (BIS 2000); (c) stress distribution (BIS 2000)

Figure 6(a) shows the typical beam section for a doubly reinforced corroded beam, wherein the different notations pertaining to dimensions and reinforcing steels have their usual meanings at time, t, from the initiation of corrosion. Figures. 6(b and c) present the strain and stress distribution across the cross-section of the beam, respectively, wherein ε_{cc} is the ultimate strain in concrete and is taken as 0.0035 (BIS 2000).

In the same figures, $\varepsilon_{st}(t)$ and $\varepsilon_{sc}(t)$ are the strains in tensile and compressive reinforcements, respectively; $x_u(t)$ is the height of compression zone; $F_{cc}(t)$ and $F_{sc}(t)$ are the forces of compression in concrete and compressive steel, respectively; $Y_{cc}(t)$ is the distance of point of application of $F_{cc}(t)$ from the edge of compression zone; $F_{st}(t)$ is the force of tension in tensile steel; f_{ck} is the 28 day characteristic cube compressive strength of concrete (BIS 2000). Uniform corrosion around the surface and along the length of the bar is assumed. Considering the simple bending theory, $\varepsilon_{st}(t)$ and $\varepsilon_{sc}(t)$ are given by Eq. (7).

$$\varepsilon_{st}(t) = \left[\frac{d(t) - x_u(t)}{x_u(t)}\right] \cdot \varepsilon_{cc} \; ;$$
$$\varepsilon_{sc}(t) = \left[\frac{x_u(t) - d_{sc}(t)}{x_u(t)}\right] \cdot \varepsilon_{cc} \qquad (7)$$

The total force of compression, $F_c(t)$ is given by Eq. (8).

$$F_c(t) = F_{cc}(t) + F_{sc}(t) \qquad (8)$$

$F_{cc}(t)$ and $Y_{cc}(t)$ are given by Eq. (9).

$$F_{cc}(t) = \kappa \cdot f_{ck} \cdot b(t) \cdot x_u(t) \cdot \left[\frac{3 \cdot \varepsilon_{cc} - 0.002}{3 \cdot \varepsilon_{cc}}\right]$$
$$Y_{cc}(t) = x_u(t) - x_u(t) \cdot \left[\frac{6 \cdot \varepsilon_{cc} - \left(\frac{0.000004}{\varepsilon_{cc}}\right)}{12 \cdot \varepsilon_{cc} - 0.008}\right] \qquad (9)$$

where κ = a factor which is decided based on the design compressive strength of the concrete in the structures and the partial safety factor appropriate to the material strength of concrete (BIS 2000). The force of compression in compressive steel, $F_{sc}(t)$, is given by Eq. (10).

$$F_{sc}(t) = \varepsilon_{sc}(t) \cdot E_{st} \cdot A_{sc}(t) \; ; \text{ for } \varepsilon_{sc}(t) \le \varepsilon_{sy}, \text{ and,}$$
$$F_{sc}(t) = \eta \cdot f_y \cdot A_{sc}(t) \; ; \text{ for } \varepsilon_{sc}(t) > \varepsilon_{sy} \qquad (10)$$

where f_y = yield strength of reinforcing steels; η = a factor which is decided based on the partial safety factor appropriate to material strength of reinforcing steels (BIS 2000); E_{st} = modulus of elasticity of reinforcing steel; ε_{sy} = yield strain for the reinforcing steels = $(\eta \cdot f_y / E_{st})$. In the present study, both κ and η are considered as 1.0. The distance, $Y_c(t)$, of point of application of total force of compression, $F_c(t)$, from the edge of compression zone is given by Eq. (11).

$$Y_c(t) = \frac{F_{cc}(t) \cdot Y_{cc}(t) + F_{sc}(t) \cdot d_{sc}(t)}{F_{cc}(t) + F_{sc}(t)} \qquad (11)$$

The force of tension, $F_{st}(t)$, in tensile steel is given by Eq. (12).

$$F_{st}(t) = \varepsilon_{st}(t) \cdot E_{st} \cdot A_{st}(t) \; ; \text{ for } \varepsilon_{st}(t) \le \varepsilon_{sy}, \text{ and,}$$
$$F_{st}(t) = \eta \cdot f_y \cdot A_{st}(t) \; ; \text{ for } \varepsilon_{st}(t) > \varepsilon_{sy} \qquad (12)$$

By equating the force of compression given by Eq. (8) and the force of tension given by Eq. (12), the height of compression zone $x_u(t)$ is evaluated. The flexural strength, $Mu(t)$, at time, t, is then determined by Eq. (13).

$$Mu(t) = F_{st}(t) \cdot \left[d(t) - Y_c(t)\right] \qquad (13)$$

3.2 Time Dependent Shear Strength

The permissible shear stress of concrete at time, t, from the initiation of corrosion is given by Eq. (14) (BIS 2000; SP16 1980).

$$\tau_c(t) = \frac{0.85 \cdot \sqrt{0.8 \cdot f_{ck}} \cdot \left(\sqrt{1 + 5 \cdot \beta(t)} - 1\right)}{6 \cdot \beta(t)}$$
$$\beta(t) = \frac{0.8 \cdot f_{ck} \cdot b(t) \cdot d(t)}{689 \cdot A_{st}(t)} \qquad (14)$$

The shear strength, $Vu(t)$, at time, t, is determined by Eq. (15).

$$Vu(t) = \tau_c(t) \cdot b(t) \cdot d(t) + \frac{\eta \cdot f_y \cdot A_{sv}(t) \cdot d(t)}{S_v} \qquad (15)$$

The maximum value of the shear strength of the corroded RC beam, $Vu_{max}(t)$, is given by Eq. (16) (BIS 2000).

$$Vu_{\max}(t) = \tau_{c\max} \cdot b(t) \cdot d(t) \qquad (16)$$

where τ_{cmax} = maximum shear stress of concrete for a given value of f_{ck} (BIS 2000). If calculated $Vu(t)$

is more than $Vu_{max}(t)$ then $Vu(t)$ is limited to $Vu_{max}(t)$ (BIS 2000).

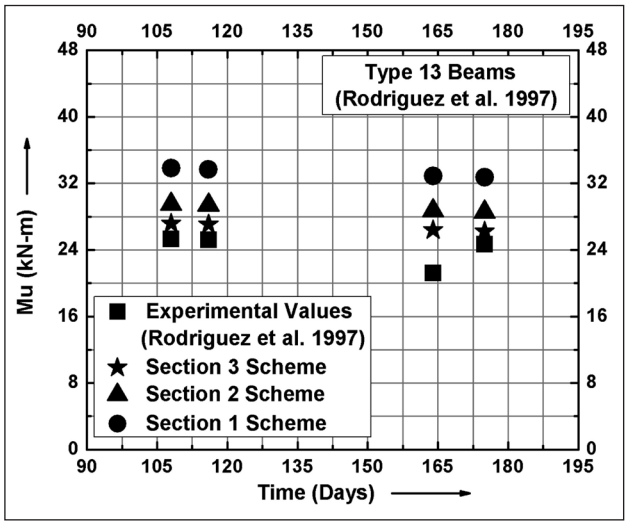

Figure 7: Time-dependent flexural strength for type 13 corroded beams of Rodriguez et al. (1997)

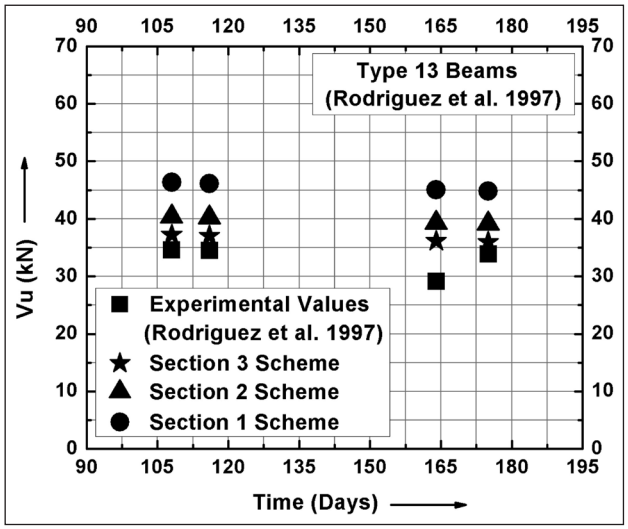

Figure 8: Time-dependent shear strength for type 13 corroded beams of Rodriguez et al. (1997)

3.3 Predictions for Time-Dependent Flexural and Shear Strengths of Corroded RC Beams – Comparison with Experimental Results

Predictions have been made for the residual flexural and shear capacity of the corrosion-degraded RC beams for which the experimental results are available (Rodriguez et al. 1997). Rodriguez et al. (1997) tested six different types of RC beams of sections 150 mm x 200 mm with spans ranging from 2050 mm to 2300 mm. The beams were provided with different ratios of tensile and compressive reinforcement, different spacing of shear reinforcement and different locations of curtailment of tensile reinforcing bars. The various reinforcing bars were corroded to different degree of corrosion in terms of attack penetration i.e. reduction in bar radius. After having corroded the reinforcement, the beams were tested up to the failure.

Figure (7 and 8) present the comparison of experimentally observed and analytically predicted values for time-dependent flexural and shear strengths, respectively, for type 13 beams of Rodriguez et al. (1997). Analytical predictions are presented for all the three deteriorated schemes for RC sections as shown in Figure 5 for comparison purposes. However, for these beams, Section 2 deteriorated scheme is expected at the end of the corrosion period. Analytical predictions are found to agree within 17 % of the experimentally observed values for flexural and shear strengths for Section 2 deteriorated scheme; this is a considerably good agreement in view of the large variability associated with the corrosion phenomena. Therefore the proposed analytical formulations for time-dependent flexural and shear strengths predict the analytical

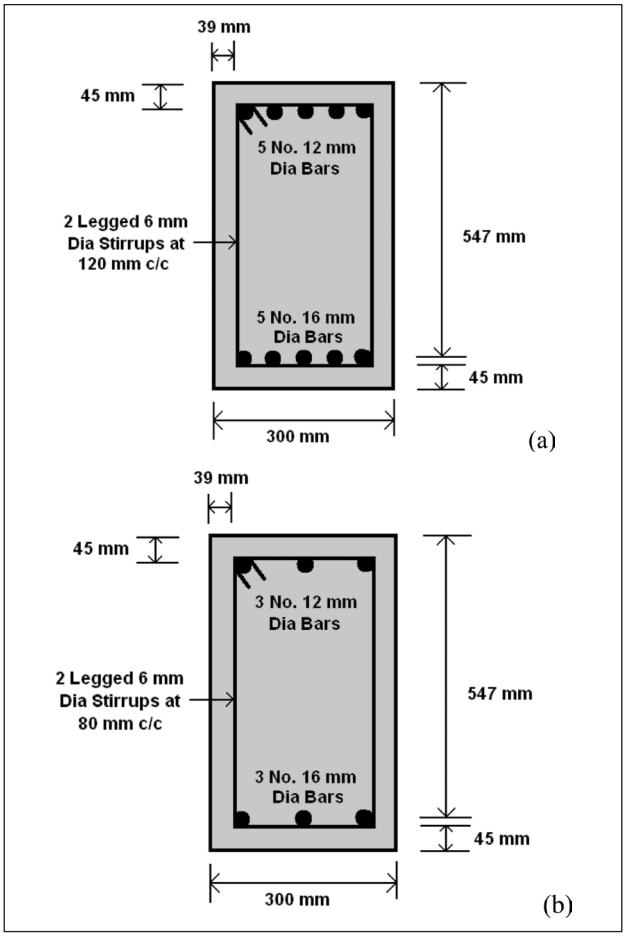

Figure 9: Typical RC beam cross-section: (a) at mid span, (b) at supports

trends which are in considerably good agreement with those of the observed experimental trends.

4. Illustration of Time Dependent Strengths of Corroded RC Beams – Probabilistic Approach

For the purpose of illustration, a simply supported RC beam with its reinforcement details as shown in Figure 9 is considered. The span of the beam is considered as 4.0 m, and it is subjected to corrosion attack. The statistical parameters for the basic variables for material strengths, dimensions and annual mean corrosion rate appropriate for the RC beam are given in Table 1. These statistical parameters are similar to the ones suggested by many researchers (Ellingwood and Ang 1974; Ellingwood 1977; Mirza et al. 1979; Mirza and MacGregor 1979a and 1979b; Ellingwood 1982; Ellingwood and Hwang 1985; Hwang et al. 1987; Israel et al. 1987; CEB-FIP 1990; ACI 1995; Frangopol et al. 1997; Enright and Frangopol 1998a and 1998b; Stewart and Rosowsky 1998; Thoft-Christensen 1998; Val et al. 1998; Hong and Zhou 1999; BIS 2000; Haldar and Mahadevan 2000; Hong 2000; Ranganathan 2000; Vu and Stewart 2000; Li 2003; Vu and Stewart 2005; Li et al. 2005).

Time-dependent flexural and shear strengths are estimated using the formulations given in the preceding sections. Since the formulations are provided based on BIS (2000) and SP16 (1980), following is adopted in the present study: (i) time-dependent flexural strength is calculated by using f_{cm} instead of $\kappa . f_{ck}$ and by using E_s instead of E_{st}, and (ii) time-dependent shear strength is calculated by using f_{cm} instead of f_{ck}.

Monte Carlo simulation is used for evaluating time-dependent mean strengths and c.o.v. associated with the strengths. Here, the "Latin Hypercube Sampling (LHS)" technique with 40 samples (Mckay et al. 1979) is used for an efficient sampling considering the variability in the variables given in Table 1. The results are presented in Figures (10 – 15) and are discussed in the following sections. The 40 random samples of the basic variables and their random combinations obtained through LHS technique are used for evaluating the sample mean of strengths and c.o.v. associated with the strengths in Figures (10 – 15). The approximated mean for strengths is evaluated by considering all the basic variables to be at their mean values. In all the figures, V_I stands for the c.o.v. of i_{COR}. Results are presented typically for a corrosion period of 60 years.

4.1 Time Dependent Flexural Strength

Figures 10(a) – 12(a) present the time-dependent flexural strength, $R_{nb}(t)$, at time t (years) from the initiation of corrosion, for different mean values of i_{COR}. In the same figures, mR_{nb} stands for the sample mean flexural strength, and R_{nb}^{m} stands for the approximated mean flexural strength. Figures. 10(b) – 12(b) present the time-dependent c.o.v., $V_{Rnb}(t)$, associated with $R_{nb}(t)$, at time t (years) from the initiation of corrosion, for different mean values of i_{COR}. These figures depict the following:

Table 1: Statistical parameters for the basic variables for material strengths, dimensions and annual mean corrosion rate

Variables		Mean	c.o.v.	Distribution
Material strengths	f_{cm}	25.8 MPa	0.18	Normal
	τ_C	0.421 MPa	0.18	Normal
	θ	2.0	0.20	Normal
	f_y	466.88 MPa	0.11	Lognormal
	E_s	200000 MPa	0.051	Lognormal
Dimensions	b	310.3 mm	0.033	Normal
	D	614.4 mm	0.017	Normal
	C_B	46.6 mm	0.123	Normal
	C_T	48.2 mm	0.105	Normal
	C_S	40.6 mm	0.099	Normal
Annual mean corrosion rate	i_{COR}	1, 3, 5 μA/cm^2	0.1, 0.2 and 0.3	Normal

Notations:
f_{cm} : Compressive strength of concrete; τ_C : Shear strength of concrete; θ: Creep coefficient; E_s : Modulus of elasticity of steel plus corrosion products combine; C_B, C_T, *and* C_S: Clear covers to bottom, top and side reinforcements, respectively.

(i) For a given i_{COR}, R_{nb}^{m} agrees well with mR_{nb} except in the time interval of 0 – 5 years, where a slight difference between them is observed. This difference is mainly attributed to the randomness associated with the time of cover peeling at bottom, top, and side resulting in the change of cross-section for the concrete. Flexural strength is mainly governed by all the basic variables (except τ_C) given in Table 1, and is a non-linear function

of those variables. Figure 6 also shows that, at time t, $R_{nb}(t)$ is evaluated after estimating various parameters, such as, beam dimensions, cross-sectional area of steels, neutral axis depth, forces of compression in concrete and compression steel and their points of application, and force of tension in tension steel and its point of application. Good agreement between the sample mean and approximated mean values of $R_{nb}(t)$ shows that the time-dependent mean flexural strength can be approximated by considering the linear terms in Taylor series expansion of performance functions for the aforementioned parameters needed to evaluate $R_{nb}(t)$ [Eqs. (5, 7 – 13)].

(ii) For a given i_{COR}, an increase in $V_{Rnb}(t)$ is observed in the time interval of 0 – 5 years for all V_I values. This is attributed to the randomness associated with the time of cover peeling at the bottom, top and side resulting in the change of cross-section for the concrete.

(iii) For a given i_{COR}, V_I has negligible effect on the mean values of the $R_{nb}(t)$; however it affects $V_{Rnb}(t)$. As V_I increases, $V_{Rnb}(t)$ also increases. This is because $R_{nb}(t)$ is a function of i_{COR}, and variation in i_{COR} values will result in the variation of corresponding $R_{nb}(t)$ values.

(iv) i_{COR} affects $R_{nb}(t)$ and $V_{Rnb}(t)$. As i_{COR} increases,

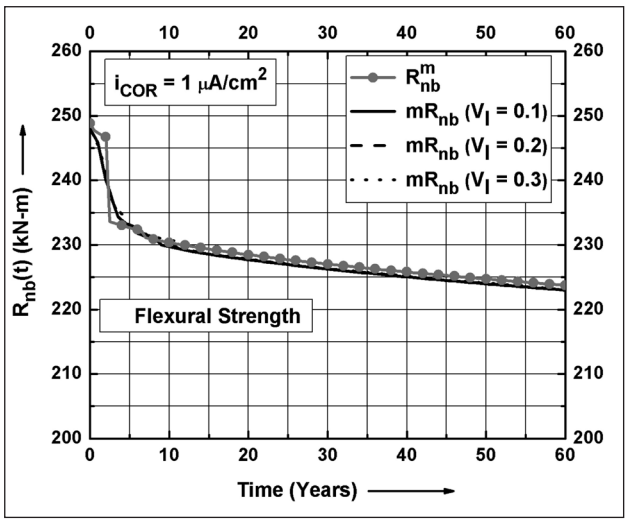

Figure 10(a): Time-dependent flexural strength (i_{COR} = 1 μA/cm²)

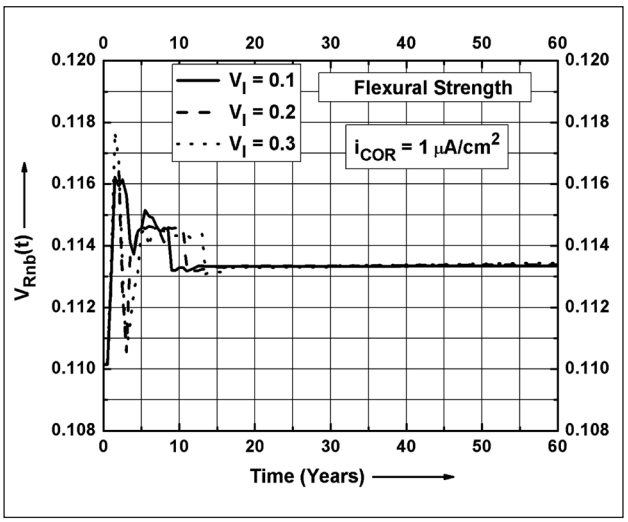

Figure 10(b): Time-dependent c.o.v. for flexural strength (i_{COR} = 1 μA/cm²)

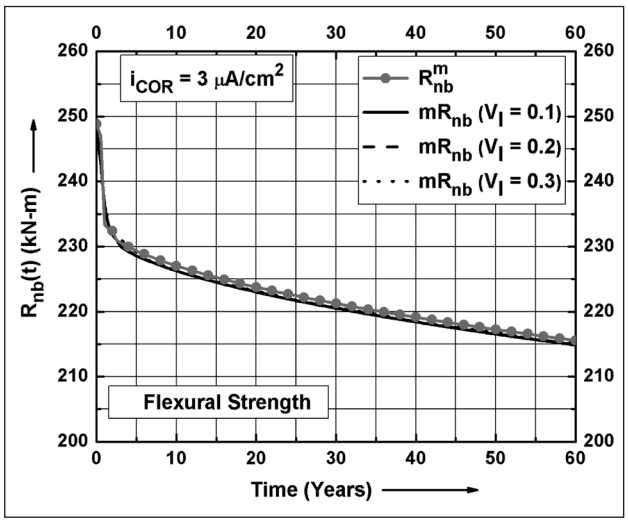

Figure 11(a): Time-dependent flexural strength (i_{COR} = 3 μA/cm²)

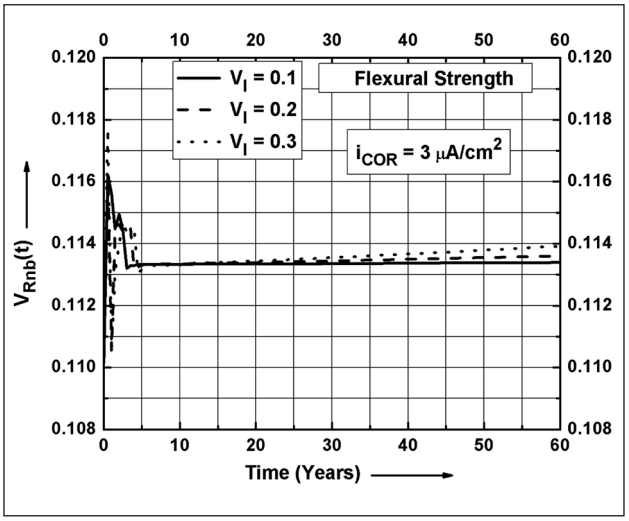

Figure 11(b): Time-dependent c.o.v. for flexural strength (i_{COR}= 3 μA/cm²)

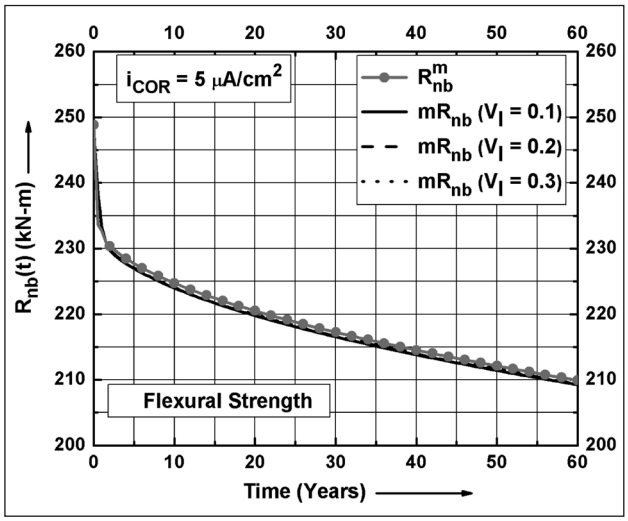

Figure 12(a): Time-dependent flexural strength (i_{COR} = 5 μA/cm²)

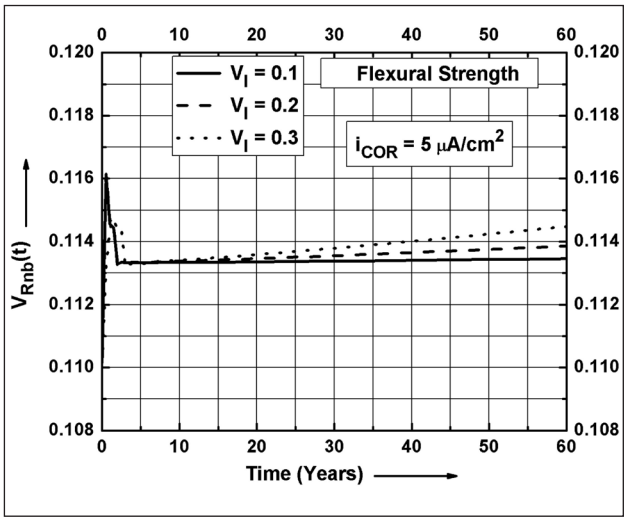

Figure 12(b): Time-dependent c.o.v. for flexural strength (i_{COR} = 5 μA/cm²)

4.2 Time Dependent Shear Strength

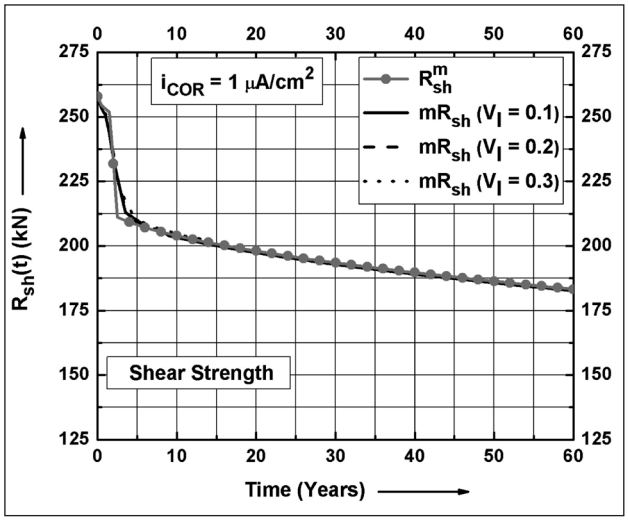

Figure 13(a): Time-dependent shear strength (i_{COR} = 1 μA/cm²)

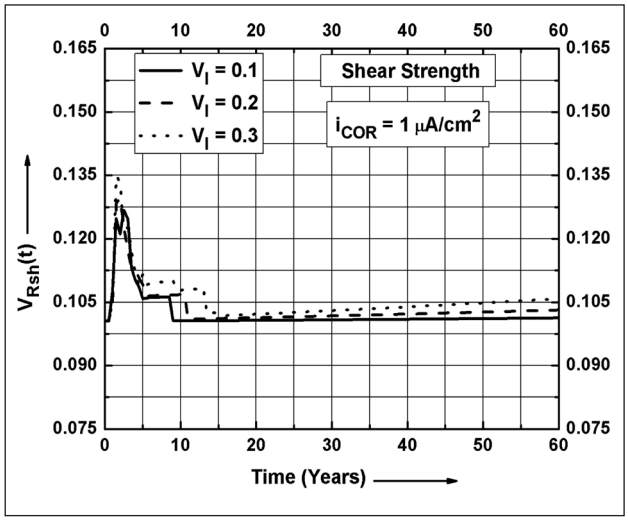

Figure 13(b): Time-dependent c.o.v. for shear strength (i_{COR} = 1 μA/cm²)

$As_{COR}(t)$ for tension steel also increases, thus further resulting in reduced $R_{nb}(t)$ and more variability for $As_{COR}(t)$. Increase in variability for $As_{COR}(t)$ will result in the increase in $V_{Rnb}(t)$ values. Here, As_{COR} is defined as the ratio of loss of cross-sectional area to the initial un-corroded area of reinforcement.

Figures. 13(a) – 15(a) present the time-dependent shear strength, $R_{sh}(t)$, at time t (years) from the initiation of corrosion, for different mean values of i_{COR}. In the same figures, mR_{sh} stands for the sample mean shear strength, and R^m_{sh} stands for the approximated mean shear strength. Figures 13(b) – 15(b) present the time-dependent c.o.v., $V_{Rsh}(t)$, associated with $R_{sh}(t)$, at time t (years) from the initiation of corrosion, for different mean values of i_{COR}. These figures depict the following:

(i) For a given i_{COR}, R^m_{sh} agrees well with mR_{sh} except in the time interval of 0 – 5 years, where a slight difference between them is observed. This difference is mainly attributed to the randomness associated with the time of cover peeling at the bottom, top, and side resulting in the change of cross-section for the concrete. Shear strength is governed by all the basic variables given in Table 1, and is a non-linear function of those variables.

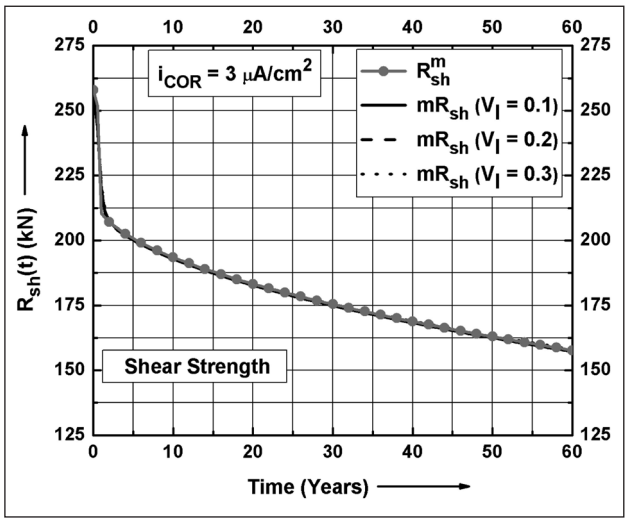

Figure 14(a): Time-dependent shear strength (i_{COR} = 3 μA/cm^2)

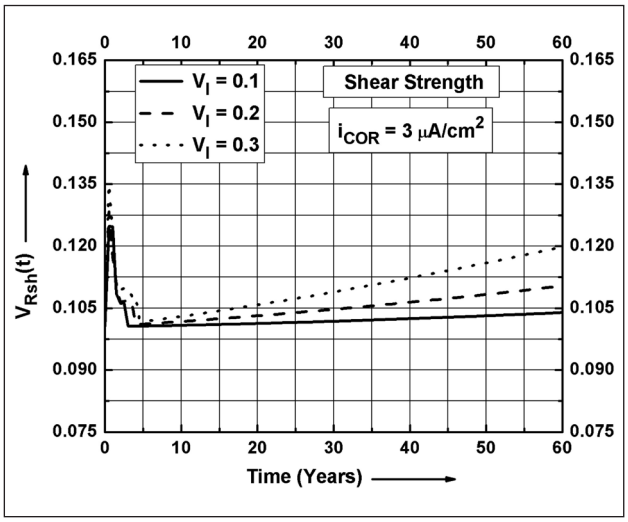

Figure 14(b): Time-dependent c.o.v. for shear strength (i_{COR} = 3 μA/cm^2)

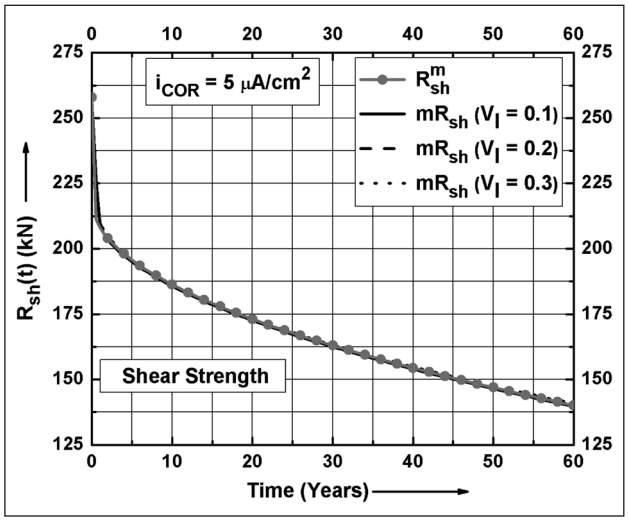

Figure 15(a): Time-dependent shear strength (i_{COR} = 5 μA/cm^2)

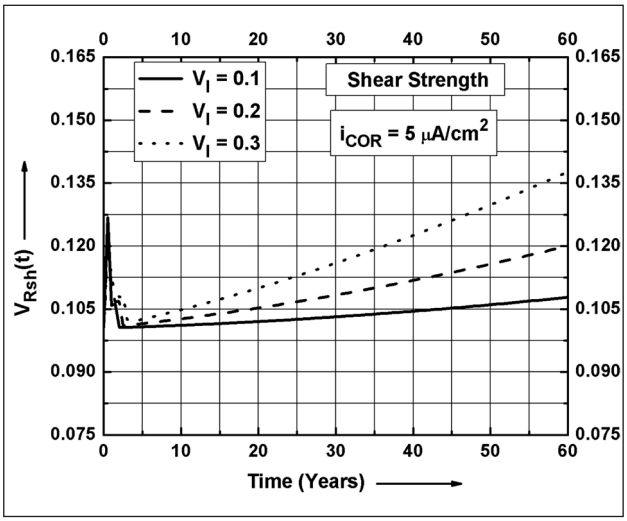

Figure 15(b): Time-dependent c.o.v. for shear strength (i_{COR}= 5 μA/cm^2)

At time t, $R_{sh}(t)$ is evaluated after estimating various parameters, such as, beam dimensions, cross-sectional area of steels, and shear strength of concrete and stirrups. Good agreement between the sample mean and approximated mean values of $R_{sh}(t)$ shows that the time-dependent mean shear strength can be approximated by considering the linear terms in Taylor series expansion of performance functions for the aforementioned parameters needed to evaluate $R_{sh}(t)$ [Eqs. (5, 14 – 16)].

(ii) For a given i_{COR}, an increase in $V_{Rsh}(t)$ is observed in the time interval of 0 – 5 years. This is attributed to the randomness associated with the time of cover peeling at the bottom, top and side resulting in the change of cross-section for the concrete.

(iii) For a given i_{COR}, V_I has negligible effect on the mean values of the $R_{sh}(t)$; however it affects $V_{Rsh}(t)$. As V_I increases, $V_{Rsh}(t)$ also increases. This is because $R_{sh}(t)$ is a function of i_{COR}, and variation in i_{COR} values will result in the variation of corresponding $R_{sh}(t)$ values.

(iv) i_{COR} affects $R_{sh}(t)$ and $V_{Rsh}(t)$. As i_{COR} increases, $As_{COR}(t)$ for shear stirrups also increases, thus further resulting in reduced $R_{sh}(t)$ and more variability for $As_{COR}(t)$. Increase in variability for $As_{COR}(t)$ will result in the increase in $V_{Rsh}(t)$ values.

(v) At time t = 0, V_{Rsh}(at t = 0) is slightly lower than V_{Rnb}(at t = 0). It is mentioned that shear strength

of beam is evaluated as sum of the shear strength contributions of concrete section and stirrups. Shear strengths of concrete section is evaluated as a product of beam dimensions and permissible shear stress of concrete, while that of stirrups is evaluated as a product of effective depth of beam, yield strength and cross-sectional area of stirrups [Eq. (14 – 16)]. Flexural strength for the given beam is mainly governed by the yielding of tensile reinforcement, and is evaluated as a product of lever arm (which is a function of effective depth of beam), yield strength and cross-sectional area of tensile reinforcement [Eq. (13)]. Since the considered variability in beam dimensions are smaller as compared to those for material strengths of concrete and steel, it may result in V_{Rsh}(at t = 0) slightly lower than V_{Rnb}(at t = 0).

5. Time Dependent Degradation Functions for Time Dependent Strengths of Corroded RC Beams

Degradation function is defined as the ratio of strength at time, t, to the initial strength for an un-corroded RC beam. Time-dependent mean degradation functions for the time-dependent flexural and shear strengths, for the considered RC beam are expressed by Eq. (17).

$$g_{nb}(t) = \frac{R_{nb}(t)}{R_{nb0}};\ g_{sh}(t) = \frac{R_{sh}(t)}{R_{sh0}} \tag{17}$$

where $R_{nb}(t)$and $R_{sh}(t)$ = flexural strength and shear strength, respectively, at time t; R_{nb0} and R_{sh0} = flexural strength and shear strength, respectively, at time t = 0; $g_{nb}(t)$ and $g_{sh}(t)$ = mean degradation functions for flexural strength and shear strength, respectively, at time t.

Figures (16 and 17) present the time-dependent mean degradation functions, $g_{nb}(t)$ and $g_{sh}(t)$, for flexural strength and shear strength, respectively, for different mean values of i_{COR}. With the increase in i_{COR}, reduction in $g_{nb}(t)$ and $g_{sh}(t)$ is observed. This is attributed to the reduction in R_{nb}^{m} and R_{sh}^{m}, respectively due to increase in i_{COR}.

6. Analytical Estimation of Time Dependent C.O.V. Associated With Degradation Function

Since time-dependent strengths and degradation functions for corroded RC beam are related to each other by Eq. (17), the time-dependent c.o.v. associated with degradation functions is evaluated by Eq. (18) (Benjamin and Cornell 1970)

$$V_{Gnb}(t) = \sqrt{\frac{V_{Rnb}^2(t) - V_{Rnb0}^2}{1 + V_{Rnb0}^2}};\quad V_{Gsh}(t) = \sqrt{\frac{V_{Rsh}^2(t) - V_{Rsh0}^2}{1 + V_{Rsh0}^2}} \tag{18}$$

where $V_{Gnb}(t)$ and $V_{Gsh}(t)$ = c.o.v. associated with degradation functions for flexural strength and shear strength, respectively, at time t; $V_{Rnb}(t)$and $V_{Rsh}(t)$ = c.o.v. associated with flexural strength and shear strength, respectively, at time t; V_{Rnb0} and V_{Rsh0} = c.o.v. associated with initial flexural strength and initial shear strength, respectively, at time t = 0. The estimation of $V_{Rnb}(t)$, $V_{Rsh}(t)$ $V_{Gnb}(t)$ and $V_{Gsh}(t)$ is addressed in the following sections.

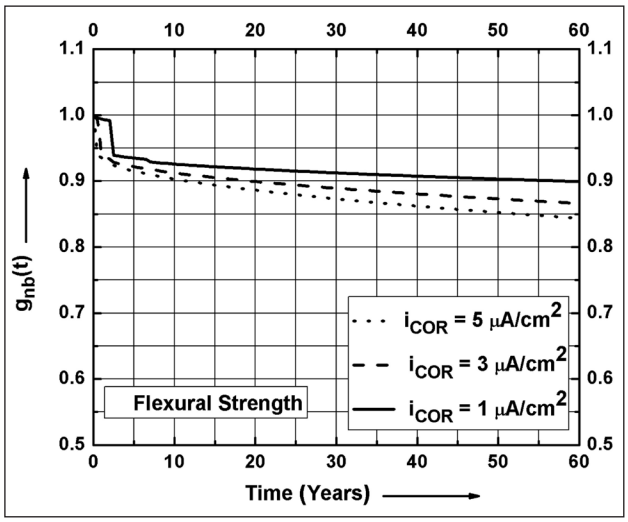

Figure 16: Time-dependent mean degradation function for flexural strength

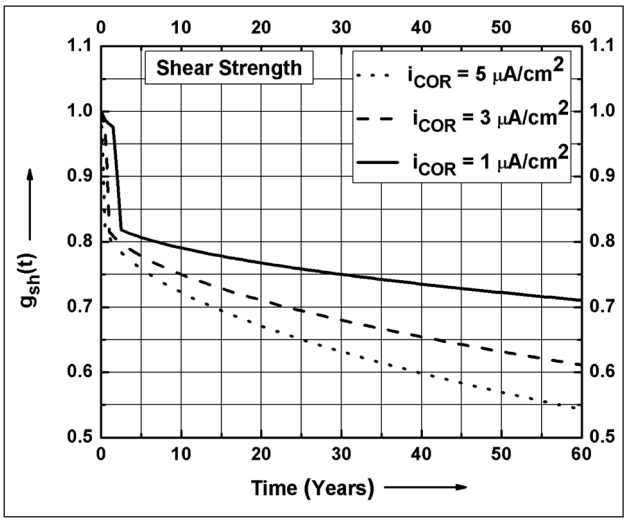

Figure 17: Time-dependent mean degradation function for shear strength

6.1 Analytical Estimation of $V_{Rnb}(t)$ and $V_{Gnb}(t)$

At time t, the flexural strength, $R_{nb}(t)$, is estimated by Eq. (13) [performance functions for $R_{nb}(t)$] for tension failure. $R_{nb}(t)$ is a function of $F_{st}(t)$, $Y_c(t)$ and $d(t)$. At time t, if σ_{Rnbt} is the standard deviation associated with $R_{nb}(t)$ then the first-order approximation of variance of $R_{nb}(t)$ is given by Eq. (19) (Haldar and Mahadevan 2000).

$$\sigma^2_{Rnbt} = \left(\frac{\partial R_{nb}(t)}{\partial F_{st}(t)}\right)^2 \cdot \sigma^2_{Fstt} + \left(\frac{\partial R_{nb}(t)}{\partial Y_c(t)}\right)^2 \cdot \sigma^2_{Yct} + \left(\frac{\partial R_{nb}(t)}{\partial d(t)}\right)^2 \cdot \sigma^2_{dt} \quad (19)$$

where, σ_{Fstt} = standard deviation associated with $F_{st}(t)$; σ_{Yct} = standard deviation associated with $Y_c(t)$; σ_{dt} = standard deviation associated with $d(t)$. First order approximation for σ_{Fstt}, σ_{Yct} and σ_{dt} are given by Eqs. (20 – 22).

$$\sigma^2_{Fstt} = \left(\frac{\partial F_{st}(t)}{\partial E_s}\right)^2 \cdot \sigma^2_{Es} + \left(\frac{\partial F_{st}(t)}{\partial X_u(t)}\right)^2 \cdot \sigma^2_{Xut} + \left(\frac{\partial F_{st}(t)}{\partial d(t)}\right)^2 \cdot \sigma^2_{dt} + \left(\frac{\partial F_{st}(t)}{\partial i_{COR}}\right)^2 \cdot \sigma^2_{icor} \quad \text{for } \varepsilon_{st}(t) \le \varepsilon_{sy} \quad (20a)$$

$$\sigma^2_{Fstt} = \left(\frac{\partial F_{st}(t)}{\partial f_y}\right)^2 \cdot \sigma^2_{fy} + \left(\frac{\partial F_{st}(t)}{\partial i_{COR}}\right)^2 \cdot \sigma^2_{icor} \text{ ; for } \varepsilon_{st}(t) > \varepsilon_{sy} \quad (20b)$$

$$\sigma^2_{Yct} = \left(\frac{\partial Y_c(t)}{\partial F_{cc}(t)}\right)^2 \cdot \sigma^2_{Fcct} + \left(\frac{\partial Y_c(t)}{\partial Y_{cc}(t)}\right)^2 \cdot \sigma^2_{Ycct} + \left(\frac{\partial Y_c(t)}{\partial F_{sc}(t)}\right)^2 \cdot \sigma^2_{Fsct} + \left(\frac{\partial Y_c(t)}{\partial d_{sc}(t)}\right)^2 \cdot \sigma^2_{dsct} \quad (21)$$

$$\sigma_{dt} = \sqrt{\sigma^2_D + \sigma^2_{CB}} \text{ ; (Before peeling of top cover)} \quad (22a)$$

$$\sigma_{dt} = \sqrt{\sigma^2_D + \sigma^2_{CB} + \sigma^2_{CT}} \text{ ;(After peeling of top cover)} \quad (22b)$$

where, σ_{Es}, σ_{fy}, σ_{icor}, σ_D, σ_{CB} and σ_{CT} = standard deviation associated with E_s, f_y, i_{COR}, D, C_B and C_T, respectively, and are evaluated based on the statistical parameters for these variables given in Table 1. σ_{Xut} is the standard deviation associated with $X_u(t)$, and the first-order approximation of variance of $X_u(t)$ for different strain conditions in reinforcing steels shall give its value. σ_{Fcct}, σ_{Ycct}, σ_{Fsct} and σ_{dsct} are the standard deviations associated with $F_{cc}(t)$, $Y_{cc}(t)$, $F_{sc}(t)$ and $d_{sc}(t)$, respectively, and the first-order approximation of variances of $F_{cc}(t)$, $Y_{cc}(t)$ $F_{sc}(t)$ and $d_{sc}(t)$ shall give their respective values. The time-dependent c.o.v., $V_{Rnb}(t)$, associated with $R_{nb}(t)$ is estimated from Eq. (23).

$$V_{Rnb}(t) = \frac{\sigma_{Rnbt}}{R_{nb}(t)} \quad (23)$$

At time t = 0, $V_{Rnb}(t = 0) = V_{Rnb0}$. Once V_{Rnb0} and $V_{Rnb}(t)$ are known, $V_{Gnb}(t)$ is evaluated from Eq. (18).

6.2 Analytical Estimation of $V_{Rsh}(t)$ and $V_{Gsh}(t)$

The shear strength, $R_{sh}(t)$, at time t, is estimated by Eq. (15) [performance functions for $R_{sh}(t)$]. $R_{sh}(t)$ is a function of $\tau_C(t)$, $b(t)$, $d(t)$, f_y and i_{COR}. For the considered corroded RC beam [Figure 9], $\tau_C(t)$ is not calculated by Eq. (14), rather τ_C is considered as a separate random variable with statistical parameters provided in Table 1. At time t, if σ_{Rsht} is the standard deviation associated with $R_{sh}(t)$ then the first-order approximation of variance of $R_{sh}(t)$ is given by Eq. (24) (Haldar and Mahadevan 2000).

$$\sigma^2_{Rsht} = \left(\frac{\partial R_{sh}(t)}{\partial \tau_C}\right)^2 \cdot \sigma^2_{TC} + \left(\frac{\partial R_{sh}(t)}{\partial b(t)}\right)^2 \cdot \sigma^2_{bt} + \left(\frac{\partial R_{sh}(t)}{\partial d(t)}\right)^2 \cdot \sigma^2_{dt} + \left(\frac{\partial R_{sh}(t)}{\partial f_y}\right)^2 \cdot \sigma^2_{fy} + \left(\frac{\partial R_{sh}(t)}{\partial i_{COR}}\right)^2 \cdot \sigma^2_{icor} \quad (24)$$

where $\sigma_{\tau c}$ = standard deviations associated with τ_C and is evaluated based on the statistical parameters for τ_C given in Table 1; σ_{bt} = standard deviation associated with $b(t)$ and first order approximation of variance of $b(t)$ shall give its value. The time-dependent c.o.v., $V_{Rsh}(t)$, associated with $R_{sh}(t)$ is estimated from Eq. (25).

$$V_{Rsh}(t) = \frac{\sigma_{Rsht}}{R_{sh}(t)} \quad (25)$$

At time t = 0, $V_{Rsh}(t = 0) = V_{Rsh0}$. Once V_{Rsh0} and $V_{Rsh}(t)$ are known, $V_{Gsh}(t)$ is evaluated from Eq. (18).

6.3 Discussion of Results for Analytical Estimation of Time-Dependent c.o.v. Associated with Time Dependent Strengths and Time-Dependent Degradation Functions

For different mean values of i_{COR}, at time t (years) from the initiation of corrosion: (i) Figures 18(a) – 20(a) present the time-dependent c.o.v., $V_{Rnb}(t)$, associated with $R_{nb}(t)$, (ii) Figures. 18(b) – 20(b) present the time-dependent c.o.v., $V_{Gnb}(t)$, associated with $G_{nb}(t)$, (iii) Figures. 21(a) – 23(a) present the time-dependent c.o.v., $V_{Rsh}(t)$, associated with $R_{sh}(t)$, and (iv)

Figures. 21(b) – 23(b) present the time-dependent c.o.v., $V_{Gsh}(t)$, associated with $G_{sh}(t)$. In the same figures V^S_{Rnb} and V^S_{Gnb}, and V^S_{Rsh} and V^S_{Gsh} are evaluated using 40 random samples; V^A_{Rnb} and V^A_{Rsh} are evaluated using the analytical formulations presented in the preceding sections; V^A_{Gnb} and V^A_{Gsh} are evaluated using Eq. (18). For the purpose of comparison: (i) in Figures. 18(a) – 20(a) V^S_{Rnb} are reproduced from Figures. 10(b) – 12(b), and (ii) in Figures. 21(a) – 23(a) V^S_{Rsh} are reproduced from Figures. 13(b) – 15(b). For a given i_{COR}, good agreement is observed between V^A_{Rnb} and V^S_{Rnb}, V^A_{Gnb} and V^S_{Gnb}, V^A_{Rsh} and V^S_{Rsh}, and V^A_{Gsh} and

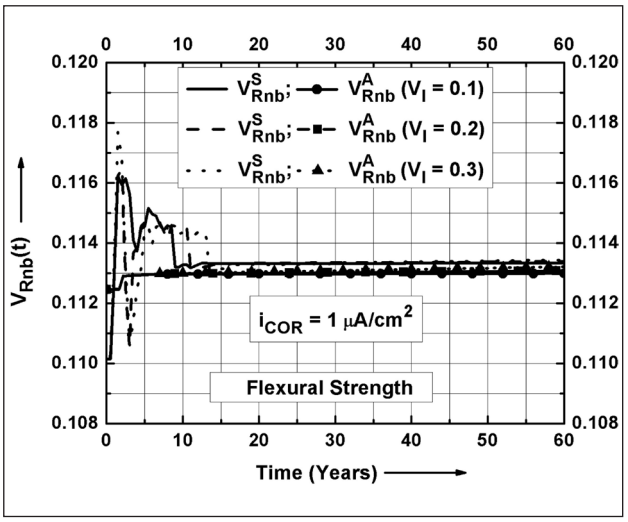

Figure 18(a): Comparison of time-dependent c.o.v V^A_{Rnb} and V^S_{Rnb} for flexural strength (i_{COR} = 1 μA/cm²)

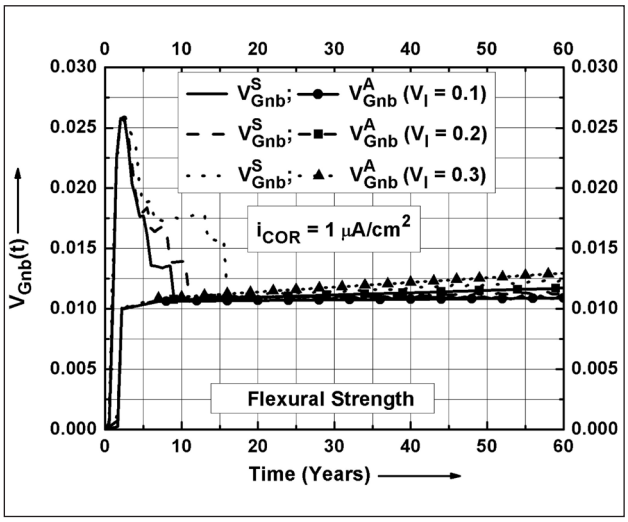

Figure 18(b): Comparison of time-dependent c.o.v V^A_{Gnb} and V^S_{Gnb} for degradation function for flexural strength (i_{COR} = 1 μA/cm²)

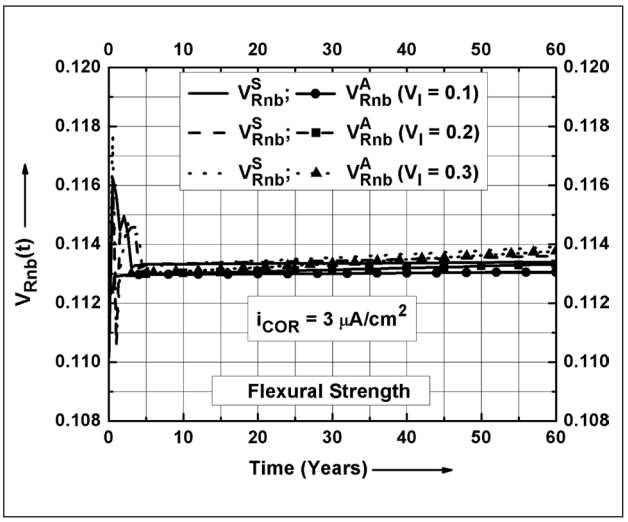

Figure 19(a): Comparison of time-dependent c.o.v V^A_{Rnb} and V^S_{Rnb} for flexural strength (i_{COR} = 3 μA/cm²)

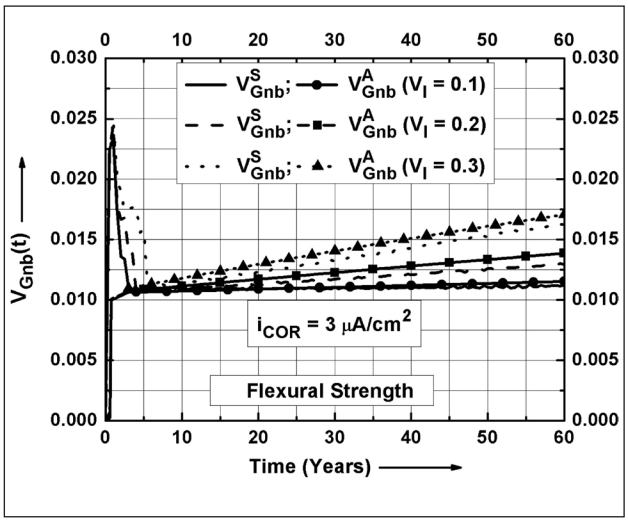

Figure 19(b): Comparison of time-dependent c.o.v V^A_{Gnb} and V^S_{Gnb} for degradation function for flexural strength (i_{COR} = 3 μA/cm²)

V^S_{Gsh}, except in the time interval of about: (a) 0 – 15 years, for i_{COR} = 1 μA/cm², (b) 0 – 5 years for i_{COR} = 3 μA/cm², and (c) 0 – 3 years for i_{COR} = 5 μA/cm². The difference in the aforementioned time intervals is mainly attributed to the randomness associated with the time of cover peeling at the bottom, top, and side resulting in the change of cross-section for the concrete. Good agreement between the analytically estimated and simulated values for the c.o.v. in the remaining time intervals shows that the first-order approximation of mean and variance of strengths can be used for estimating c.o.v. for both strengths and degradation functions.

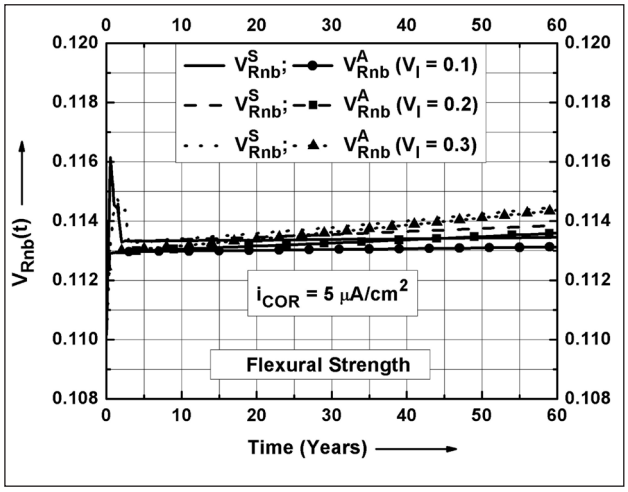

Figure 20(a): Comparison of time-dependent c.o.v V^A_{Rnb} and V^S_{Rnb} for flexural strength (i_{COR} = 5 μA/cm²)

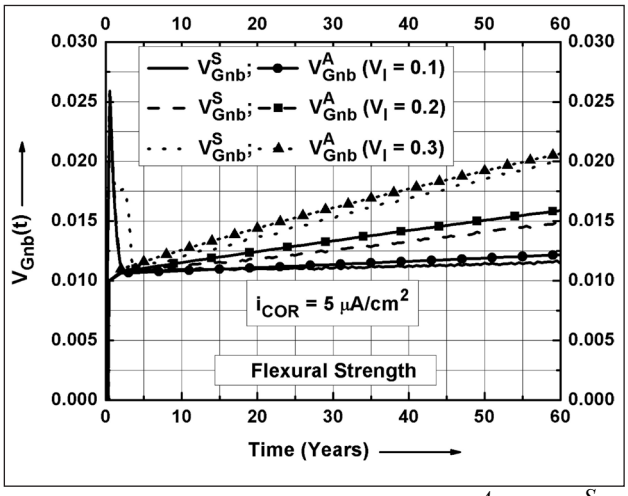

Figure 20(b): Comparison of time-dependent c.o.v V^A_{Gnb} and V^S_{Gnb} for degradation function for flexural strength (i_{COR} = 5 μA/cm²)

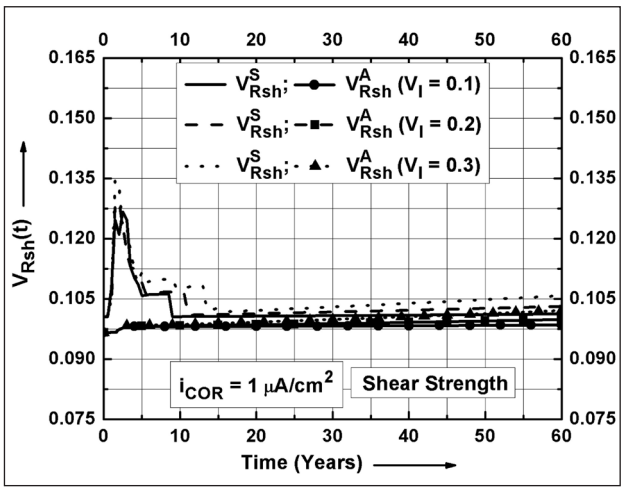

Figure 21(a): Comparison of time-dependent c.o.v V^A_{Rsh} and V^S_{Rsh} for shear strength (i_{COR} = 1 μA/cm²)

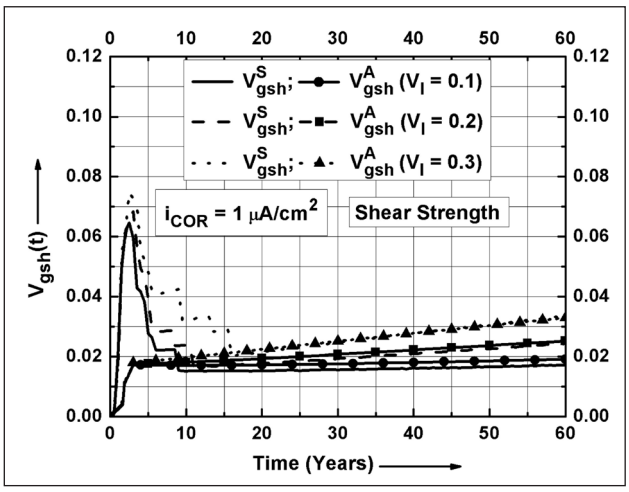

Figure 21(b): Comparison of time-dependent c.o.v V^A_{Gsh} and V^S_{Gsh} for degradation function for shear strength (i_{COR} = 1 μA/cm²)

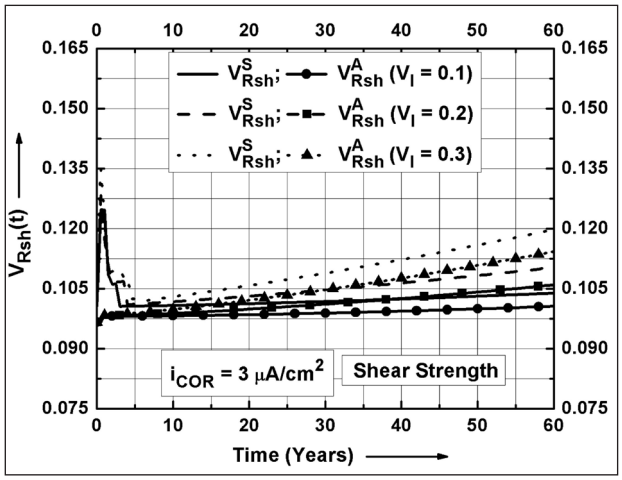

Figure 22(a): Comparison of time-dependent c.o.v V^A_{Rsh} and V^S_{Rsh} for shear strength (i_{COR} = 3 μA/cm²)

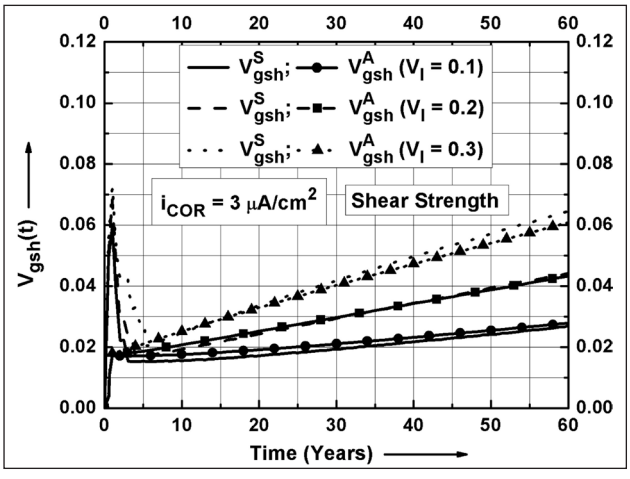

Figure 22(b): Comparison of time-dependent c.o.v V^A_{Gsh} and V^S_{Gsh} for degradation function for shear strength (i_{COR} = 3 μA/cm²)

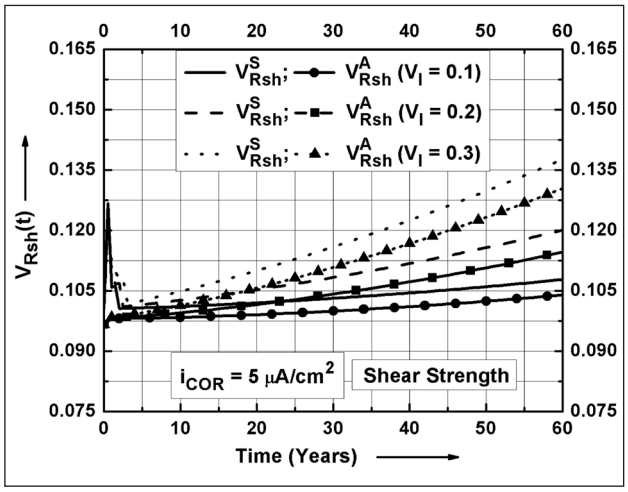

Figure 23(a): Comparison of time-dependent c.o.v V^A_{Rsh} and V^S_{Rsh} for shear strength (i_{COR} = 5 μA/cm^2)

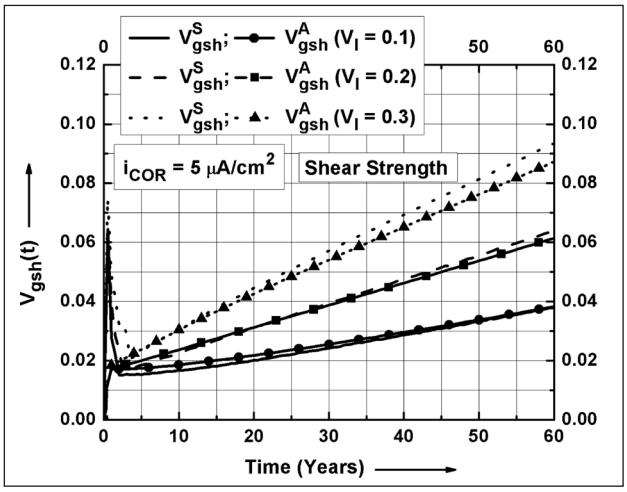

Figure 23(b): Comparison of time-dependent c.o.v V^A_{Gsh} and V^S_{Gsh} for degradation function for shear strength (i_{COR} = 5 μA/cm^2)

7. Conclusions

Following conclusions are drawn from the present study:

(i) Correlations with the experimental results indicate that the equations proposed for estimating the time-dependent mass loss of the reinforcement, W_s, reduced diameter of reinforcement, D_r, loss of cross-sectional area of reinforcement, A_{cor}, and corrosion penetration depth, X, are capable of providing their reasonable estimates that are in line with the available experimental trends.

(ii) Correlations with the experimental results indicate that good agreement is observed between analytical predictions and experimental results, for ultimate flexural and shear strengths for corrosion-affected RC beams. These findings also highlight the fair estimation of: (i) time to peeling of cover concrete using the proposed methodology to arrive at the time-dependent reduced concrete section, and (ii) W_s to arrive at the time-dependent reduced cross-section of reinforcing steel.

(iii) A methodology to evaluate time-dependent strengths and c.o.v. associated with strengths is presented for corrosion-affected RC beams, by using LHS technique.

(iv) For corrosion-affected RC beams, it is shown that time dependent mean flexural and shear strengths can be approximated by considering the linear terms in Taylor series expansion of their performance functions.

(v) For corrosion-affected RC beams, time-dependent c.o.v. associated with the strength is influenced by the c.o.v. associated with annual mean corrosion rate, i_{COR}, at late stages of degradation (say 40 – 60 years).

(vi) Good agreement is observed between the analytical and simulated estimations for the time-dependent c.o.v. associated with flexural and shear strengths.

(vii) Good agreement is observed between the analytical and simulated estimations for the time dependent c.o.v. associated with the degradation functions for the flexural and shear strengths.

(viii) Analytical estimation of c.o.v. associated with strengths and degradation functions substantially reduces the computational efforts involved in their estimation using LHS technique.

Acknowledgement

The first author gratefully acknowledges the financial support provided by Japan Society for the Promotion of Science under JSPS RONPAKU Dissertation Ph.D. program for pursuing Ph.D. at Nagoya University, Nagoya, Japan.

References

1. ACI (1995), Building Code Requirement for Structural Concrete (ACI 318-95) and Commentary (ACI 318R-95), American Concrete Institute, Michigan, USA.
2. Andrade, C., C. Alonso and Molina, F. J. (1993), "Cover cracking as a function of rebar corrosion: part I – experimental test." Materials and Structures, 26, 453-464.
3. Bazant, Z. P. (1979), "Physical model for steel corrosion in sea structures – theory." Journal of the Structural Division, ASCE, 105(6), 1137-1153.
4. Benjamin, J. R. and C. A. Cornell (1970), "Probability, Statistics, and Decision for Civil Engineering." Mcgraw-Hill, New York, USA.

5. Bhargava, K., A. K. Ghosh, Y. Mori and S. Ramanujam (2003), "Analytical Model of Corrosion-Induced Cracking of Concrete Considering the Stiffness of Reinforcement." Structural Engineering and Mechanics – An International Journal, 16(6), 749-769.
6. Bhargava, K., A. K. Ghosh, Y. Mori and S. Ramanujam (2005), "Modeling of Time to Corrosion-Induced Cover Cracking in Reinforced Concrete Structures." Cement and Concrete Research, 35(11), 2203-2218.
7. Bhargava, K., A. K. Ghosh, Y. Mori and S. Ramanujam (2006), "Model for Cover Cracking due to Rebar Corrosion in RC Structures." Engineering Structures, 28(8), 1093-1109.
8. Bhargava, K. (2008), Time-dependent degradation and reliability assessment of RC structures subjected to reinforcement corrosion, Doctor of Engineering Dissertation, Graduate School of Environmental Studies, Nagoya University, Nagoya, Japan.
9. BIS (2000), IS 456: 2000, Indian Standard, Plain and Reinforced Concrete – Code of Practice, Fourth Revision, Bureau of Indian Standards, New Delhi, India.
10. CEB–FIP (1990), CEB-FIP Model Code 1990, Comite Euro-International du Beton-Federation International de la Precontrainte, Thomas Telford, London, UK.
11. Ellingwood, B. R. and A. H. S. Ang (1974), "Risk-based evaluation of design criteria." Journal of the Structures Division, ASCE, 100(ST9), 1771-1788.
12. Ellingwood, B. (1977), "Statistical analysis of RC beam-column interaction." Journal of the Structures Division, ASCE, 103(ST7), 1377-1388.
13. Ellingwood, B. (1982), "Safety checking formats for limit states design." Journal of the Structures Division, ASCE, 108(ST7), 1481-1493.
14. Ellingwood, B. and H. Hwang (1985), "Probabilistic descriptions of resistance of safety-related structures in nuclear plants." Nuclear Engineering and Design, 88, 169-178.
15. Enright, M. P. and D. M. Frangopol (1998a), "Service-life prediction of deteriorating concrete structures." Journal of Structural Engineering, ASCE, 124(3), 309-317.
16. Enright, M. P. and D. M. Frangopol (1998b), "Probabilistic analysis of resistance degradation of reinforced concrete bridge beams under corrosion." Engineering Structures, 20(11), 960-971.
17. Frangopol, D. M., K. Y. Lin and A. C. Estes (1997), "Reliability of reinforced concrete girders under corrosion attack." Journal of structural Engineering, ASCE, 123(3), 286-297.
18. Haldar, A. and S. Mahadevan (2000), Reliability Assessment Using Stochastic Finite Element Analysis, First Edition, John Wiley & Sons, Inc., New York, USA.
19. Hong, H. P. and W. Zhou (1999), "Reliability evaluation of RC columns." Journal of Structural Engineering, ASCE, 125(7), 784-790.
20. Hong, H. P. (2000), "Assessment of reliability of aging reinforced concrete structures." Journal of structural Engineering, ASCE, 126(12), 1458-1465.
21. Hwang, H., B. Ellingwood, M. Shinozuka and M. Reich (1987), "Probability-based design criteria for nuclear plant structures." Journal of Structural Engineering, ASCE, 113(5), 925-942.
22. Israel, M., B. Ellingwood and R. Corotis (1987), "Reliability-based code formulations for reinforced concrete buildings." Journal of Structural Engineering, ASCE, 113(10), 2235-2252.
23. Li, C. Q. (2003), "Life cycle modeling of corrosion affected concrete structures – Propagation." Journal of Structural Engineering, ASCE, 129(6), 753-761.
24. Li, C. Q., W. Lawanwisut and J. J. Zheng (2005), "Time-dependent reliability method to assess the serviceability of corrosion-affected concrete structures." Journal of Structural Engineering, ASCE, 131(11), 1674-1680.
25. Liu, Y. (1996), Modeling the time to corrosion cracking of the cover concrete in chloride contaminated reinforced concrete structures, Ph.D. Dissertation, Virginia Polytechnic Institute and State University, Blacksburg, Virginia, USA.
26. Liu, Y. and R. E. Weyers (1998), "Modelling the time-to-corrosion cracking in chloride contaminated reinforced concrete structures." ACI Materials Journal, 95(6), 675-681.
27. Mangat, P. S. and M. S. Elgarf (1999), "Flexural strength of concrete beams with corroding reinforcement." ACI Structural Journal, 96(1), 149-158.
28. Mckay, M. D., R. J. Bechman and W. J. Conover (1979), "A comparison of three methods for selecting values of input variables in the analysis of output from a computer code." Technometrics, 21(2), 239-245.
29. Mirza, S. A., M. Hatzinikolas and J. G. MacGregor (1979), "Statistical description of strength of concrete." Journal of the Structures Division, ASCE, 105(ST6), 1021-1037.
30. Mirza, S. A. and J. G. MacGregor (1979a), "Variations in dimensions of reinforced concrete members." Journal of the Structures Division, ASCE, 105(ST4), 751-766.
31. Mirza, S. A. and J. G. MacGregor (1979b), "Variability of mechanical properties of reinforcing bars." Journal of the Structures Division, ASCE, 105(ST5), 921-937.
32. Ranganathan, R. (2000), Structural Reliability Analysis and Design, Second Jaico Impression, Jaico Publishing House, Mumbai India.
33. Rasheeduzzafar, S. S. Al-Saadoun and A. S. Al-Gahtani (1992), "Corrosion cracking in relation to bar diameter, cover and concrete quality." Journal of Materials in Civil Engineering, ASCE, 4(4), 327-343.
34. Rodriguez, J., L. M. Ortega and J. Casal (1997), "Load carrying capacity of concrete structures with corroded reinforcement." Construction and Building Material, 11(4), 239-248.
35. SP16 (1980), Design Aids for Reinforced Concrete to IS: 456-1978, Bureau of Indian Standards, New Delhi, India.
36. Stewart, M. G. and D. V. Rosowsky (1998), "Time-dependent reliability of deteriorating reinforced concrete bridge decks." Structural Safety, 20, 91-109.
37. Thoft-Christensen, P. (1998), "Assessment of the reliability profiles for concrete bridges." Engineering Structures, 20(11), 1004-1009.
38. Torres-Acosta, A. A., (1999), Cracking induced by localized corrosion of reinforcement in chloride contaminated concrete, Ph.D. Dissertation, Department of Civil and Environmental Engineering, University of South Florida, Tampa, Florida, USA.
39. Val, D. V., M. G. Stewart and R. E. Melchers (1998), "Effect of reinforcement corrosion on reliability of highway bridges." Engineering structures, 20(11), 1010-1019.
40. Vu, K. A. T. and M. G. Stewart (2000), "Structural reliability of concrete bridges including improved chloride-induced corrosion models." Structural Safety, 22, 313-333.
41. Vu, K. A. T. and M. G. Stewart (2005), "Predicting the likelihood and extent of reinforced concrete corrosion-induced cracking." Journal of Structural Engineering, ASCE, 131(11), 1681-1689.

SRESA JOURNAL SUBSCRIPTION FORM

Subscriber Information (Individual)

Title	First Name	Middle Name	Last Name

Street Address Line 1 _____

Street Address line 2 _____

City	State/Province	Postal Code	Country

Work Phone	Home Phone	E-mail address

Subscriber Information (Institution)

Name of Institution/ Library _____

Name and Designation of Authority for Correspondence _____

Address of the Institution/Library _____

Subscription Rates

	Subscription Quantity	Rate	Total
Annual Subscription (in India)	_____	Rs 10,000	_____
(Abroad)	_____	$ 500	_____
	_____		_____
	_____		_____

Payment mode (please mark)

Cheque ☐ Credit Card ☐ Master Card ☐ Visa ☐ Online Banking ☐ Cash ☐ De mand Draft ☐

Credit card Number _____

Credit Card Holders Name _____

Credit Card Holde _____

Guidelines for Preparing the Manuscript

A softcopy of the complete manuscript should be sent to the Chief-Editors by email at the address: editor@sresa.org.in. The manuscript should be prepared using 'Times New Roman' 12 font size in double spacing, on an A-4 size paper. The illustrations and tables should not be embedded in the text. Only the location of the illustrations and tables should be indicated in the text by giving the illustration / table number and caption.

The broad structure of the paper should be as follows: a) Title of the paper – preferably crisp and such that it can be accommodated in one or maximum two lines with font size of 14 b) Name and affiliation of the author(s), an abstract of the paper in ~ 100 words giving brief overview of the paper and d) Five key words which indicates broad subject category of the paper. The second page of the paper should start with the title followed by the Introduction

A complete postal address should be given for all the authors along with their email addresses. By default the first author will be assumed to be the corresponding author. However, if the first author is not the corresponding author it will be indicated specifically by putting a star superscript at the end of surname of the author.

The authors should note that the final manuscript will be having double column formatting, hence, the size of the illustration, mathematical equations and figures should be prepared accordingly.

All the figures and tables should be supplied in separate files along with the manuscript giving the figure / table captions. The figure and table should be legible and should have minimum formatting. The text used in the figures and tables should be such that after 30% reduction also it should be legible and should not reduced to less than font 9.

Last section of the paper should be on list of references. The reference should be quoted in the text using square bracket like '[1]'in a chronological order. The reference style should be as follow:

1. Pecht M., Das D, and Varde P.V., "Physics-of-Failure Method for Reliability Prediction of Electronic Components", Reliability Engineering and System Safety, Vol 35, No. 2, pp. 232- 234, 2011.

After submitting the manuscript, it is expected that reviews will take about three months; hence, no communication is necessary to check the status of the manuscript during this period. Once, the review work is completed, comments, will be communicated to the author.

After receipt of the revised manuscript the author will be communicated of the final decision regarding final acceptance. For the accepted manuscript the author will be required to fill the copy right form. The copy right form and other support documents can be down loaded from the SRESA website: http://www.sresa.org.in

Authors interested in submitting the manuscript for publication in the journal may send their manuscripts to the following address:

Society for Reliability and Safety
RN 68, Dhruva Complex
Bhabha Atomic Research Centre,
Mumbai – 400 085 (India)
e-mail : editor@sresa.org.in

The Journal is published on quarterly basis, i.e. Four Issues per annum. Annual Institutional Subscription Rate for SAARC countries is Indian Rupees Ten Thousand (Rs. 10,000/-) inclusive of all taxes. Price includes postage and insurance and subject to change without notice. For All other countries the annual subscription rate is US dollar 500 ($500). This includes all taxes, insurance and postage.

Subscription Request can be sent to SRESA Secretariat (please visit the SRESA website for details)

SRESA Journal of

Life Cycle Reliability and Safety Engineering

Contents

Vol. 1 Issue No. 3 July – September 2012 ISSN – 2250 0820